

**UCGE Reports
Number 20097**

Department of Geomatics Engineering

**Design and Analysis of a Low Cost
GPS Aided Navigation System**

(URL: <http://www.geomatics.ucalgary.ca/links/GradTheses.html>)

by

James F. McLellan

January 1992



THE UNIVERSITY OF CALGARY

**DESIGN AND ANALYSIS OF A LOW COST
GPS AIDED NAVIGATION SYSTEM**

by

JAMES F. McLELLAN

A DISSERTATION

**SUBMITTED TO THE FACULTY OF GRADUATE STUDIES
IN PARTIAL FULFILLMENT OF THE REQUIREMENTS FOR THE
DEGREE OF MASTER OF ENGINEERING**

DEPARTMENT OF SURVEYING ENGINEERING

CALGARY, ALBERTA

JANUARY, 1992

© James F. McLellan 1992

ABSTRACT

A low cost GPS aided navigation system can provide continuous position and navigation to a navigator, and coupled with a communication system, can be an integral part of a fleet management system. Also, information gathering, processing and dissemination has become an important part of our society. From a mobile perspective, it is critical to know where the vehicle is located along with information such as status, payload and destination. GPS will revolutionize these navigation related activities as it can operate world wide, 24 hours per day (full constellation), and in any kind of weather.

The focus of this thesis deals with the development of a fleet management system called NavTrax™. NavTrax™ encompasses navigation, communication and central office subsystems. This thesis concentrates on the development of the navigation system, including both hardware and software. The system is designed to provide continuous position, self initialization and immediate response at turn-on.

The Magnavox MX 4200 and GPS Engine were selected since they are two of the few low cost GPS receivers which output both raw pseudo ranges (position) and carrier phase rate (velocity), such that they can be combined with dead reckoning sensors via a kinematic filter.

Because GPS sensors, at best, have a 25 to 40 second delay (can be up to two to three minutes) in initialization, it is necessary to save the last position and to design a filter that can start off from previous coordinates and produce a position using dead reckoning sensor information until the GPS signal has been acquired. The GPS filter used in NavTrax™ is an eight state filter of three positions, three velocities and two time related biases. The GPS filter is taken as the reference filter and is fed directly into a master filter

where fusion takes place. The master filter contains six states including three velocities and three positions. The system was designed such that additional sensors could be readily added or changed.

Dead reckoning sensors utilized in this research include a flux gate compass (azimuth), a rate gyro (change in azimuth), and a transmission type odometer (speed). Each of the dead reckoning sensors has its own local filter which feeds into the master filter where fusion takes place. Information is passed from the master filter back into each local filter. Full covariance information is utilized on each sensor, and rigorous covariance propagation is carried out, thus the quality of the solution is known at all times.

The filter can be run on its own for some period of time purely on the basis of the kinematic model and dead reckoning sensor information. In periods of long lapses of GPS information, map matching will be required in order to prevent lost situations. Map matching was not made part of this thesis, however, it will be incorporated as part of future developments. The objective was to build a land navigation system that would not have to rely on an expensive, high quality single line road network in order to function properly.

The end result of employing the above methodology is that the filter responds quickly and guarantees position determination at all times. Blunders can also be detected readily in the sensor data. Tests were performed in a high density urban environment to judge the performance of the integrated system, which has proven to be superior to containing only GPS. Without Selective Availability and continuous tracking of four or more satellites, the accuracy of the system is about 20 m. Without GPS, the dead reckoning system is accurate to about one to two percent of the distance travelled.

ACKNOWLEDGEMENTS

I would like to express my appreciation to my supervisor, Dr. Gerard Lachapelle, for his continued support and encouragement throughout my M. Eng. program.

This dissertation was completed while employed full time by Pulsesearch, A Division of Nowasco, and in the role as Manager of the Navigation Systems Group. The Navigation Systems Group are responsible for the design, development, testing and analysis of the NavTrax™ system. Much of the latter work in this dissertation is based on internal reports and technical papers written at Pulsesearch have been referenced throughout this work. The original work on AVLN2000™ completed at The University of Calgary, under the leadership of Dr. Edward Krakiwsky, served as catalyst to Pulsesearch in embarking on fleet management systems as a business venture.

Appreciation is expressed sent to Mr. John Adams for his technical support and encouragement to complete an M. Eng. degree. Special thanks also goes to Dr. Edward Krakiwsky for his advice and discussions. Thanks also goes to Dr. M. E. Cannon for her consultation in developing GPS mathematical models. Appreciation is also given to my colleagues at Pulsesearch who performed many tests and wrote software in support of this dissertation. John B. Schleppe was especially helpful in development of the sensor filtering.

A special recognition and thanks is due to my wife, Eleanor, who supported me greatly while writing this dissertation. Thank you for your patient support, love and understanding during this multi-year effort.

TABLE OF CONTENTS

THESIS APPROVAL	ii
ABSTRACT	iii
ACKNOWLEDGEMENTS	v
TABLE OF CONTENTS	vi
LIST OF TABLES	xi
LIST OF FIGURES	xii
NOTATION	xvi
ACRONYMS AND ABBREVIATIONS	xviii
CHAPTER 1 INTRODUCTION	1
1.1 Canada's Road Network	2
1.2 Problem Definition	3
1.3 Solution	3
CHAPTER 2 LAND NAVIGATION REQUIREMENTS	6
2.1 General Requirements	6
2.2 Functional Requirements	10
2.3 User Requirements by Thompson - Hickling	11
2.4 Pulsesearch Market Study	11
2.5 The Market	15
2.6 Vehicle Navigation Systems	20
CHAPTER 3 NAVIGATION SYSTEM DESIGN	23
3.1 System Overview	23

3.2 System Design	24
3.3 The NavTrax™ Filter	32
CHAPTER 4 FILTERING METHODOLOGY	34
4.1 Dynamic and Kinematic Modelling	34
4.2 Kalman Equations	36
4.3 Bayes Filtering Equations	39
4.4 Federated Filtering Concept	40
4.5 Federated Filter Design	48
4.6 Federated Filter Implementations	49
CHAPTER 5 GPS PROCESSING	55
5.1 Processing Overview	55
5.2 Broadcast Ephemeris Computations	57
5.2.1 Keplerian Orbital Elements	57
5.2.2 Broadcast Ephemeris Computational Procedure	61
5.2.3 Computation of Satellite Velocity	65
5.3 Observation Reductions	69
5.3.1 Computation of Distance and Elevation to Satellite	69
5.3.2 Clock Corrections	70
5.3.3 Ionospheric Modelling	72
5.3.4 Tropospheric Modelling	74
5.4 Carrier Smoothed Code Measurement	75
5.4.1 Effect of the Ionosphere on Carrier Smoothing	79

5.5 Observation Weighting	81
5.6 Cycle Slip Detection in the Carrier Phase Data	83
5.6.1 Phase Velocity Method	83
5.6.2 Pseudorange Method	85
5.6.3 Treatment of Cycle Slips	85
5.7 Pseudorange and Carrier Phase Measurements	85
5.7.1 Range Model	86
5.7.2 Phase and Phase Difference Models	93
5.7.3 Phase Rate Model	98
5.8 Complementary GPS Observables	106
5.9 Kinematic State Space Model	109
CHAPTER 6 DEAD RECKONING AND MASTER FILTER	115
6.1 Dead Reckoning Sensors	115
6.2 Distance Filter	117
6.2.1 Differential Odometry	117
6.2.2 Single Odometer	122
6.3 Compass	125
6.3.1 Etak Flux Gate Sensor	128
6.3.2 Model	130
6.4 Rate Gyro	139
6.4.1 Etak Turn Sensor	142
6.4.2 Murata GYROSTAR™	143

6.4.3 Model	145
6.5 Velocity Filters	148
6.5.1 Heading Filter	148
6.5.2 Propagation of Velocity to Azimuth and Speed	150
6.5.3 Conversion of Speed and Heading to Velocity	151
6.6 NavTrax™ Master Filter	151
CHAPTER 7 SENSOR ASSESSMENT	155
7.1 Dead Reckoning Sensors	155
7.1.1 Compass	156
7.1.2 Rate Gyro	160
7.1.3 Odometer	162
7.2 GPS	164
CHAPTER 8 TEST DESCRIPTION AND RESULTS	167
8.1 NavTrax™ Testing	167
8.2 Field Trials In the Calgary Police Department	178
CHAPTER 9 SUMMARY AND CONCLUSIONS	180
REFERENCES	182
APPENDIX A COORDINATE TRANSFORMATION FORMULAE	189
A.1 Transformation of (ϕ, λ, h) to (x, y, z)	189
A.2 Transformation of (x, y, z) to (ϕ, λ, h)	189
A.3 Error Propagation of ϕ, λ, h to X, Y, Z	191
A.4 Transformation of (ϕ, λ) to (x, y) UTM Grid Coordinates	192

A.5 Transformation of (x, y) UTM Grid Coordinate to (ϕ, λ)	193
A.6 Error Propagation between Grid and Ellipsoid Coordinates	195
APPENDIX B NAVIGATION ALGORITHMS	198
B.1 Navigation Algorithms	198
B.2 Cartesian Formulation	199
B.3 Geodetic	200

LIST OF TABLES

Table 2.1: Vehicle Navigation User Requirements	12
Table 2.2 Total Number of Highway Vehicles in Canada	16
Table 2.3 Total Number of Urban Vehicles in Canada	17
Table 2.4 Total Number of Off-Highway Vehicles in Canada	18
Table 2.5 Some GPS Based AVLN Systems	22
Table 5.1 Standard Deviation of Phase Measurements	83
Table 5.2 Values For GPS Filter	114
Table 6.1 Heading Sensors	116
Table 6.2 Distance Sensors	116
Table 6.3 Sensors and Their Output	117
Table 6.4 Values for Odometer Filter	124
Table 6.5 Values for Compass Filter	138
Table 6.6 Gyro Principles and Design	141
Table 6.7 Values for Heading Rate Filter	147
Table 6.8 Values for Heading Rate Filter	149
Table 6.9 Values for Master Filter	154

LIST OF FIGURES

Figure 2.1. Fleet Management System Components	7
Figure 2.2 Components of a Generic AVLN System	9
Figure 2.3 Requirements - Major Highway	19
Figure 2.4 Requirements - Urban	19
Figure 3.1 System Overview	24
Figure 3.2 - Processing Overview	25
Figure 3.3 - I/O Controller	26
Figure 3.4 Navigation Module	27
Figure 3.5 Decentralized-Federated Filter	30
Figure 3.6 Data Flow Diagram	33
Figure 4.1.Federated Filter Design and Implementation Scheme	41
Figure 4.2 Federated Filter #1: MF Memory, Zero-Reset	51
Figure 4.3 Federated Filter #2: MF/LF Memory, Partial Fusion	52
Figure 4.4 Federated Filter #3: LF Memory, Full Fusion	53
Figure 4.5 Federated Filter #4: LF Memory, No-Reset	54
Figure 5.1 GPS processing with Differential Corrections	56
Figure 5.2 Keplerian Orbital Elements	59
Figure 5.3 GPS Orbit Description	60

Figure 5.4 Satellite Coordinate Computation	62
Figure 5.5 Smoothed Pseudorange Weighting Values	79
Figure 5.6 Carrier Smoothed Pseudoranges - Dual Ramp Method	80
Figure 5.7 Pseudorange Model	87
Figure 5.8 Phase Difference Model	94
Figure 5.9 Phase Rate Model	99
Figure 5.10. Exponential Autocorrelation Function	111
Figure 6.1 Odometry Sensor	118
Figure 6.2 Differential Odometer Geometry	119
Figure 6.3 Earth's Magnetic Field	126
Figure 6.4 Etak Flux Gate Sensor Block Diagram	129
Figure 6.5 Flux Gate Coordinate Frames	131
Figure 6.6 Compass to Body Frame Rotation	132
Figure 6.7 Compass Observations as an Ellipse	135
Figure 6.8 Compass Observations as a Circle	136
Figure 6.9 Heading Rate Determination	142
Figure 6.10 Outline of a Piezoelectric Vibratory Gyroscope	143
Figure 6.11 Outline of a Triangle Bar Gyroscope	144
Figure 6.12 GYROSTAR Rate Gyro Output Detection	145
Figure 7.1 Temperature Profile	156

Figure 7.2 Etak Compass Response	157
Figure 7.3 Compass Y Power Drain Test	159
Figure 7.4 Compass X Power Drain Test	160
Figure 7.5 GYROSTAR Rate Gyro Response	161
Figure 7.6 Etak Rate Gyro Response	161
Figure 7.7 Distance Error Growth Rate due to Tire Pressure	163
Figure 7.8 Distance Error Growth Rate due to Velcoity	164
Figure 7.9 Urban Tracking	165
Figure 7.10 Suburban Tracking	166
Figure 8.1 Initial Filter Screen	169
Figure 8.2 Initial NavTrax Screen - Overview	170
Figure 8.3 Latitude Error Growth - Overall	171
Figure 8.4 Longitude Error Growth - Overall	171
Figure 8.5 NavTrax Screen - MacLeod Trail	172
Figure 8.6 Latitude Error Growth - MacLeod Trail	173
Figure 8.7 Longitude Error Growth Rate - MacLeod Trail	173
Figure 8.8 Filter Screen - Downtown	174
Figure 8.9 NavTrax Screen - Downtown	175
Figure 8.10 - Latitude Error Growth Rate - Downtown	176
Figure 8.11 Longitude Error Growth Rate - Downtown	176
Figure 8.12 Latitude Error Growth Rate - Deerfoot	177

Figure 8.13 Longitude Error Growth Rate - Deerfoot 177

Figure B.1 Velocity Equations 201

NOTATION

Parameter	Description
A	design matrix
a	semi-major axis of Earth's reference ellipsoid
alt	altitude angle: $alt = 90^\circ - z$ (i.e. tilt from horizon, z is the zenith distance)
b	semi-minor axis of Earth's reference ellipsoid
$BASE$	perpendicular distance between front and rear wheel axles
C_F^α	covariance matrix for \hat{x}_F
C^l	covariance matrix of observations
C^u	covariance matrix of driving noise
C^α	covariance matrix of parameters
c	speed of light
d^L	total distance observed by left wheel odometer at time t_k
d^R	total distance observed by right wheel odometer at time t_k
e^2	eccentricity of Earth's reference ellipsoid
h	geodetic height
I	identity matrix
l	observation vector
P	GPS pseudorange measurement
t_{k-1}, t_k	two successive times of measurement

<i>TRACK</i>	Constant width between left and right wheel plane when wheels aligned parallel in forward pointing direction
z	zenith distance: angle down from zenith to object ($z = 90^\circ - alt$)
az_{mag}	azimuth observed from magnetic fluxgate compass in reference to magnetic North at time t_k
Δaz	change in heading (azimuth)
V_N	velocity north
V_E	velocity east
V_U	velocity up
\hat{x}	vector of estimated parameters
\hat{x}_F	final combined solution
ϕ	geodetic latitude
λ	geodetic longitude
λ	L1 GPS carrier wavelength
α	inverse of correlation time of the stochastic Markov process
ρ	geometric range from receiver to satellite
Φ	Kalman filter transition matrix
Φ	carrier phase observation at time t_k
$\dot{\Phi}$	carrier phase rate observation at time t_k

ACRONYMS AND ABBREVIATIONS

Acronym	Description
ARCS	Automatic Remote Control System
AVLN	Automatic Vehicle Location and Navigation
C/A code	Clear/Acquisition code
CAD	Computer aided dispatch
CT	Conventional Terrestrial coordinate system
DLC	Differential Loran C
DGPS	Differential Global Positioning System
DOC	Department of Communications
DOT	Department of Transportation
DR	Dead Reckoning
ECEF	Earth Centered Earth Fixed Cartesian coordinate reference system
GAST	Greenwich Apparent Sidereal Time
GDOP	Geometry Dilution of Precision
GIS	Geographic Information System
GPS	Global Positioning System (NAVSTAR satellite system)
HDOP	Horizontal Dilution of Precision
I/O	input / output
INS	Inertial Navigation System
ION	Ionosphere
IVHS	Intelligent Vehicle-Highway System

JIT	Just In Time
LC	Loran C
LF	local filter
MDT	mobile display terminal
MF	master filter
MHz	megahertz
MM	Map Matching
NAV	navigation
OECD	Organization for Economic Cooperation and Development
RA	Right Ascension coordinate system
SA	Selective Availability
SCADA	System Control And Data Acquisition
TEC	Total Electron Count
TROP	troposphere
UHF	ultra high frequency
UTM	Universal Transverse Mercator conformal map projection
VDOP	Vertical Dilution of Precision
VHF	very high frequency
WGS84	World Geodetic System, 1984

CHAPTER 1

INTRODUCTION

Intelligent Vehicle Highway Systems (IVHS) are the new wave in North American transportation circles and are generally understood to be made up of the following elements [McLellan et al., 1991b]:

- (1) advance traffic control systems;
- (2) driver information systems;
- (3) fleet management systems; and
- (4) vehicle control systems.

Happening almost concurrently, but in mobile communication circles, is Vision 2000 Inc., a non-profit corporation setup and spearheaded by Communications Canada, with approximately 50 member companies and government organizations. It has set a future goal to provide personal communication between **anyone, anywhere, and at anytime**. At first glance, this initiative looks like one of pure communications, however, the inclusion of the word **anywhere** is understood to encompass both the positioning (coordinates) and location (map) worlds. Hence, Vision 2000 in Canada has embraced the IVHS initiative and recognizes the importance of navigation related technologies in the world of mobile communications.

IVHS and Vision 2000 are the general framework within which the research herein is being performed.

1.1 Canada's Road Network

Land navigation takes place both "off road" and "on road". Canada's road and street network is 840,000 km in length, of which 64% is unpaved, but is still widely used. The rural areas account for 86% of the road network with the remaining 14% concentrated in the urban areas. 1986 statistics, however, show that urban travel constitutes 55% of total highway travel. The Provincial and Municipal governments jointly own 98% of all roads leaving only 2% ownership to the Federal and Territorial governments [Krakiwsky et al., 1990; McLellan et al., 1991b].

In 1986 about 16 million vehicles were registered in Canada according to Statistics Canada. About 75% of these vehicles are private automobiles. The average vehicle is driven about 20,000 km per year. It is estimated that there are about 200,000 straight trucks and road tractors operating on Canada's highways. In addition to this amount, there are about 10,000 vehicles in Canada performing off highway work such as utility inspection and information gathering [McLellan et al., 1989].

There is a growing emphasis of how to best manage these vehicles. In Canada, efficiency and safety is of prime concern. Governments are reluctant to build new roads and freeways. Companies, in ever increasing competition, are being forced to maintain rigid schedules (just in time (JIT) delivery). Gridlock is a problem in some of the major urban centres (Toronto and Montreal), but is not the major problem facing Canadian companies.

In the United States and Europe, the above statistics are orders of magnitude larger, hence their concerns and problems are somewhat different than those in Canada (gridlock is a major problem). Defined in the following Sections are the problems encountered and it will be demonstrated how low cost navigation systems incorporating space technology can be part of the solution.

1.2 Problem Definition

The Organization for Economic Cooperation and Development [OECD, 1988] has estimated that billions of dollars are lost annually by industrialized nations due to the lack of navigation related information for drivers. The President of IVHS America at the 1991 ISATA meeting in Florence, Italy, stated that about two billion vehicle hours of delay per year are incurred in the USA due to traffic congestion and the non-optimal use of the U.S. road network system. This translates into lost revenue of about \$30 billion per year. This figure is predicted to increase by 500 % by the year 2005 if no corrective action is taken [McLellan et al., 1991a]. The lack of road related information for drivers and dispatchers of fleets of vehicles, again, is identified as a serious problem. In order to solve this problem, it can be seen that the issue of communicating with **anyone, anywhere and anytime** must be addressed.

Rather than waiting for some all encompassing solution, the strategy in Canada and the United States is to make early in-roads into making vehicles and highways more "intelligent" - the rationale being that useful technologies already exist and are ready to be exploited. All that is needed is for a judicious and clever selection to be made and, then, an optimal integration of these technologies is necessary to solve particular classes of IVHS problems. The U.S. Congress has recently committed \$160 million per year for the next five years to solving these IVHS problems. In Canada, "Round Table" discussions are underway by DOT, Ottawa, to come up with a Canadian strategy.

1.3 Solution

The problem of **anywhere** will be addressed in this document. Included will be the design and development of a navigation system which is relatively low cost, robust and fault tolerant.

The Global Positioning System (GPS) has revolutionized the geodetic and navigation industries, shifting the focus from ground-to-ground measurements to ground-to-sky measurements. Conventional survey methods link stations via terrestrial measurements requiring that the stations be intervisible. It is this intervisibility that has in the past precluded the development of low cost navigational systems for Land Positioning Systems. Loran C, Omega and various other systems have been used extensively in air and sea applications, but have had limited use in land applications. Loran C is gaining wider acceptance but is still has limited coverage in many parts of the world, notably in the northern part of the Canadian western provinces.

The deployment of the Block II Global Positioning System (GPS) satellites coupled with low cost sensor hardware has generated a great deal of interest in the public sector for provision of low cost navigation systems. One of the limitations with using GPS as a primary positioning system is the requirement to have line of sight visibility to four or more satellites at all times. Currently there are two contributing factors to this limitation: first, not all satellites have yet been launched, thus there are still periods when less than four satellites are visible; secondly, line of sight tends to be frequently blocked when operating in urban canyons (areas of tall buildings and trees and in tunnels). To be acceptable for many applications, the navigation system must be capable of providing continuous position, regardless of the operating environment. The system must also be low cost and user friendly in order to gain wide acceptance.

The focus of this dissertation is to show an optimal way in which to integrate the various low cost sensors to provide continuous position for an Automatic Vehicle Location and Navigation (AVLN) system. It is this continuous integration coupled with continuous calibration of sensor biases which leads to a superior accuracy from low cost sensors. The implementation described herein is a first generation fleet management system developed

at Pulsesearch Navigation Systems, called NavTrax™.

In Chapter 2, an overview of Land Navigation Requirements is presented. In Chapter 3, the Navigation System Design is given and forms the basis for the remainder of the thesis. Discussed in Chapter 4 are various methods of kinematic modelling, while kinematic GPS processing is treated in Chapter 5 and Dead Reckoning in Chapter 6. Various tests performed on the individual sensors and their results are treated in Chapter 7. Chapter 8 contains an assessment of the navigation system based on various field tests. The thesis concludes with a summary and future recommendations in Chapter 9.

CHAPTER 2

LAND NAVIGATION REQUIREMENTS

In this Chapter, general criteria are first defined for land navigation, and then functional requirements are specified. Two user studies are cited which help define the specific requirements of user groups, that is, the works of Thompson-Hickling and Pulsesearch. A brief overview of current land navigation systems under development is given in the final section.

2.1 General Requirements

The objectives of managing the mobile operations of a fleet of vehicles are four-fold [McLellan et al., 1992], namely:

- (1) to minimize response time;
- (2) to increase the capacity of goods delivered;
- (3) to improve the service to the customer in the form of information on where the response vehicle is at any given moment; and
- (4) to maximize the use of resources (vehicles and personnel) available.

This multifaceted objective can be met, if and only if, the most appropriate resource(s) can be selected. The correct selection is only possible if one has total knowledge and control over all resources. This means that the realtime location and status of all vehicles must be known.

Realtime positions (coordinates) of the vehicles must be continuously computed at all times, as these coordinates are used as pointers into the road network data base to obtain locations (addresses) and road related information. The velocity vector for each vehicle

needs to be computed, yielding speed and heading, which is used to deduce whether the vehicle is stationary or moving, and the direction it is travelling. Accurate positioning of the vehicle helps determine whether the vehicle is on a freeway, on a parallel service road, or in a cul-de-sac. All of these quantities contribute to the automatic status determination of each vehicle, hence, putting the fleet under full control.

There are four main components of a fleet management system (Figure 2.1), namely [McLellan et al., 1991a]:

- (1) navigation;
- (2) SCADA (system control and data acquisition);
- (3) communication; and
- (4) information modelling and decision making.

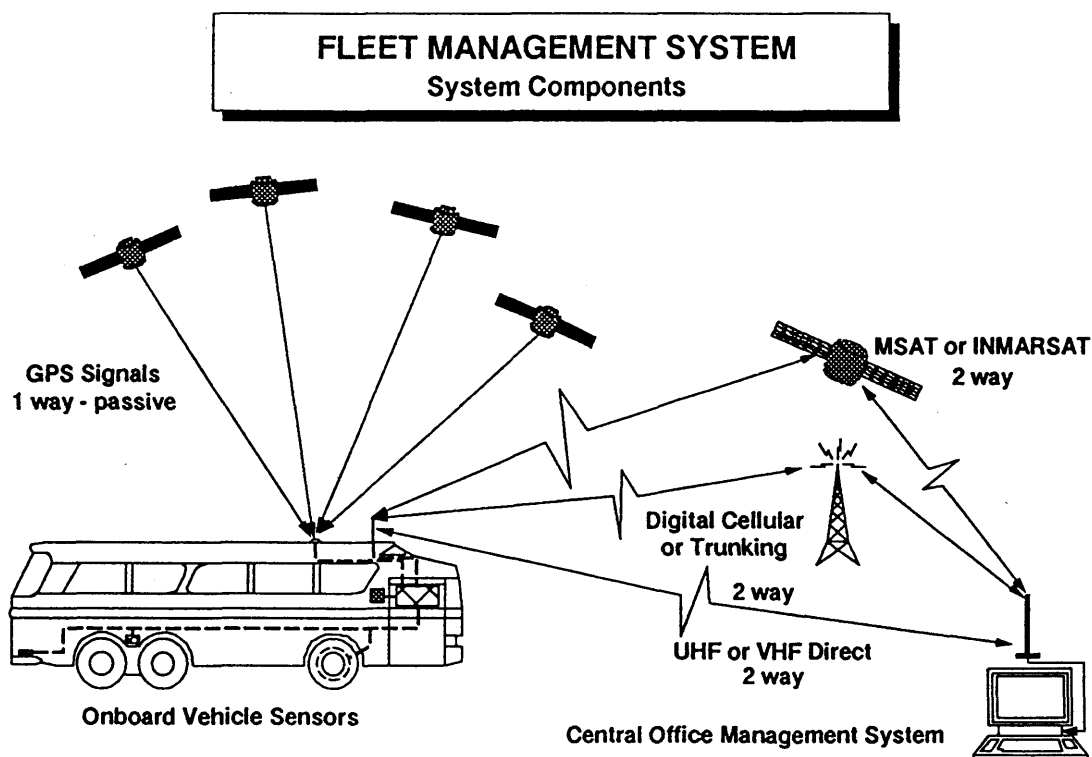


Figure 2.1. (McLellan et al., 1991b)

SCADA, reporting on vehicle related information such as engine health, oil and tire pressure, etc., and information modelling are beyond the scope of this dissertation. Various methods of communications for fleet management operations include cellular, very high frequency (VHF) and ultra high frequency (UHF) private mobile radio, trunking (800 to 900 Mhz) and satellite.

A critical factor in the success of an integrated navigation module is that it must be relatively low cost. This means that expensive navigation hardware must be avoided in preference of innovative mathematical models and filter designs [McLellan et al., 1992]. It must, however, be very reliable, self starting, fault tolerant and robust.

In fleet management applications there are several questions which a successful system must be capable of responding to, and they are as follows [McLellan et al., 1989]:

- (1) Where am I? (Driver);
- (2) Where am I going? (Driver);
- (3) Where are you? (Dispatcher); and
- (4) Who should go? (Dispatcher).

The importance of these questions depends upon the application for which the fleet management system is servicing. In Section 2.4 some results from a market study which looked at both urban and major highway classifications are given.

Krakiwsky et al., [1987] state that an AVLN system allows a land based user to:

- (1) position a vehicle using GPS and on-board dead reckoning sensors;
- (2) display the position on a computer screen;
- (3) access a single line road digital network and relate the position to a location; and
- (4) obtain directions (visual and audio) using an expert system on how to proceed from one location to another.

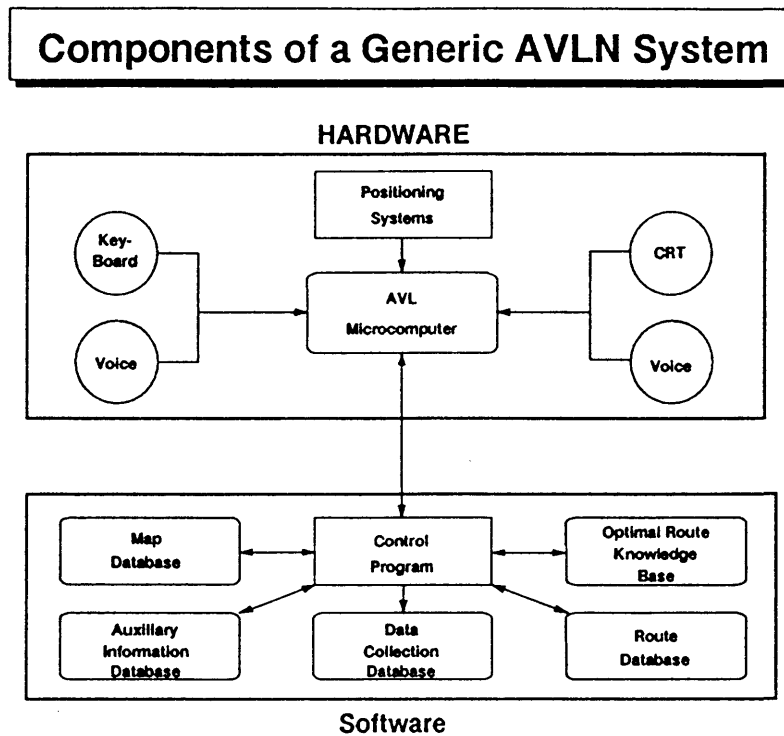


Figure 2.2 (after Krakiwsky [1991])

In Figure 2.2, a break-down of the above requirements into the main hardware and software components is given. These two components are treated as the two main elements of an AVLN system. Many systems, such as those with position reporting only capabilities, will have only a subset of the components shown therein.

A navigation system with positioning sensors coupled with a communications system to a central dispatch centre can answer questions (3) and (4) posed above. To gain general acceptance, the positioning system in the vehicle has to remain transparent to the driver most of the time. Many of the systems which are based solely on differential odometers and map matching, using an on-board data base of the street network, will require manual updating by the driver, especially in rural areas. The use of GPS as a primary positioning

sensor will enable the vehicle's position to be determined **anywhere** and **anytime** with no operator intervention. Map matching involves using the vectors contained in the road network to update heading and position.

For some applications, single point GPS positioning methodology integrated with dead reckoning sensors will yield an acceptable accuracy of 30 to 100 m assuming that selective availability is turned on. There are a number of applications, however, that are increasingly demanding a 5 to 30 m accuracy. This higher accuracy is due to several reasons; first, in navigating to an exact address, the average lot width is about 15 m, thus the requirement is set at plus or minus one lot; secondly, a vehicle which appears to be on a parallel collector road rather than a freeway will not be tolerated, especially for emergency response vehicles. This can be solved either by adding map matching algorithms coupled with reliable and accurate maps to the navigation solution, or by improving the accuracy the GPS pseudoranges. The pseudoranges can be improved by employing differential GPS (DGPS) technology, which would require the broadcasting of differential GPS range corrections that can be picked up by AVLN systems. Traffic information is also required for best route determination and route guidance.

The AVLN system must be self starting such that no user initialization is required. Operator intervention should, however, be built in as option for sophisticated users. It must yield continuous positions automatically, self calibrate sensor biases, and be robust in that temporary sensor failure should not lead to lost situations. Consumers will not tolerate systems that are neither robust nor user friendly.

2.2 Functional Requirements

Navigation related requirements are understood to be composed of the following functions [McLellan et al., 1989]:

- (1) positioning (determination of the coordinates of the mobile vehicle);

- (2) location (relation of coordinates to a single line road network);
- (3) allocation (dispatching of the most appropriate vehicle, based on, for example, distance, travel time, and status, to do the job);
- (4) route determination (selection of the best route to be taken based upon a certain set of criteria); and
- (5) guidance (issuance of route guidance instructions on how to proceed along the best route chosen).

The position (coordinates) of fleet vehicles are communicated to the dispatch centre for a variety of reasons including allocation, fleet monitoring and safety.

2.3 User Requirements by Thompson - Hickling

The importance of the above five mentioned functions have been determined through a user survey performed in Canada by Thompson - Hickling [1989] for a selected set of fleet operations ranging from urban transit operations, to ambulance services, and commercial trucking operations (Table 2.1). The contemplated benefits that would accrue from improved navigation are listed along with reporting time intervals and accuracy requirements.

2.4 Pulsesearch Market Study

Pulsesearch also performed extensive market surveys and analyses in Western Canada [McLellan et al., 1989] and have confirmed the above results. These results have been further confirmed through beta site testing of a fleet management system (Calgary Police Department and Amoco Resources) and detailed discussions with prospective users of the system. Allocation of vehicles and route guidance appears to be a more critical problem in areas of intense traffic congestion such as Los Angeles, while in medium sized cities the problem still remains, but only at a moderate level.

**Table 2.1: Vehicle Navigation User Requirements
(after Thompson-Hickling [1989]; Krakiwsky et al [1990])**

APPLICATION	VEHICLE TYPE	ACCURACY 2D-95% (m)	REPORT RATE (min)	PURPOSE AND EXPECTED BENEFITS
Urban Transit	Buses	15-65	<1	To keep buses on schedule.
Taxi	Taxis	65-200	<1	More efficient dispatching.
Inter-city Bus	Buses RVs	65-200	N/Av	Scheduling User Connections.
Rail	Trains Rail cars	Which track; Location	1-15	Better monitoring of tracks & trains.
Utilities	Trucks & Off road	15-65	1-5	Faster response to emergencies & repairs.
Ambulance	Ambulances	10-20	<1	Faster response to emergencies. Better use of available vehicles.
Police	Cars	10 - 20	1-10	Better response time. Improved fleet management. Safety of officers.
Fire	Cars Trucks	10-20	Continuous	Realtime locations for monitoring & dispatching.
Canada Post	Trucks Cars	200+	1-15	Ability to monitor more closely operations of contract couriers (eventually re-route).
Correctional Services	Parolees Cars	16-65	1-15	Monitor progress of prisoner transfer. Check on parolee's locations.
Local Gov't	Cars Trucks	65 to 200	1-15	Better service to public.
Courier Service	Couriers	N/Av	1-15	En route communication to increase delivery efficiency.
Commercial Trucking	Large & small trucks	65-200	16-30	Better loading & faster delivery.

Discussions with police, ambulance and fire departments have shown that realtime positioning-location is needed by the dispatcher to an accuracy of 10 to 30m, thus, necessitating the use of differential GPS technology (DGPS). The reason given for this stringent requirement is that there can be no ambiguity as to what street, and in which direction the vehicle is heading. Examples of problem areas giving rise to possible ambiguities are downtown alleys, wharf and pier areas, and service roads paralleling freeways. Not being able to correctly locate the vehicle could lead to a serious dispatching error, causing loss of life and property.

In the fire protection environment, the average travel time to an incident is about four to seven minutes. The realtime location of the mobile equipment is required at the dispatch centre so that it is known exactly when the hoses and personnel are dropped off at specific hydrants and when the vehicle has reached its 911 destination call. If problems are encountered, then additional equipment must be immediately dispatched. In areas of heavy traffic congestion, it must be discerned whether the vehicle is only slowly approaching the incident, or indeed, if it has already arrived; this determination is only possible with an accurate positioning system. In departments working within areas where there is little expansion in the road network, such as with many of the cities in the Los Angeles area, the drivers tend to know the best route to the incident.

In areas, however, where urban sprawl is prevalent and new roads are being added quickly to the network, route guidance can be an invaluable tool. In some cities, such as Calgary, it is intended that the new roads be added to the network at the stage when the subdivision plan is submitted for approval, thereby resulting in automatic updating and a current network.

Clearly, from the above stated requirements, continuous and accurate positioning is required for selected major user sectors. Given that there will be blockage of the GPS signal

in "urban canyons", tree covered areas, and in tunnels, it will be necessary to augment GPS with other sensors such as those of the dead reckoning (DR) variety. The integration of GPS and DR technologies is discussed in greater detail in the following Chapters.

When selecting a primary navigation system, Loran C (LC) must be considered as well as GPS. Critical factors which must be considered are price, accuracy, size, robustness, coverage and availability. The best land accuracy that can be achieved with LC is 50 to 100 m with enroute calibration [Lachapelle et al., 1989; Lachapelle and Townsend, 1990; 1991]. Accuracies of 8 to 20 m have been obtained in marine applications such as harbour entries [Viehweg et al., 1988], but can not typically be attained on land due to ground conductivity variations and spatial weather variation effects [Lilley and Edwards, 1986].

There are large parts of the world that are not covered by Loran C (in Canada, most notably northern Alberta, Saskatchewan and Manitoba). GPS has the added advantage (over Loran C) of being universal and thus is capable of operating worldwide, which is critical in so far as a manufacturing decision is concerned. It can be argued that GPS is not currently available 24 hours per day worldwide, however, there are plans to do so by the end of January 1993.

Loran C is being accepted more readily by the aviation industry due to concerns of integrity and government policy concerning signal availability and selective availability (S/A) of GPS. This may not be the case, however, as time goes on.

Previous arguments for choosing Loran C over GPS was often due to price differential. However, a number of manufacturers such as Magnavox, Rockwell, JRC and Magellan are producing GPS board sets which are very price competitive (\$450 to \$1,000). For the above reasons, GPS has been chosen over LC for the primary absolute positioning sensor.

One remaining closing point is the matter of user friendliness and robustness. It is deemed that GPS based systems are superior to pure terrestrial, dead reckoning based

systems, mainly because the latter require intense initialization via address inputs by the user. This shortcoming, coupled with the necessity to have sophisticated and complete map data bases with highly reliable addressing and geocoding, also contributed to the decision to choose GPS over terrestrial sensors as the primary positioning device [Krakiwsky, 1991].

2.5 The Market

The fleet management market characteristics and size in Canada and the United States has been analyzed by McLellan et al. [1989] and consisted of the following steps:

- (1) Literature search to identify existing systems, their capabilities and users;
- (2) Accurate estimation of potential market size for Dispatch AVLN Systems through the use of a questionnaire;
- (3) Preparation of presentation (slide shows and vehicle demonstrations) for potential customers;
- (4) Meetings with potential customers to analyze their needs and price sensitivity;
- (5) Analyze methods of creating data bases and determine content and structure as well as methods of maintenance;
- (6) Analysis of various methods for communication between dispatch and mobile vehicles; and
- (7) Targeting several customers who have high potential for system purchase and who also have similar requirements.

The market study initially done by Pulsesearch included personal and telephone interviews with companies and organizations in Calgary, Edmonton, Regina, Winnipeg and Toronto. Numbers shown in the following tables were based on information gathered in Western Canada and only include the number of vehicles that were thought to be potential users of the system at the time when the survey was conducted. Numbers shown for eastern and central Canada were based on population provided by Statistics Canada using a pro-

portional number of vehicles compared to Western Canada. The estimates provided in these tables are considered conservative and are expected to increase rapidly as systems become available and users see the benefits.

Since the initial survey, additional research and analysis was done in Vancouver and Los Angeles. The response to system requirements became somewhat more demanding as the people subsequently interviewed were increasingly computer literate and management of mobile resources also became a higher priority. The explosion in computer technology has also changed peoples expectations. Fleet management systems with navigation capabilities have also been installed in several major U.S. cities which has raised public awareness.

Shown in Table 2.2 is the estimated Dispatch AVLN market size for highway transport in Canada, while Table 2.3 contains data for off highway type vehicles (e.g., utility fleets), and Table 2.4 are urban statistics. Road Tractors are defined as vehicles where the truck and trailer are two separate units. Straight trucks include vehicles where the truck and trailer are a single unit.

Table 2.2 Total Number of Highway Vehicles in Canada
(after McLellan et al. [1989])

Classification	Western ²	Central ^{1,3}	Eastern ^{1,3}	Total
Straight Trucks	62,090	75,565	9,773	147,428
Road Tractors	14,438	29,268	2,620	46,326
Total	76,528	104,833	12,393	193,754

Sources:

1. Statistics Canada 1986
2. Pulsesearch Western Canada Survey
3. Extrapolation of Pulsesearch Survey

The Urban category includes primarily Trucks, Cars and Vans. Vehicles in this category can be divided into Public Service, Commercial and Utilities, as shown in Table 2.3. This table is an estimate for the urban category of vehicles in Canada.

**Table 2.3 Total Number of Urban Vehicles in Canada
(after McLellan et al. [1989])**

Classification	Western ²	Central ^{1,3}	Eastern ^{1,3}	Total
Police	1,462	2,135	307	3,904
Fire	486	710	102	1,298
Ambulance	137	200	29	366
Utilities				
-Gas	550	803	116	1,469
-Hydro	195	285	41	521
-Telephone	145	212	30	387
-Streets	550	803	116	1,469
-Water	145	212	30	387
-Sewer	116	169	24	310
Urban Commercial				
-Security	110	161	23	294
-Waste	415	606	87	1,108
-Concrete	600	876	126	1,602
-Construction	2,700	3,942	567	7,209
Total	7,611	11,112	1,598	20,321

The off-highway category includes average cost Straight Trucks and Road Tractors. Vehicles in this category are primarily hauling less than truck loads between inter-city destinations as well as secondary roads and rural destinations. Shown in Table 2.4 is an estimate for this category of vehicles in Canada.

Table 2.4 Total Number of Off-Highway Vehicles in Canada
(after McLellan et al. [1989])

Classification	Western ²	Central ^{1,3}	Eastern ^{1,3}	Total
Straight Trucks	2,007	3,779	588	6,374
Road Tractors	1,593	1,930	539	4,062
Total	3,600	5,709	1,027	10,336

Sources:

1. Statistics Canada 1986
2. Pulsesearch Western Canada Survey
3. Extrapolation of Pulsesearch Survey

User needs in the major highway and urban sectors of the market are examined from both the drivers and dispatchers' points of view. These results are shown in Figures 2.3 and 2.4. It is clear that navigation related information is required for both the driver and dispatcher.

An analysis of the results has shown that the requirements for the major highway classification are mainly for operational information at the dispatch centre. The urban classification requires information both at the dispatch centre and in the vehicle. Many trucking companies interview indicated that they did not want the drivers viewing screens as they were driving.

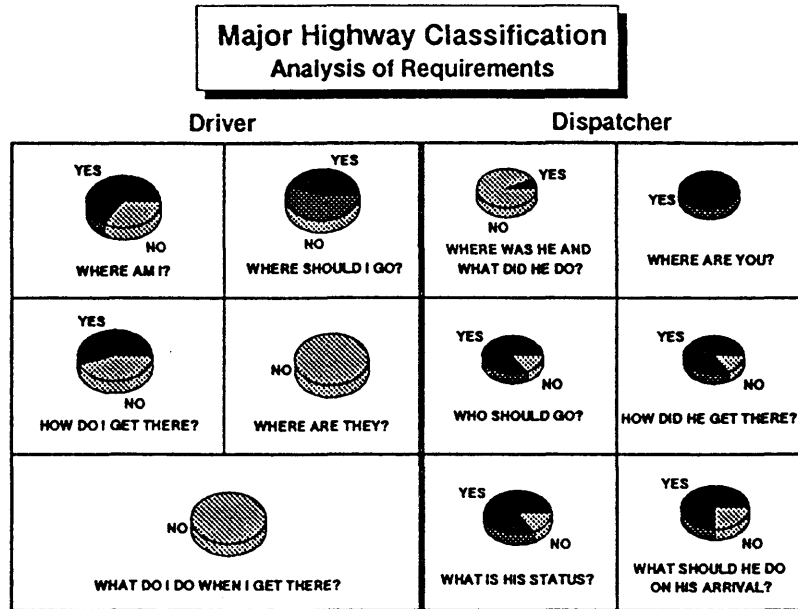


Figure 2.3 (after McLellan et al. [1989])

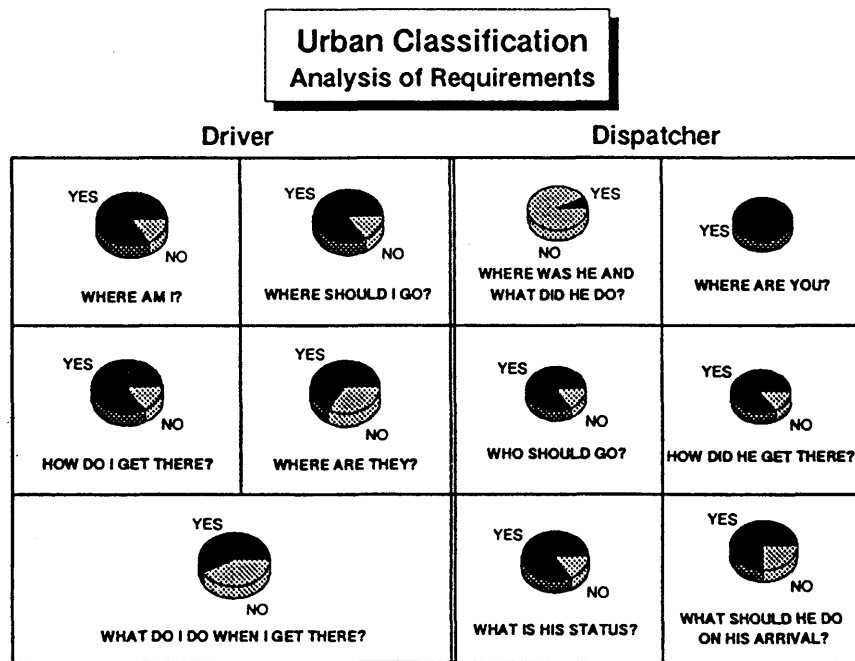


Figure 2.4 (after McLellan et al. [1989])

2.6 Vehicle Navigation Systems

The development of the first AVLN systems occurred in the U.S.A. with the Automatic Remote Control System (ARCS) for the delivery of newspapers [French 1974]. The Fleet Location and Information Reporting System (FLAIR[™]) for the tracking of police vehicles in St. Louis was developed by Boeing in 1977. Shortly after FLAIR, GEC-Marconi, in 1978, developed the LANDFALL (Links and Nodes Data Base for Automatic Land Vehicle Location) system for the tracking of police vehicles in London, U.K.

A second wave of development in the 80's comprised the following list of systems that are terrestrially based, that is, they do not use satellite positioning technology:

- (1) Etak Navigator[™] [1985] in the USA by Honey and Zavoli;
 - (2) the AUTOGUIDE [1986] system in the UK by the Dept. of Transportation;
 - (3) The ALI-SCOUT [1986] system in Germany by Siemens;
 - (4) the CARIN [1987; Car Information and Navigation System] in Holland by Phillips;
 - (5) the Clarion Etak [1988] in Japan;
 - (6) the MARIA [1988] system in Japan by Mitsubishi Corp;
 - (7) the NAVICO [1988] system in Japan by Navigation and Comm. Co. and Sumitomo Electric;
 - (8) NISSAN System [1988] in Japan by Nissan, Hitachi, Kanto, and Deiki Co.;
 - (9) SANYO System [1988] in Japan by Sanyo Electric Co.;
 - (10) SONY System [1988] in Japan by Sony Corp.;
 - (11) TOYOTA System [1988] in Japan by Toyota Corp.;
 - (12) the Travepilot [1989], upscaled Etak Navigator[™] in Europe and USA by Bosch;
- and

(13) NAVMATE System [1990] in Japan and USA by ZEXEL Corp.

The above list is not exhaustive and notably excluded are AVLN systems that are terrestrial RF (e.g., Decca, Omega, Loran C) based.

Satellite based systems have been identified by Krakiwsky [1991] and are listed in Table 2.5. This class of AVLN systems is under development mainly in Japan and the U.S.A., with Canada demonstrating a strong showing. Activity in Europe in the GPS satellite domain is beginning to pick up commencing with the 1989-90 time period.

All of the AVLN systems listed above have a system design approximated by the generic system shown in Figure 2.2. There are both hardware and software components of these systems. The digital map data base is seen to be clearly a part of the software segment and plays the key role in the location world of relating mathematical coordinates of the vehicles' position to the real world.

The remainder of this dissertation is devoted to detailing the NavTraxTM system listed in Table 2.5. This system is believed to be superior over some of the other systems listed, due to the capability to continuously calibrate sensor biases and for fault detection, identification and recovery (FDIR). This ability makes the system more robust and will require little, if no user re-initialization.

Table 2.5 Some GPS Based AVLN Systems (after Krakiwsky, [1991])

Country	Date of Entry	Name of System	Originator/ Co/Company	1	2	3	4
Japan	1983	DRIVE GUIDE	Nissan Co.	x			
	1983	MAZDA SATNAV	Mazda Co.	x			
	1985	MMC SATNAV	MMC Co.	x			
	1985	SUZUKI NAV	Suzuki Co.	x			
	1985	TOYOTA FX-V	Toyota Corp.	x			
	1986	TELECOM VAN	Mazda Co.		x		
	1987	MADIX-III	Nippondenso Co.	x			
	1989	MAZDA SCNS	Mazda Co.	x		x	
	Unknown	NISSAN GPS NAV	Nissan Co.	x	x		
	USA	1983	CLASS	Chrysler Corp.	x		x
1984		NAV TEST CAR	General Motors Corp.	x		x	
1990		NAV-COM AVLS	Nav-Com Inc.		x		x
1990		TRIMBLE AVLS	Trimble Navigation Ltd.	x	x		x
Canada		1988	AVLN 2000	Univ. Of Calgary			
	1989	ALTA INV SYSTEM	Alberta Transportation- /Univ. of Calgary				x
	1990	NavTrax	Pulsesearch Navigation Systems, SaskTel Mobile Communications	x	x		x
	1992	NavARC	Pulsesearch Navigation Systems	x			x
Germany	1989	LOCATION SYSTEMS	Nukem GmbH				
	1989	VELOC	AEG Marinetechnik		x		
U.K.	1990	NAVSTAR IVN	Navstar		x		

- 1 Autonomous
- 2 Dispatch
- 3 Route Information (Guidance)
- 4 Inventory with differential GPS to improve accuracy

CHAPTER 3

NAVIGATION SYSTEM DESIGN

An overview of the NavTraxTM system design is given in Section 3.1. In Section 3.2, the System design is given along with a detailed description of each sensor and its function. An introduction to the role of federated filtering is given in Section 3.3. Details on implementation and testing are given in subsequent Chapters.

3.1 System Overview

A fleet management system has three main subsystems (Figure 3.1), namely:

- (1) the in-vehicle subsystem;
- (2) the communications subsystem; and
- (3) the dispatch centre subsystem.

The optimal integration of these three components is the key to developing a successful fleet management product.

The in-vehicle subsystem consists of hardware and software components and performs specific functions as follows [McLellan et al., 1992]:

- (1) navigation and location computation;
- (2) status determination and reporting to dispatch office; and
- (3) receipt of messages from central dispatch.

Typical hardware components consist of a GPS receiver and an array of dead reckoning sensors for navigation and a selectable communication system. Possible communication systems could include UHF/VHF private radio systems, 800 to 900 Mhz trunking, cellular telephone or satellite. In most large metropolitan areas in North America it is often difficult

to secure additional radio spectrum for private mobile radio systems. Trunking systems are being installed to provide wide area coverage to multiple users. A UHF private radio system was used for system trials using an experimental frequency provided by the Department of Communications (DOC).

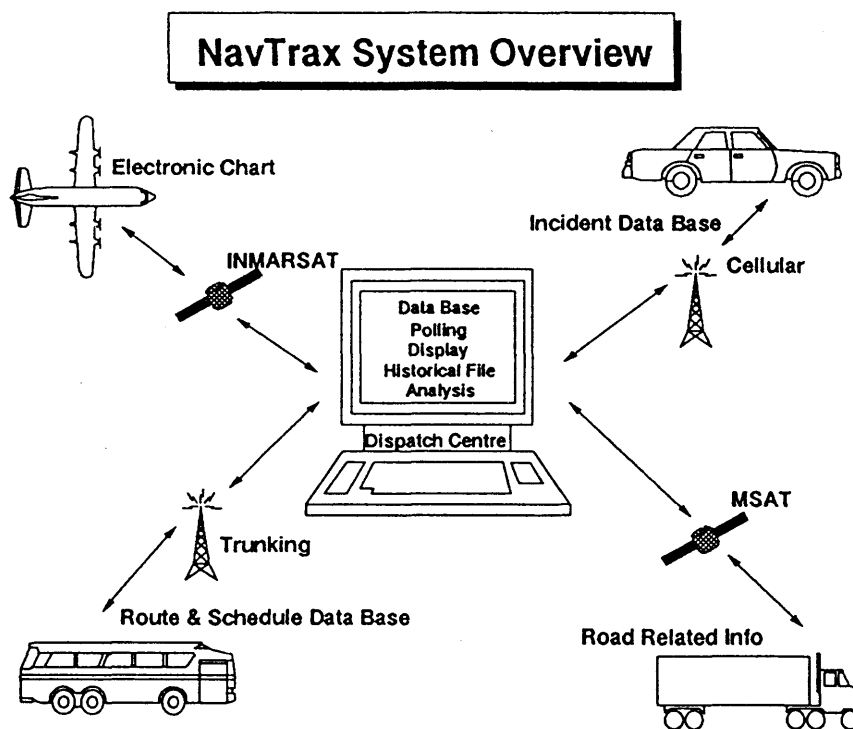


Figure 3.1. (after McLellan et al. [1992])

3.2 System Design

The design of the overall system is modular and decentralized. In-vehicle computations are extensive with only results (location and status) being reported to the dispatch centre. This minimizes the amount of data that needs to be communicated.

The onboard positioning sensors selected are GPS, odometer, fluxgate compass and rate gyro. These components are suitable for most applications and will be able to operate anywhere in the world. An altimeter is optionally included in some applications requiring continuous height, such as seismic operations.

The major processing modules for the positioning system are shown in Figure 3.2. The primary positioning sensor is the GPS system. In order to solve for position using GPS, a minimum of three satellites (with known height) must be tracked simultaneously with suitable geometry.

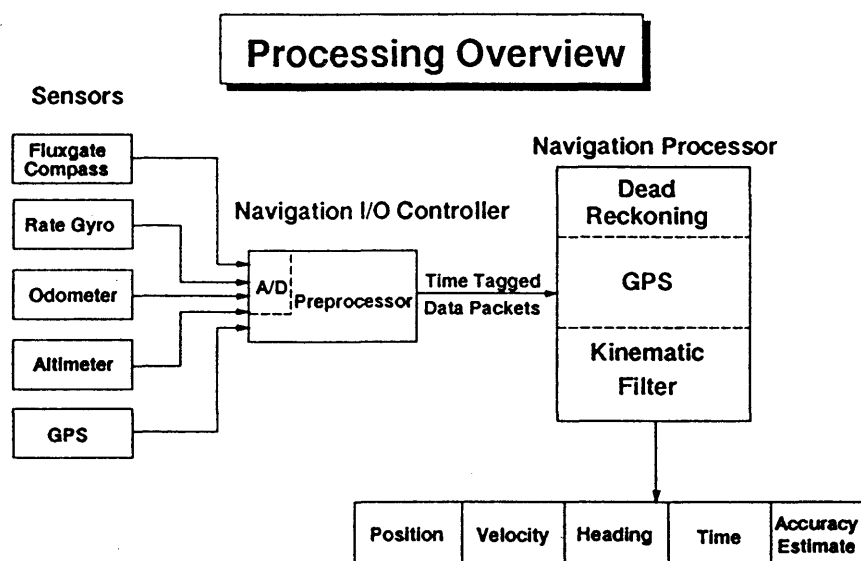


Figure 3.2 (after McLellan et al. [1989])

Sensor information is collected, time tagged and pre-processed with a special purpose Navigation I/O controller board utilizing an Intel 196 processor chip, while navigation computations are performed by an Intel 386 CPU. Software modules consist of sensor pre-processing, position computation, status determination and location reporting.

The Navigation I/O controller board (Figure 3.3) controls all the data I/O and pre-processes raw input sensor data. There are four serial ports which can be configured as all

RS 422 or 2-RS422 and 2-RS232. An 8 channel 14 bit A/D converter and 3 - 8 bit parallel ports are also on the board. The board is built with 32 K of Non-volatile RAM and 24 K of ROM. Also, a 16 key, keypad can be accommodated. Input power can range from 8-24 VDC.

The navigation module is the heart of the in-vehicle subsystem and it is therein that the realtime position (coordinates) are continuously computed (Figure 3.4). The general navigation equations for both cartesian and geodetic coordinate frames are given in Appendix B. It is these navigation equations which help define the transition matrices and are used for position prediction. The navigation sensors used are the following [McLellan et al., 1991a]:

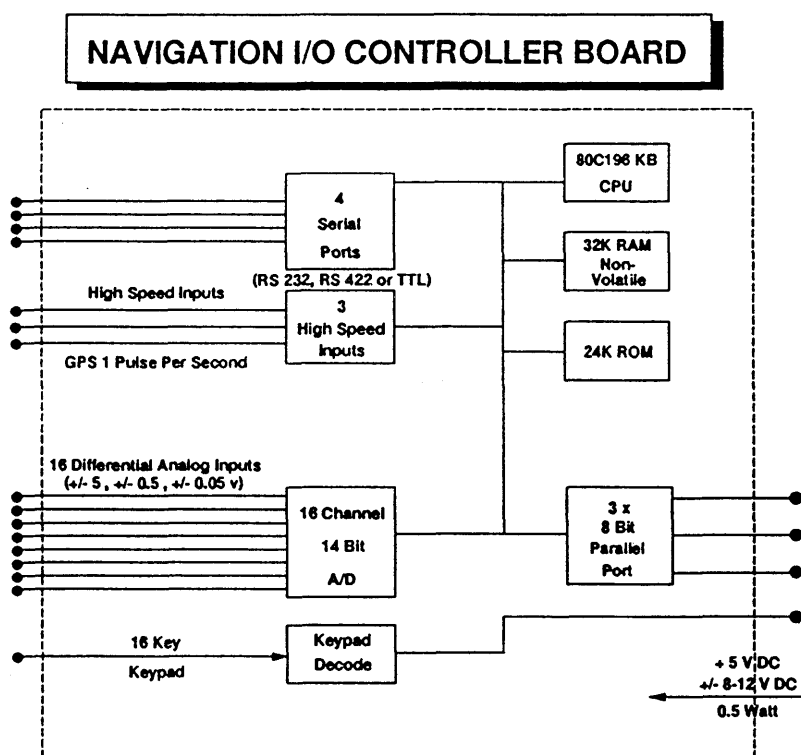


Figure 3.3

- (1) GPS pseudo range and carrier phase for position and velocity;
- (2) rate gyro for azimuth change;
- (3) compass for azimuth; and
- (4) odometer for speed.

A general overview of the filter techniques are given below. Detailed information is given in Chapters 4, 5 and 6, where the implementation is made.

A very important characteristic of the positioning filter is the use of a decentralized - federated filter [Carlson 1987, 1988a]. Each sensor has its own filter: the reference filter is GPS based, while each dead reckoning sensor has its own local filter for determination of biases and in which fault detection is made. The reference filter and all local filters feed into the master filter where fusion of all information is made. The master filter then feeds back into the reference filter and local filters on the basis of an information sharing principle where total information is conserved (Figure 3.4). More details are given in Figure 3.5.

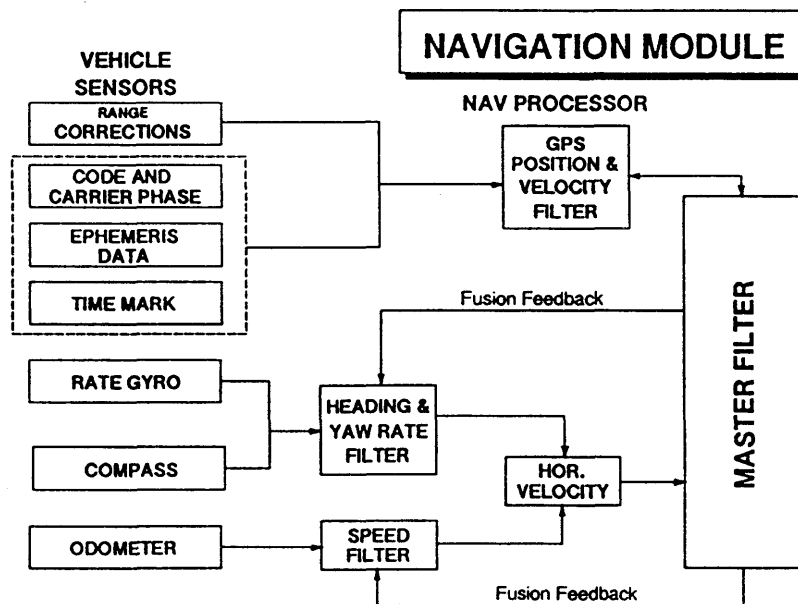


Figure 3.4

The fusion feed back from the master filter to each local filter allows for frequent and automatic calibration of each sensor separately. In this manner, outliers, blunders and spurious data in each sensor can be eliminated and re-calibration can take place. Only clean data moves from each local filter into the master (fusion) filter. Thus it can be stated that the filter is a robust - fault tolerant filter where faults are detected and identified, and the system can recover before lost situations arise. It should be noted that this is the first attempt at implementing this type of filter. Subsequent testing and determination of fusion values will be required for optimizing this federated configuration.

The time mark shown in Figure 3.4 goes from the GPS sensor to the I/O controller board. A system interrupt is generated when this pulse is received (Figure 3.3 - GPS 1 Pulse Per Second). The system clock is corrected continuously by counting the clock ticks and scaling them accordingly. If the GPS sensor has a time recovery option, and it is turned on, the GPS sensor time is continuously corrected to GPS time via the Kalman filter values. The time mark is typically accurate to 100 to 200 nanoseconds depending upon selective availability.

All dead reckoning sensor observations are then time stamped with GPS time before they are passed onto the navigation processor. This is critical as the raw data from the GPS receiver is one to two seconds old by the time it is passed onto the navigation processor. The information from the dead reckoning sensors is captured at a higher rate and with a much smaller delay.

The master filter has a common set of state vector elements, namely, three positions and three velocities. All the local filters possess state vector elements which are a subset of these in addition to their own internal bias states. Also computed in the master filter is the covariance matrix of the state vector which gives information on the quality of the solution. When poor satellite geometry or lack of sufficient dead reckoning sensor data is

available, this weakness is reflected in the resultant covariance matrix for the state vector. In this way, one can ascertain how much trust should be placed on the position (coordinates) of the vehicle. This confidence region can then be translated into an ambiguity window in determining the location of the vehicle. In other words, if more than one intersection or road (link) appears within the confidence window, then there is an ambiguous location determination; otherwise a unique location of the vehicle has been defined.

The NavTrax™ System is designed primarily for after market custom installation into a variety of vehicles ranging from aircraft to land vehicles [McLellan et al., 1991a; McLellan et al., 1992]. The requirement to fulfill the needs of a variety of users dictated that the system architecture be capable of integrating a number of diverse sensors. A comprehensive evaluation of various types of dead reckoning and GPS sensors was performed. The objective was to use sensors which were low cost, easy to install and would give adequate performance. The investigation resulted in the optimal combination of flux gate compass, rate gyro and transmission odometer. An altimeter is included on aircraft installations and on land applications, such as 3D seismic surveys, where height is essential. A modular approach to system architecture in both hardware and software was selected to facilitate production and to meet various customer applications and accuracy requirements.

GPS is thus integrated with a flux gate compass (azimuth), rate gyro (yaw rate), and odometers (speed). Odometers are of the transmission variety and output distance travelled over time which is converted to speed. The data from the selected sensors are combined via a family of kinematic filters with output being position, velocity, heading, time and an accuracy estimate for these states.

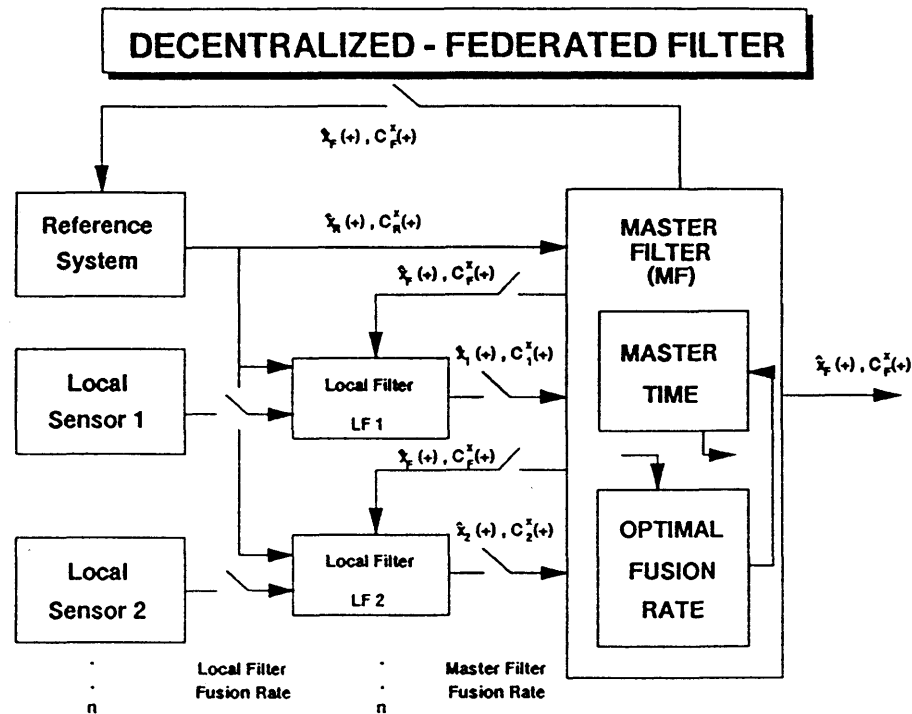


Figure 3.5

The kinematic filter used in NavTrax™ is a decentralized - federated filter (Figure 3.5). GPS is chosen as the reference filter because its model has the most extensive state vector of position and velocity. Each sensor has its own local filter with its states being a subset of the reference filter.

The compass tends to be very sensitive to external magnetic field disturbances such as bridges, railway tracks and overpasses. Spurious readings as large as 180° are often encountered. Tests have shown the presence of large errors due to the operation of power windows and air conditioning [McLellan et al., 1992]. The vertical magnetic field in Calgary is about three times stronger than the horizontal field, thus, the inclination of the sensor has a large effect on the heading determination (eg., 1° tilt causes 2° heading error). Attempts were made to measure the pitch and roll and compensate for these errors, however, the greatest degree of pitch and roll tended to occur on sharp turns and caused large acceleration

values to be present on the pitch and roll readings. Empirical testing has led to using a standard error of about 5° for this sensor. If it were not for the above external effects, a value of about three to four degrees could be used which reflects the sensor noise level.

The rate gyro used proved to be very sensitive to temperature fluctuations. This can be a serious problem in Canada, where in the winter variations of 40° C are encountered when driving in and out of parking garages. Testing has also shown that vibrations can affect readings as well. In some cases up to 10° per minute of heading error have accumulated. Typically errors of 1° - 2° are encountered. The drift is generally linear. The rate gyro overall is quite responsive to heading changes.

The compass and rate gyro are combined into a heading filter which exploits the absolute heading determination, though noisy, with the relative yaw rate of the rate gyro which drifts over time. The filter solves for heading and yaw rate as well as calibration parameters. The filter is periodically updated using the GPS derived heading and from map matching when available.

Wheel mounted odometers were initially tested, which allows for change in azimuth determination as well as distance travelled. The combination of fluxgate headings and differential odometer heading rate changes produced adequate results. From discussions with various users groups, however, it was learned that they are regarded as an inconvenience from the installation and maintenance points of view. Maintenance is especially difficult in vehicles that are often in off road conditions. On the other hand, transmission odometers are concealed and installed in the transmission where the speed odometer cable is connected. Errors sources are primarily due to wheel slippage and changes in wheel circumference due to tire pressure and velocity changes. Bias ply tires, often encountered on trucks, can see error growth up to several per cent of the distance travelled due to circumference change, while radial tires, however, are affected only minimally in this regard.

A six channel C/A code GPS receiver from Magnavox was selected as being optimum in terms of price and capabilities. The improvement in accuracy of a six channel versus four channel receiver was considerable. The continuous tracking on dedicated channels is very critical when operating in urban canyons and tree covered areas; an improvement is also seen in re-acquisition time and continuous tracking capabilities with six channel receivers. This receiver also measures carrier phase which is used to smooth the noisy code measurements. The carrier phase measurements are numerically differentiated over time to yield phase rates which yields a solution for the three velocity components. The receiver also outputs raw data which is required in some applications.

3.3 The NavTrax™ Filter

A decentralized filter (Figure 3.5) was chosen to prevent a fault in any local sensor from contaminating other sensors and thus the solution (see Chapter 4).

The combination of the individual (partial results) from each local filter is accomplished in a fusion algorithm in the master filter. The master filter then returns information to each local filter at which time the fused information is combined with the new sensor data, and, as well, a decision is made whether to re-calibrate the particular sensor (Figure 3.5).

Central to the approach taken is the choice of a kinematic model that describes the motion of the vehicle. A constant velocity model has been selected and it is deemed appropriate given the accuracy required (best: 2 to 5 m) and the GPS data of 1 hz. This kinematic information is shared by the master and local filters according to the conservation of information principle espoused by Carlson [1988b]. In short, the NavTrax™ navigation module can be said to be fault tolerant and robust.

A data flow diagram is given in Figure 3.6 showing the information that is being passed between the various processes. It can be seen from the data flow that the federated filter is a modification of Figure 3.5 in that the states in the local filters are not the same as the master filter and some propagation must take place. One of the objectives of this research is to test this configuration.

The odometer plays a key role in the filtering in that it is assumed that the vehicle is stationary after a short period of time when no pulses are received. This allows both the velocity and heading rates to be set to zero. This is analogous to a zero velocity update in inertial processing. This also key to determining the reference offset of the rate gyro.

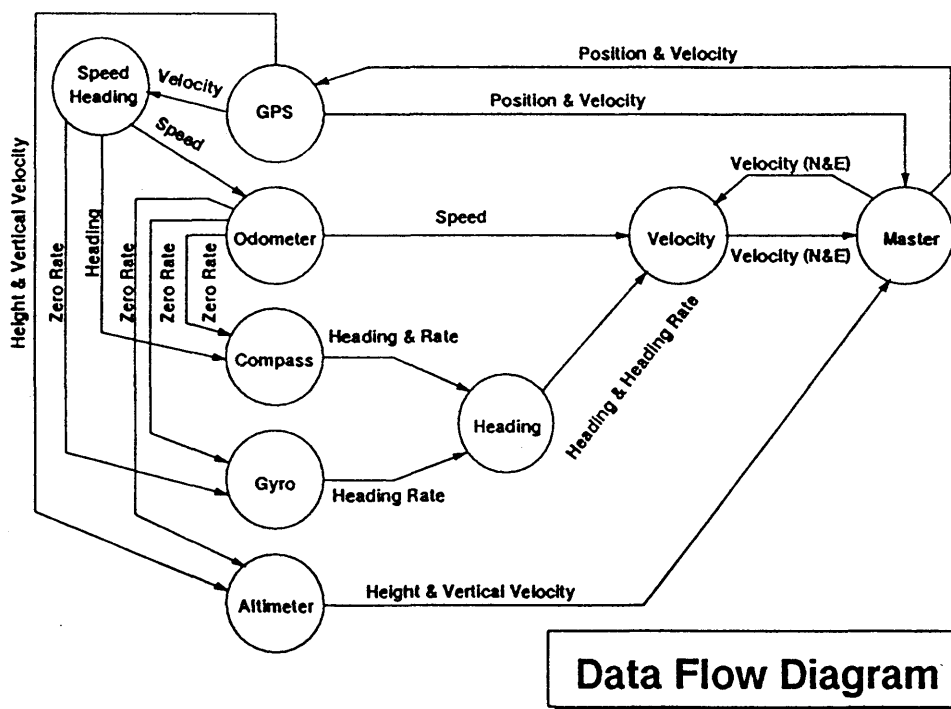


Figure 3.6

At this juncture, the system overview and design has been completed, and the remainder of the thesis will deal with the models of each sensor group, namely, GPS (Chapter 5) and Dead Reckoning (Chapter 6).

CHAPTER 4

FILTERING METHODOLOGY

The standard Kalman and Bayes filtering equations remain the cornerstone of the federated filter to be used, hence, they are listed below for eventual use. It is important to point out at this juncture that the main characteristic of the federated filter is that it is a filter implementation in a decentralized fashion rather than the customary centralized approach where one large Kalman filter is used. Consequently, the federated filter employs several smaller Kalman (or Bayes) filters running in parallel but at different rates. Fundamental to the filtering problem is the description of the kinematics of the vehicle, hence it is treated at the outset.

4.1 Dynamic and Kinematic Modelling

The Kalman [1960] filter equations are rooted in the modeling of a vehicle in three dimensional space [Wong, 1987; Schwarz et al., 1989]. This model is based upon:

- (1) the knowledge of the forces causing the motion (dynamics); or
- (2) the measurement of the vehicle's motion (kinematics).

The latter approach is adopted as this is the reality when dead reckoning or GPS positioning literally traces out the vehicle's trajectory. In equation form, kinematic modelling of a vehicle's position at time t_{k+1} , relative to t_k , is given by the following series expansion:

$$r_{k+1} = r_k + \dot{r}_k \Delta t + \frac{\ddot{r}_k \Delta t^2}{2} + \dots, \quad (4.1)$$

where

$$\mathbf{r}_k = [x_k \ y_k \ z_k]^T \quad (4.2)$$

is the position vector,

$$\dot{\mathbf{r}}_k = [\dot{x}_k \ \dot{y}_k \ \dot{z}_k]^T \quad (4.3)$$

is the velocity vector,

$$\ddot{\mathbf{r}}_k = [\ddot{x}_k \ \ddot{y}_k \ \ddot{z}_k]^T \quad (4.4)$$

is the acceleration vector, and Δt is the small, but, finite time difference along the trajectory.

For the low dynamic and low accuracy applications in vehicle navigation, a constant velocity model can be used, namely ($\ddot{\mathbf{r}}_k = 0$):

$$\mathbf{r}_{k+1} = \mathbf{r}_k + \dot{\mathbf{r}}_k \Delta t, \quad (4.5)$$

where Δt has a value of about 0.10 to 0.25 sec for dead reckoning sensors and 1.0 sec for GPS solutions. Clearly, GPS rates can be higher than the 1.0 sec value when sufficient computer processing power exists and raw data is available at higher rates. Further, recall that in AVLN we are dealing with a low accuracy requirement (a few metres to a few 10's of metres), thereby giving even more credence to the constant velocity model cited above in eqn (4.5). Furthermore, land vehicles moving on a street or highway have minimal acceleration over the above mentioned time interval of 0.1 and 1.0 sec.

Gelb [1974] and Brown [1973] demonstrate how to make use of the measured quantities in a so-called state space model. In this approach, the departures of \mathbf{r} and $\dot{\mathbf{r}}$ from a reference trajectory \mathbf{r}_o and $\dot{\mathbf{r}}_o$ is described by a system of differential equations

$$\dot{\mathbf{x}} = \mathbf{F}\mathbf{x} + \mathbf{G}\mathbf{u}, \quad (4.6)$$

where the departures are modelled by the state vector \mathbf{x} , the system dynamics or kinematics (in this case) are described by the dynamics matrix \mathbf{F} , and $\mathbf{G}\mathbf{u}$ is driving noise

due to the kinematic model imperfections such as accelerations occurring (during Δt) whilst applying the constant velocity model, and lack of continuity (discreteness) resulting from low measurement rates relative to vehicle motion.

The formal mathematical solution of the differential equation (eqn 4.6) is normally combined with the measurements that are made during the kinematic process namely:

$$l = f(x), \quad (4.7)$$

where f is a non-linear model indirectly linking the observables l to the state vector x . The linearized version of eqn (4.7) is used, namely:

$$l+r = Ax, \quad C' \quad (4.8)$$

where r is the measurement residual, C' is the measurement covariance matrix, and the design matrix $A = \partial f/\partial x$ is also known as the Jacobian matrix.

4.2 Kalman Equations

Gelb [1974] derives the solution to the combination of the two eqns (4.6) and (4.8), which is the well known set of Kalman Filter equations. Krakiwsky [1990] also derives these equations from the surveying least squares point of view and compares them to the less known Bayes equations.

The set of equations are in two parts, namely:

- (1) the prediction equations denoted by (-) to signify the absence of the measurements at the current epoch t_k ; and
- (2) the filtering equations denoted by (+) to signify the presence of the measurements at the present epoch t_k .

The time t_{k-1} denotes the epoch immediately in the past at which measurements were made, while the " $\hat{}$ " denotes Kalman estimates.

The Kalman prediction equations are the following:

$$\hat{x}_k(-) = \Phi_{k-1,k} \hat{x}_{k-1}(+) , \quad (4.9)$$

$$C_k^x(-) = \Phi_{k-1,k} C_{k-1}^x(+) \Phi_{k-1,k}^T + C_{k-1,k}^u , \quad (4.10)$$

where C^x is the covariance matrix of the state vector \mathbf{x} , $C_{k-1,k}^u$ is the covariance of the driving noise, while $\Phi_{k-1,k}$ is the transition matrix whose relation to the dynamics matrix F , introduced in eqn (4.6), is described below.

The Kalman filtering update equations are the following:

$$\hat{x}_k(+) = \hat{x}_k(-) + K[l_k - A_k \hat{x}_k(-)] , \quad (4.11)$$

$$C_k^x(+) = [I - KA_k] C_k^x(-) , \quad (4.12)$$

$$K = C_k^x(-) A_k^T [A_k C_k^x(-) A_k^T + C_k^l]^{-1} , \quad (4.13)$$

where K is known as the Kalman gain matrix encapsulating the measurement update.

Transition and Dynamic Matrices

Below is a description of the relationship of the transition matrix Φ to the dynamics matrix F , along with a discussion of the covariance matrix of the kinematic system noise C^u .

If the mean value of the driving noise Gu over Δt is assumed to be zero, and also that F remains constant (assumption correct for constant velocity model), then the solution to the differential eqn (4.6) is given by

$$x(\Delta t) = \Phi(\Delta t, 0) x(0) , \quad (4.14)$$

with the initial conditions $x(0) = \text{constant}$, hence, defining the transition matrix $\Phi_{k-1,k}$.

The transition matrix Φ can be derived numerically or analytically. Assuming F remains constant

$$\Phi_{k-1,k} = e^{F\Delta t}.$$

A truncated Taylor series approach is used to obtain Φ numerically, namely:

$$\Phi_{k-1,k} = I + F\Delta t, \quad (4.15)$$

where $\Delta t = t_k - t_{k-1}$. The transition matrix $\Phi_{k-1,k}$ is also called the total transition matrix when Δt is large (a few seconds) and it is obtained from the following product of individual transition matrices corresponding to n shorter time intervals:

$$\Phi_{k-1,k} = \prod_{i=1}^n \Phi(t_i, t_{i-1}). \quad (4.16)$$

Covariance Matrix Of The System Noise

The covariance matrix, C^u of the system noise, Gu , over Δt is defined by [Carlson, 1988a; Schwarz et al., 1989]

$$C^u(\Delta t) = E[Gu, (Gu)^T]_{k-1,k},$$

but computed from [Schwarz et al., 1989]

$$C^u(\Delta t) = \int_{t=0}^{\Delta t} \Phi Q(\tau) \Phi^T d\tau, \quad (4.17)$$

where Q is the spectral density matrix of the system noise. Gelb [1974], using eqn (4.15), derives the following simplified expression:

$$C^u(\Delta t) = Q\Delta t.$$

The reason behind the use of the integral in eqn (4.17) is due to the fact that the kinematic process is governed by eqn (4.6), namely:

$$\dot{x} = Fx + Gu, \quad (4.18)$$

and that when dealing in the state vector space x (rather than \dot{x}), integration is needed to get the spectral density from \dot{x} space of eqn (4.6) into the x space of eqn (4.9). Hence, when dealing with the implementation of kinematic systems in practise, integration of spectral densities will have to be performed.

4.3 Bayes Filtering Equations

Morrison [1969] has given a set of filtering equations, called Bayes equations, which Krakiwsky [1990] has proven to be mathematically equivalent to the Kalman filtering equations. The difference between the Kalman and Bayes expressions has been analyzed from the computational point of view by Krakiwsky [1990] and clear advantages are shown for each. Also, Carlson [1988a] has also adopted the Bayes type equations for use in the information sharing concept contained in his decentralized federated filter approach. Using the proofs in Krakiwsky [1990], a mathematical basis for the Bayes equations used in Carlson [1988a] is given.

The Bayes equations in the Krakiwsky [1990] notation are given immediately below. The prediction equations are the following:

- (1) the prediction of the state vector

$$\hat{x}_k(-) = \Phi_{k-1,k} \hat{x}_{k-1}(+) \quad , \quad (4.19)$$

- (2) the corresponding predicted covariance matrix

$$C_k^x(-) = \Phi_{k-1,k} C_{k-1}^x(+) \Phi_{k-1,k}^T + C_{k-1,k}^u \quad , \quad (4.20)$$

where all matrices have been defined earlier within the context of the Kalman equations. Note that these prediction equations are identical to the Kalman expressions given by eqns (4.9) and (4.10).

The covariance matrix for the filtered state vector is

$$C_k^x(+)=\left\{[C_{k-1}^x(-)]^{-1}+A_k^T C_k^l A_k\right\}^{-1}, \quad (4.21)$$

where it is noted that the structure is of the "summation of the normal equations" form since the first term is the inverse of a covariance matrix which is a normal equation matrix; while the second term is clearly another normal equation matrix. Eqn (4.21) is mathematically equivalent to eqn (4.12) but different from the computational point of view [Krakiwsky, 1990], in that the former requires an inversion of the size of new observations, while in the latter, two inversions of the size of the state vector are required.

The filtered state vector is

$$\hat{x}_k(+)=\hat{x}_k(-)+K[l_k-A_k\hat{x}_{k-1}(-)], \quad (4.22)$$

where the Bayes gain matrix is

$$K=C_k^x(+)A_k^T C_k^{l^{-1}}. \quad (4.23)$$

Clearly, the Bayes expressions are computationally more efficient when accumulating many observations which are larger in number than the size of the state vector. The Bayes expressions are the algorithms to be used in the decentralized-federated filter approach given in Chapter 4.5.

4.4 Federated Filtering Concept

There is ample motivation to search for a filtering method that would have the following characteristics:

- (1) improved system robustness (resist and avoid blunders as in magnetic compass-outputs, and cycle slips in GPS phase measurements);
- (2) improved fault detection and identification (FDI), and fault recovery (FR); and
- (3) automatic self calibration (e.g. odometers, compass, rate gyro).

The decentralized-federated filter is based upon the principle of "information sharing" in which (Figure 4.1):

- (1) the total system information is divided among n local filters;
- (2) local time propagation and measurement update processing (including local sensor update and calibration) is performed locally; and
- (3) the updated local information is then re-combined in the master filter to form a new total sum - a fused solution.

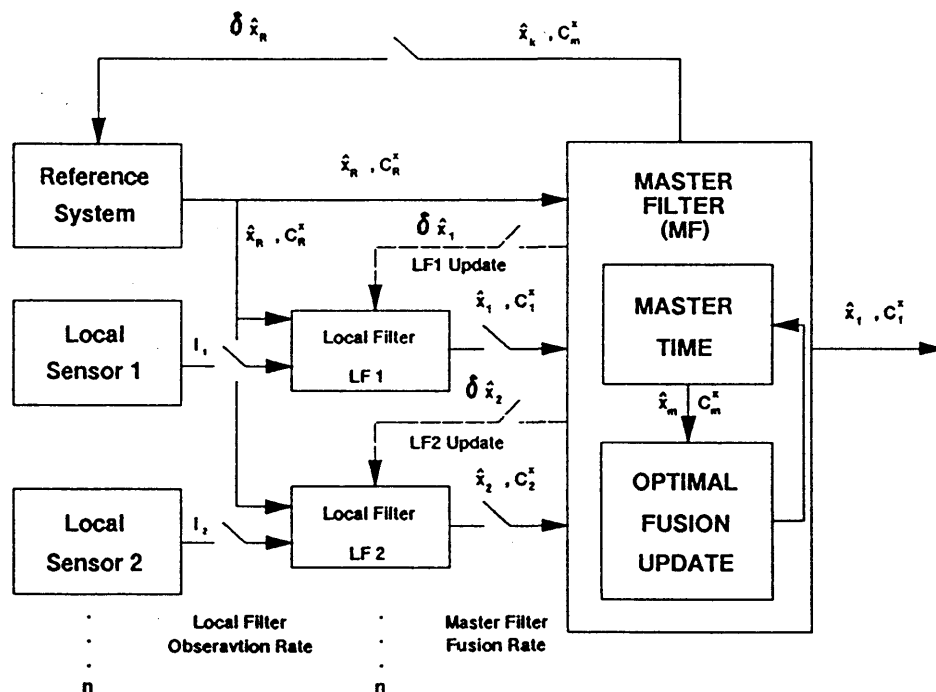


FIGURE 4.1. Federated Filter Design and Implementation Scheme

Note that the reference system is taken as the primary sensor, e.g. INS integrating INS with other local sensors such as GPS for measurement updates. Within the context of this work GPS was chosen as the reference system and the compass, rate gyro and odometers as local sensors. The main distinguishing characteristic of the reference system is that it must run continuously, whereas local filters can run sporadically and at different rates.

Reference filters usually have more complex models than the local filters. The reference filter continuously feeds into the master filter and the master filter feeds back into the reference filter at the same rate. It is within the master filter that fusion (combination) of information from the local filters takes place. This is how the reference filter obtains a correction $\delta\hat{x}_R$. The master filter can feedback into the local filters as well.

Carlson [1988a] lists the advantages of this information-sharing principle as follows:

- (1) increased total system throughput by parallel processing in several local filters;
- (2) increased system throughput by using local filters for data compression;
- (3) improved overall system reliability by maintaining multiple component solutions usable as backups (e.g., if the compass malfunctions the system should still supply a solution based upon the other sensors); and
- (4) reduced system development testing and maintenance cost through the use of this theoretically correct formulation rather than ad hoc designs.

Information Sharing Principles

Carlson [1988a] defines the fully centralized filter solution (denoted by f) respectively by the state vector and covariance matrix, namely:

$$\hat{x}_f, C_f \quad (4.24)$$

where the normal Kalman subscripts $k-1, k$ have been dropped for reasons of simplicity and replaced by f . Solutions and covariance matrices for the i^{th} local filter (LF) (e.g., GPS pseudorange; compass; altimeter; rate gyro) are denoted by

$$\hat{x}_i, C_i, \quad (4.25)$$

where $i = 1, n$.

The master filter (MF) (e.g., dead reckoning; GPS) solution is denoted by

$$\hat{x}_m, C_m. \quad (4.26)$$

The subscript $j = 1, n, m$ includes all the local filters and the master filter m .

For statistically independent solutions (e.g., dead reckoning and GPS), their combination can be effectuated by the following additive information algorithm (addition of normal equations) or fusion algorithm:

$$C_f^{-1} = N_f = N_1 + N_2 + \dots + N_n + N_m, \quad (4.27)$$

where C is the covariance matrix, and the information matrix (normal equation coefficient matrix) $N = C^{-1}$.

Also, in terms of the solution vector,

$$C_f^{-1} \hat{x}_f = N_f \hat{x}_f = N_1 \hat{x}_1 + N_2 \hat{x}_2 + \dots + N_n \hat{x}_n + N_m \hat{x}_m. \quad (4.28)$$

$$\hat{x}_f = C_f \{ C_1^{-1} \hat{x}_1 + C_2^{-1} \hat{x}_2 + \dots + C_n^{-1} \hat{x}_n + C_m^{-1} \hat{x}_m \}, \quad (4.29)$$

which is the formula for the multivariate weighted mean. The above formula applied to the univariate world reduces to

$$\bar{x} = \frac{\frac{x_1}{\sigma_1^2} + \frac{x_2}{\sigma_2^2} + \dots + \frac{x_n}{\sigma_n^2} + \frac{x_m}{\sigma_m^2}}{\frac{1}{\sigma_1^2} + \frac{1}{\sigma_2^2} + \dots + \frac{1}{\sigma_n^2} + \frac{1}{\sigma_m^2}}, \quad (4.30)$$

which is the well-known formula for the univariate weight mean. Eqn (4.29) can be used in lieu of the expressions given by Wei and Schwarz [1990] for obtaining a global estimate from several local filtered estimates that run in parallel.

The federated filter employs the above by first constructing (obtaining) the LF and MF solutions and then combining (or re-combining) them at any time. This particular construction avoids the need to carry and account for LF-LF or LF-MF cross covariances. By combining via the normal equations (eqns (4.27), (4.28)), the problem of accounting for cross covariances vanishes. This concept of addition of the normal equations is well known to the geodetic community.

In the next development of "information sharing", Carlson [1988] introduces the "conservation of information principle", namely the fully centralized solution can be divided amongst the local filters and master filter as follows:

$$C_f^{-1} = N_f = N_1\beta_1 + N_2\beta_2 + \dots + N_n\beta_n + N_m\beta_m \quad , \quad (4.31)$$

where the $\beta_j, j = 1, n, m$ cause a fraction of the full solution to be attributed to the LF's (n) and MF (m). Further

$$C_j^{-1} = C_f^{-1}\beta_j = N_f\beta_j \quad , \quad (4.32)$$

$$C_j = C_f\beta_j^{-1} = C_f\gamma_j \quad , \quad (4.33)$$

$$\hat{x}_j = \hat{x}_f \quad , \quad j = 1, n, m \quad , \quad (4.34)$$

where each local solution is set equal to the full solution, but the covariance information is proportioned with $C_f\beta_j^{-1} = C_f\gamma_j$. The equation

$$\beta_m + \sum_{i=1}^n \beta_i = 1 \quad (4.35)$$

characterizes the "conservation of information principle". In federated filtering when the normal equations are employed, β_i are used in information sharing, while when the covariance matrices are employed, $\gamma = \beta^{-1}$ is used (Figure 4.4).

The consequence of the above is that the LF's and MF solutions can be re-combined using eqn (4.30) to yield the correct total solution \hat{x}_f once blunders have been removed from the LF's and MF. Some researchers liken the β_i to weights, while others regard them as information proportionment quantities. Experience using them is necessary before this subtly can be fully and deeply understood. At first glance, however, it can be said that weighting is effectuated via the C_f^{-1} matrices, while the β_j and γ_j act as factors for distributing the total system information to the LF's and MF.

Measurement Update Process

In the measurement update process each LF i incorporates discrete measurements from its unique sensor i (e.g. GPS pseudorange or phase; magnetic compass azimuth; odometer). Measurement information is added to each LF (Figure 4.2) by the addition of normal equations, namely:

$$C_i^{-1}(+) = C_i^{-1}(-) + A_i^T C_i^{-1} A_i \quad , \quad (4.36)$$

$$N_i(+) = N_i(-) + N_i \quad , \quad (4.37)$$

and for the solution

$$C_i^{-1}(+) \hat{x}_i(+) = C_i^{-1}(-) \hat{x}_i(-) + A_i^T C_i^{-1} A_i \quad , \quad (4.38)$$

$$N_i(+) \hat{x}_i(+) = N_i(-) \hat{x}_i(-) + A_i^T C_i^{-1} l_i \quad , \quad (4.39)$$

where (+) denotes post measurement values for the i^{th} LF.

The correct total solution is obtained from the fusion algorithm (eqns (4.28), (4.30)), namely:

$$C_f^{-1}(+) = C_m^{-1} + \sum_{i=1}^n [C_i^{-1} + A_i^T C_i^{-1} A_i] \quad , \quad (4.40)$$

$$N_f(+) = N_m + \sum_{i=1}^n N_i + \sum_{i=1}^n A_i^T C_i^{-1} A_i \quad , \quad (4.41)$$

$$N_f(+) = N_f(-) + \sum_{i=1}^n A_i^T C_i^{-1} A_i \quad . \quad (4.42)$$

The above solution is what would be achieved by employing a batch solution or a single centralized Kalman filter solution.

Kinematic Process

Carlson [1988a] calls the kinematic process the discrete time propagation process. This process can also be accomplished via independent, parallel operations of the LF's and MF, provided the common process noise information is divided in the same fashion as the fused solutions for measurement updates discussed immediately above. Recall (eqn (4.6)) the kinematic process is given by

$$\dot{\mathbf{x}} = \mathbf{F}\mathbf{x} + \mathbf{G}\mathbf{u} \quad , \quad (4.43)$$

and hence the covariance propagation from t_{k-1} to t_k (without measurement update) is

$$(C_k^x(-))_j = (\Phi_{k-1,k})_j (C_k^x(+))_j (\Phi_{k-1,k}^T)_j + (C_{k-1,k}^u)_j \quad , \quad (4.44)$$

where $j = 1, 2, \dots, n, m$, namely the LF $()_i$ and MF $()_m$ values of Φ, C^x and C^u . Special mention of the C^u covariance matrix should be made at this juncture, that is, we do not evaluate it as Carlson states, namely:

$$(C_{k-1,k}^u)_j = G_j C_j^u G_j^T \quad , \quad (4.45)$$

because G_j and C_j^u in the $\dot{\mathbf{x}}$ space are not known. Information in the x space is available, namely (eqn (4.17)):

$$(C_{k-1,k}^u)_j = \int_{\tau=t_{k-1}}^{\tau=t_k} \Phi Q(\tau) \Phi^T d\tau \quad , \quad (4.46)$$

where $Q(\tau)$ is the spectral density matrix of the system noise. According to the eqn (4.18) $(C_{k-1,k}^u)_j = Q \Delta t$. The Q values are defined in Chapters 5 and 6.

Federated Filtering Equations

Carlson [1988a] does not give the filtering equations for the federated filtering method. Morrison [1969] and Krakiwsky [1990] give the equations necessary to implement this method; the equations are called the Bayes filtering equations. Wei and Schwarz [1990] also list an alternative set of equations but no name has been attached to them. The Bayes filter equations, using the notation of Krakiwsky [1990] and the concepts of decentralized filtering by Carlson [1988a], are listed immediately below:

The predicted state vector using $j = 1, 2, n, m$ solutions is (eqn (4.19)).

$$\hat{x}_k(-) = \sum_{j=1}^m (\Phi_{k-1,k})_j \hat{x}_k(-)_j \quad . \quad (4.47)$$

The predicted covariance matrix is (eqns (4.20);(4.44)) is

$$C_k^x(-) = \sum_{j=1}^m (C_k^x(-))_j$$

$$C_k^x(-) = \sum_{j=1}^m \left\{ (\Phi_{k-1,k})_j (C_k^x(+))_j (\Phi_{k-1,k})_j^T + (C_{k-1,k}^u)_j \right\} \quad . \quad (4.48)$$

The covariance matrix for filtered state vector (eqns (4.21);(4.40);(4.41)) is

$$C_k^x(+) = \left\{ [C_k^x(-)]^{-1} + \sum_j (A_k^T C_k^l A_k)_j \right\}^{-1} \quad , \quad (4.49)$$

where a summation of all the normal equations for the local filters takes place.

The Bayes filtered state vector is (eqns (4.22); (4.23))

$$\hat{x}_k = \hat{x}_k(-) + \sum_j K_j [l_k - (A_k)_j \hat{x}_k(-)_j] \quad , \quad (4.50)$$

where

$$K_j = [C_k^x(+)_j (A_k)_j^T (C_k^l)_j]^{-1} \quad . \quad (4.51)$$

Note in the Bayes equations, two inverses of order of the state vector are needed (eqn (4.49)) while the third inverse of order of the observations (eqn (4.51)) is usually not needed for uncorrelated white noise on the observations.

4.5 Federated Filter Design

Let us now take the federated filter equations one step further, that is, into the filter design and implementation stage. Return to Figure 4.2 and note that the main difference between the federated filter and the standard Kalman filter implementation is that the Kalman approach is a one step process, while the federated - Bayes approach is a two step process, namely:

- (1) first, each local sensor sends data to its own local filter for processing ($j = 1$ in eqns ((4.47); (4.48); (4.49); (4.50))); and
- (2) then the results \hat{x} are sent to the master filter for fusion-combination ($j = 1, n, m$) eqns ((4.47);(4.48);(4.49);(4.50)).

Other distinguishing characteristics of the federated filter are the following:

- (1) feedback and update δx_j to each local filter is made;
- (2) the master filter sends back a correction $\delta \hat{x}_R$ to the reference filter; and
- (3) the reference filter sends information (\hat{x}_R, C_R^T) to each local filter.

All of the above is performed within context of the information sharing concept proposed by Carlson [1988a].

It should be reiterated that the federated filter (Bayes) is mathematically equivalent to the Kalman filter equations. Krakiwsky [1990] already has demonstrated this fact, but, has also pointed out that they are different from the computational points of view in that different

sizes of matrix inversions are necessary. This latter fact translates into the fact that the Bayes equations should be used in federated filtering because many observations are being accumulated during the period before cross talk filter updates.

In summarizing the findings of this section, the following conclusions of Carlson [1988a] are stated.

- (1) One may wish to perform the fusion (total combination of solutions) and reset (of the local filters) less often because of the following:
 - (a) to reduce computational load of fusion and reset operations;
 - (b) to reduce data bus loads between LF processors and the MF fusion processor;
 - and
 - (c) to eliminate the need to synchronize fusion-reset operations with the LF measurement update cycles.
- (2) Operating the LF's and the MF independently and taking multiple LF steps between fusion updates simply ignores some information (knowledge of common process noise) that could in principle be used at each inner step. The solution is optimal (minimum variance-unbiased) for that subset of data and hence the solution may not be globally (as in a centralized filter approach) optimal. Global optimality may not be of prime importance in that some accuracy may be sacrificed in order to gain the following:
 - (a) throughput-speed via parallel processing;
 - (b) fault detection, identification and recovery (FDIR); and
 - (c) real time system simplicity.

4.6 Federated Filter Implementations

The decentralized and information sharing characteristics of the federated filter design leads to a family of filter designs. The spectrum covered by these designs ranges from the

LF's retaining none of the information (zero-reset feedback) while the MF retains all, to a design in which the LF's retain all the information (full fusion feedback). These possibilities are treated below and will be seen to have application to the parallel filtering of GPS pseudoranges and phase measurements, and then their subsequent combination with DR, azimuth, change in azimuth and altimetry sensors.

The following four federated filter designs are those of Carlson [1988b]. The first federated filter design is called the master filter (MF) memory, zero-reset feedback (Figure 4.2). Its characteristics are as follows:

- (1) the MF retains all the used information from the Bayes filter equations (i.e. $\beta_m = 1$) with long term memory;
- (2) the local filters (LF's) retain zero information ($\beta_j = 0$) and act as data compression (summation of normal equations) with short term memory. (Clearly, β_j is not a weight, but is connected to information sharing).

The advantages of this design are as follows:

- (1) the LF's can implement low order (simple) math models and sensor models between zero resets;
- (2) higher order models can be implemented in the larger MF - operating at a reduced rate;
- (3) databus loads are halved since there is no feedback of fusion reset situations to the LF's; and
- (4) real time operations are simplified since the LF's do not have to wait for the MF to feedback solutions.

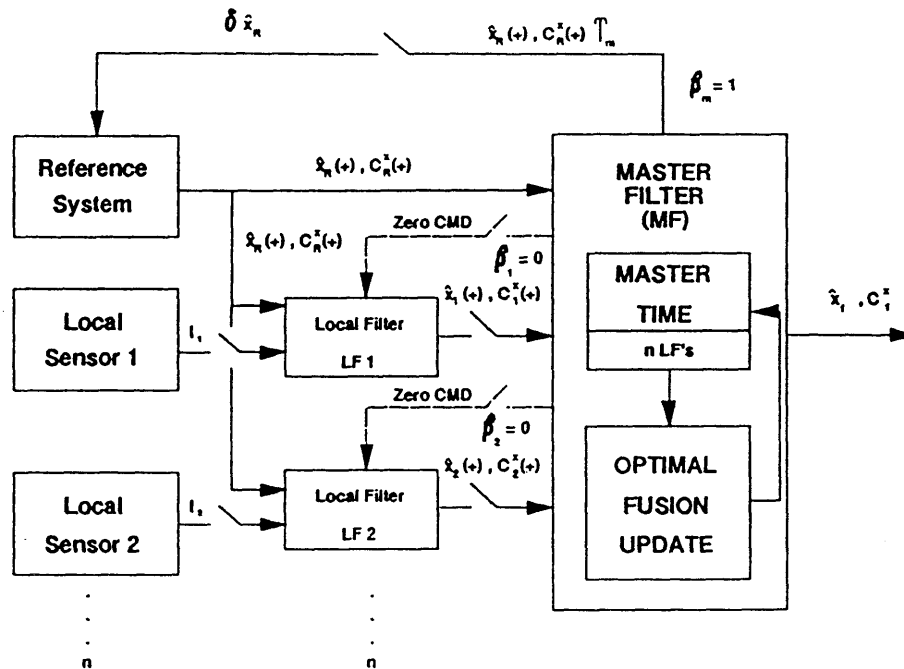


FIGURE 4.2. Federated Filter #1 : MF Memory, Zero-Reset Feedback

$$(\beta_m = 1 ; \beta_i = 0)$$

The second and third designs (Figures 4.3, 4.4) are characterized by fusion feedback -partial and full, respectively. Their main characteristics and advantages are described in the following:

- (1) the less accurate LF's can operate at higher accuracies than when operating alone (design #1); thereby allowing greater fault-detection and backup capabilities;
- (2) design #2 allows the MF to maintain higher order system models for e.g. INS, as compared to the LF's;
- (3) design #3 reduces the LF process noise multipliers from $n+1$ ($i=m$) to n ($j=1, n$) when there is no need for MF retained information.

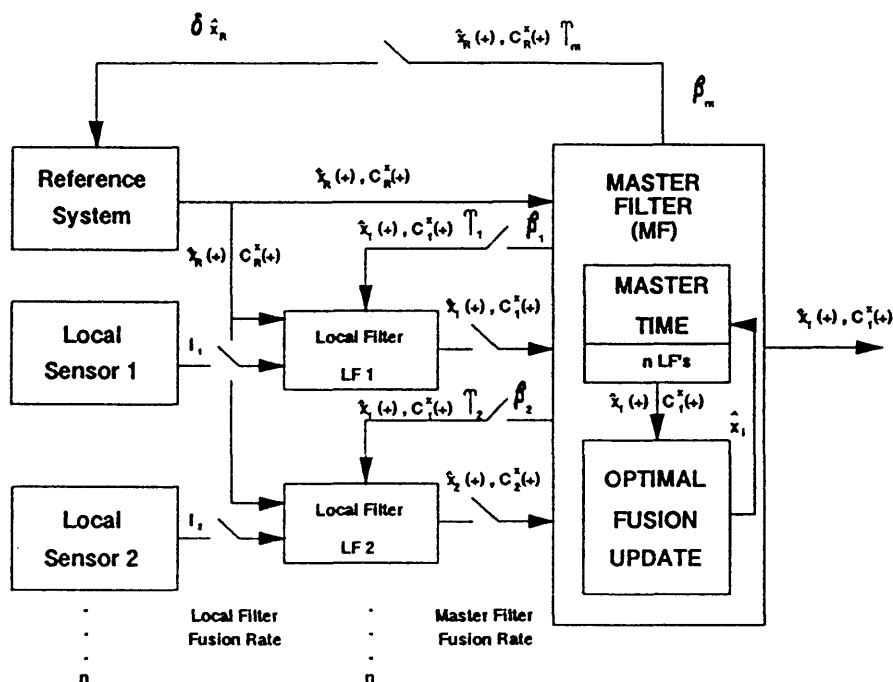


FIGURE 4.3. Federated Filter #2 : MF/LF Memory, Partial Fusion Feedback

$$(\beta_m \approx \beta_i \approx 1/(n+1) ; \text{eg. } n=3, \beta_m = \beta_i = 0.33)$$

Design #4: LF Memory, No reset feedback; has the following characteristics - advantages:

- (1) it is the least accurate but most fault tolerant;
- (2) the MF retains none of the fused information, while the LF's together retain all the information;
- (3) the LF's retain their original (pre-fusion) solutions without change, rather than the split solutions as in designs #2 and 3;
- (4) the MF, rather than reset to zero, propagates the fused solution forward to the next fusion time (t_k) to make the best estimate available for output at intermediate time points (this propagated solution is not used, however, in the next fusion update as it duplicates the total LF information as of the last update); and

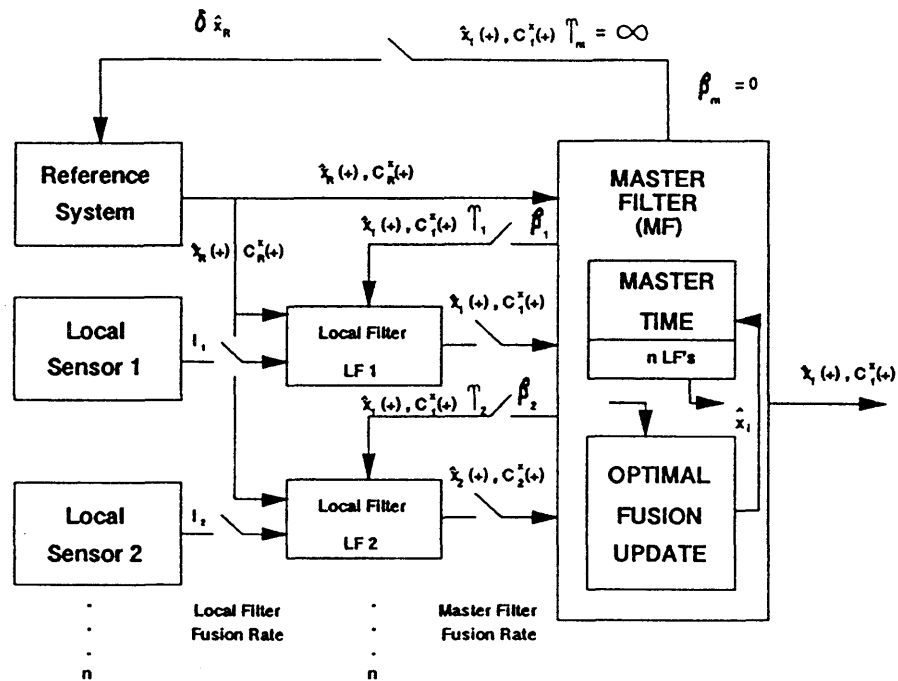


FIGURE 4.4. Federated Filter #3 : LF Memory, Full Fusion Feedback

$$(\beta_m = 0; \beta_i = 1/n)$$

- (5) this design is highly fault tolerant in that a fault in one local sensor cannot contaminate any other LF solution, while the good LF solutions can still be used after the faulty solution has been isolated and the solution is sub optimal but more accurate than individual LF solutions.

Federated filter local filter solutions i are fused together in the master filter by use of the following Bayes filter type equations [Krakiwsky, 1974, 1990; Carlson, 1988a; Wei and Schwarz, 1990 Gao et al., 1991]:

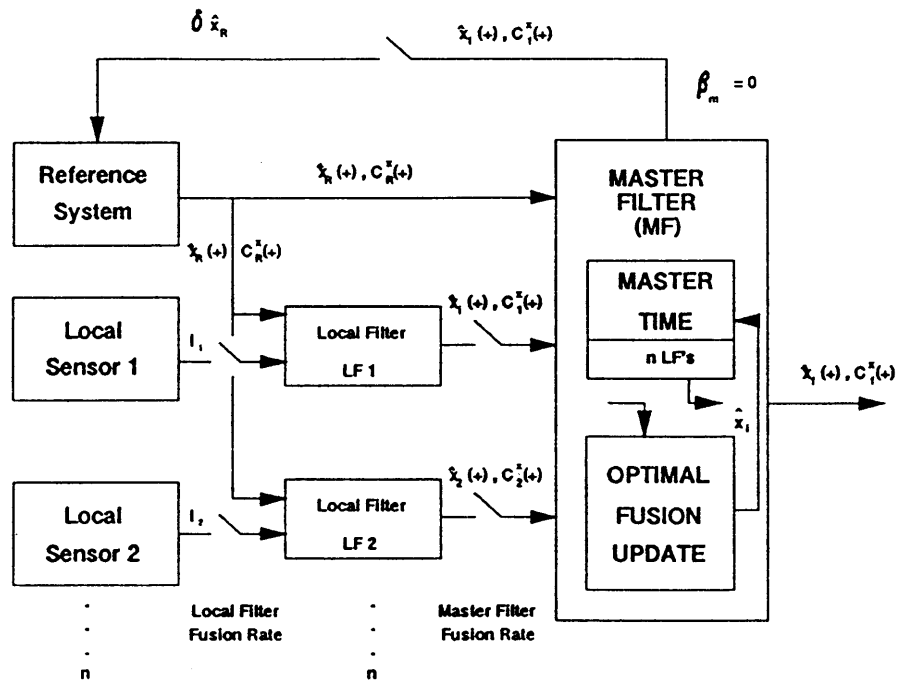


FIGURE 4.5. Federated Filter #4 : MF Memory, No-Reset Feedback

$$x_k(+) = C_k^{x(+)} \{C_k^x(-)\}^{-1} x_k(-) + \sum_{i=1}^n C_k^{x(+)} \{C_{ik}^x(+)\}^{-1} x_{ik}(+) - \sum_{i=1}^n C_k^x(+) \{C_{ik}^x(-)\}^{-1} x_{ik}(-) \quad (4.52)$$

$$\{C_k^{x(+)-1}\} = \{C_k^x(-)\}^{-1} + \sum_{i=1}^n \{C_{ik}^x(+)\}^{-1} - \sum_{i=1}^n \{C_{ik}^x(-)\}^{-1} \quad (4.53)$$

An alternative to these equations are those of the "multivariate weighted mean" given in eqn (4.29).

CHAPTER 5

GPS PROCESSING

Chapter 5 encompasses the knowledge needed for GPS processing. Section 5.1 includes a processing overview summarizing the various computation modules. Section 5.2 contains details on satellite orbit computations while Section 5.3 deals with observation reductions. Section 5.4 gives the methodology for generating carrier smoothed pseudoranges and Section 5.5 furnishes details regarding observation weighting. Section 5.6 contains various methods for detecting cycle slips and some of the disadvantages of using a low cost receiver. Section 5.7 lists the various design matrices in both Cartesian and geodetic formulation. Section 5.8 shows how the various GPS observations may be combined and Section 5.9 includes the kinematic state space model.

5.1 Processing Overview

The following is a brief overview of the computation steps involved in processing pseudorange and carrier phase data [Cannon, 1991b]. Detailed mathematical formulation is given in subsequent sections. Figure 5.1 divides the processing into three major sections, namely: observation pre-processing, prediction and updates.

- (1) **Decode raw data:** Form pseudorange, carrier phase measurements as well as transmit time for each satellite tracked from the raw measurement data. The validity of the measurements (i.e. SNR and/or Costas ratio) are checked.
- (2) **Compute satellite coordinates, tropospheric and ionospheric corrections:** It is not necessary to compute a new tropospheric and ionospheric correction at a 1 Hz rate, but instead compute it once every 5 seconds, for example.

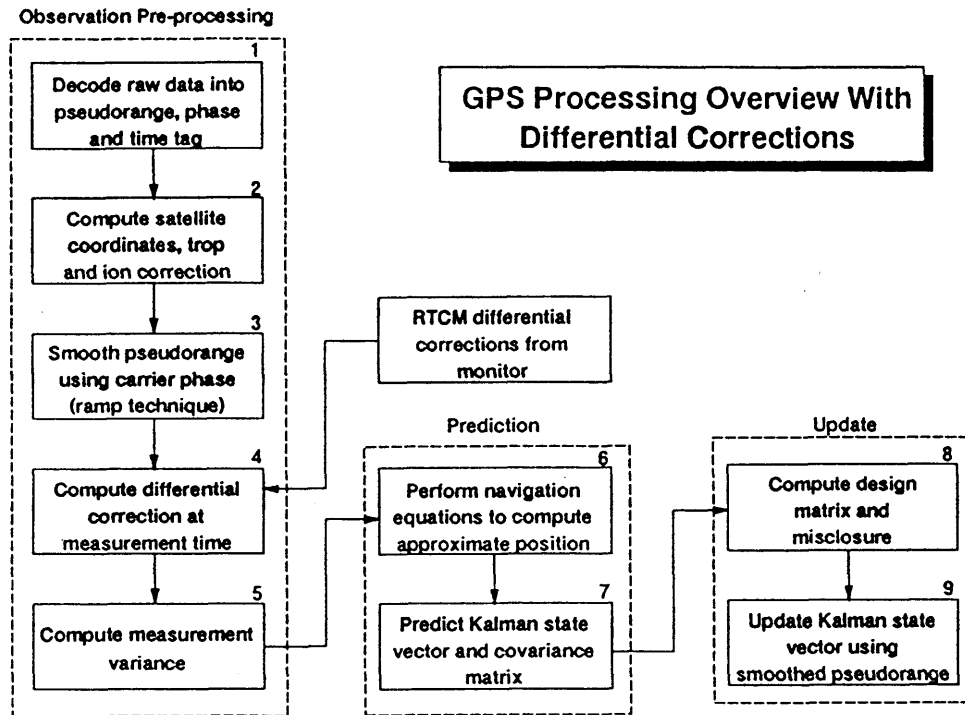


Figure 5.1.

- (3) **Smooth Code Using Carrier:** The noise on the code is smoothed using the carrier phase [Hatch, 1982, 1986]. A variation of this which employs dual ramps was implemented in order to minimize multipath and ionospheric divergence. The integrity of the smoothed code is monitored using the pure code (which is accurate to 1-3 m) and the ramp is reset if the difference between the two measurements becomes too large. This module also entails the cycle slip detection procedure.
- (4) **Compute differential corrections:** Differential corrections at the time of measurement are computed. It must also be determined if there are differential corrections for all satellites tracked. If not, then the carrier smoothed measurement will be de-weighted with respect to those satellites having differential corrections. Differential corrections to the phase rate do not have to be computed since the differential correction rate is transmitted as part of the RTCM corrections.

- (5) **Compute measurement variance:** The variance of the smoothed pseudorange and phase rate are computed and reflect the residual errors which may be present in the observation. In this way, measurements taken to satellites with low elevation would have a higher variance. Also, the variance reflects the amount of smoothing that has been done (i.e. smoothed measurement has lower noise than pure pseudorange).
- (6) **Evaluate navigation equations:** The position of the receiver at the current measurement epoch is predicted using the estimated velocities. The clock offset is also predicted using the estimated clock drift.
- (7) **Kalman prediction equations:** The state vector and covariance matrix are predicted to the current epoch using the transition matrix and process noise. The process noise matrix is made to be adaptable, depending on the vehicle dynamics. The use of an adaptive filter is made after fusion feedback.
- (8) **Compute design matrix and misclosure:** Each satellite is processed sequentially so that no matrix inversions are required i.e. only a one by one must be inverted.
- (9) **Kalman update equations:** Standard Kalman update equations are used to process the measurements. Blunder detection algorithms are also built-in to this module.

5.2 Broadcast Ephemeris Computations

5.2.1 Keplerian Orbital Elements

The idealized satellite motion caused solely by an Earth centred gravitational field is called Keplerian motion, which may be deduced from Newton's laws of motion. The main characteristics of Keplerian motion are listed immediately below [Wells et al, 1986]:

- (1) The motion relative to the Right Ascension (RA) system (inertial system) occurs in a stationary plane which contains the centre of mass of the Earth. The orbit is conic with one of the foci located at the Earth's centre of mass, the geocentre (Kepler's first law).

- (2) The closest and farthest points of the orbit to the Earth's centre of mass, called perigee and apogee, respectively, are stationary in inertial space.
- (3) The size and shape of the elliptical orbit are constant.

The stationarity of the orbital plane, perigee, size, and shape of the orbit, together with constant period, lead to the fact that the Keplerian motion can be described by six parameters $(\sqrt{a}, e, i_o, \omega, \Omega_o, M_o)$, of which only one is a function of time. The definition of these parameters are as follows (Figure 5.2):

- (1) The Right Ascension of the ascending node (Ω) is the geocentric angle between the nodal directions and vernal equinox measured eastward in the equatorial plane.
- (2) The inclination (i), is the angle between the equatorial and orbital planes.
- (3) The argument of perigee (ω) is the angle between the nodal and perigee directions measured in the orbital plane.
- (4) The semi-major axis of the elliptical orbit is (a).
- (5) The eccentricity of the orbit is (e).
- (6) The anomaly is an element describing the position of the satellite in the orbital ellipse. One of the three types of anomalies is normally used in practise. The true anomaly f is shown in Figure 5.2. The axes x_1, x_2, x_3 are those of the RA system. The conventional terrestrial system (CT) axes x_T, y_T, z_T are shown in Figure 5.3.

There are four points (Figure 5.2) of importance along the orbital ellipse and are defined below [Wells et al., 1986]:

- (1) The ascending node, which is at one end of the line of intersection of the orbital plane and the equatorial plane, as the satellite passes from the southern hemisphere into the northern hemisphere.
- (2) The perigee is the point at which the satellite most closely approaches the Earth.

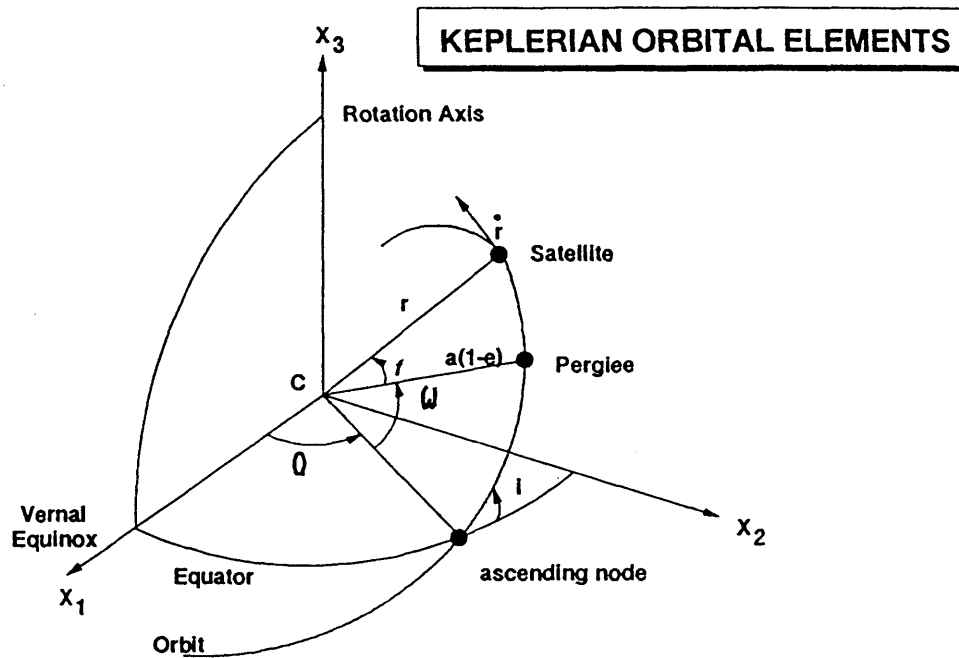


Figure 5.2 (after Wells et al., 1986)

- (3) The reference position is the position of the satellite at the reference time t_{oe} (the time for which the mean anomaly M_o , i_o , and Ω_o are given).
- (4) The satellite position is what is to be determined. It is separated from perigee by the true anomaly f , and from the ascending node by the argument of latitude $u = \omega + f$.

Broadcast ephemerides for the GPS satellites are readily available in the navigation message modulated on the GPS carrier signals. The parameters describing the orbital motion of the satellite are very similar to those of a Keplerian representation. Because the broadcast ephemeris is the result of an extrapolation of a post-processed orbit into the future (which have been precisely determined by numerical integration of the equations of motion), these parameters are Keplerian in appearance only, i.e., they only describe the satellite orbit for the period for which they are intended (about 1.5 hours from the reference epoch).

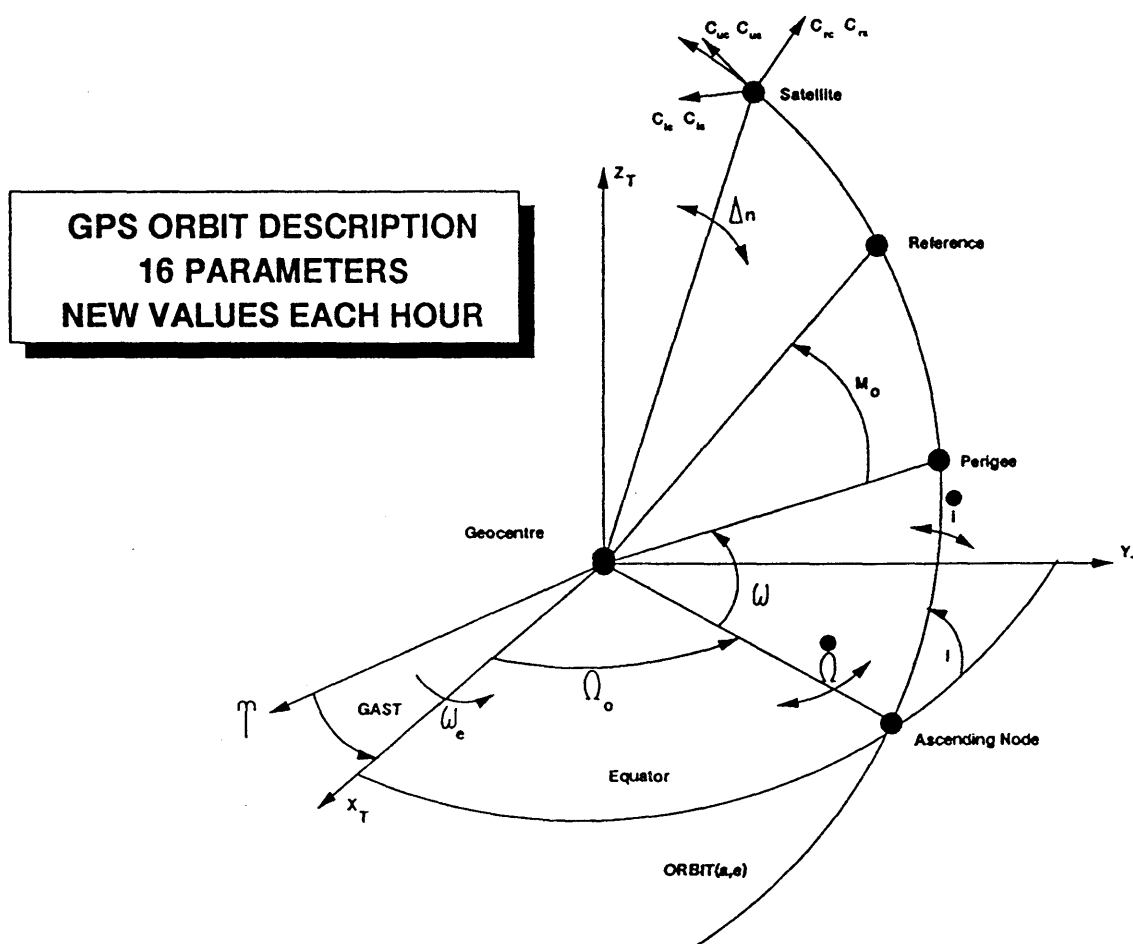


Figure 5.3(after Wells et al., 1986)

The six parameters $(\sqrt{a}, e, i_o, \omega, \Omega_o, M_o)$ describe a smooth elliptical orbit, along with the mean motion n , with the satellite position being a function of time since t_{oe} . The additional parameters $\Delta n, \dot{\Omega}, \dot{i}$, and the six sine and cosine coefficients, describe the deviations of the actual satellite motion from this smooth ellipse, where the dot is the time derivative. These parameters primarily describe the perturbation effects of the non-sphericity of the Earth while also absorbing the smaller perturbation due to the sun and moon gravitational and solar radiation pressure.

Each broadcast ephemeris parameter set is intended for use only during the one hour period to which they refer. Extrapolation of the broadcast ephemeris well beyond this period leads to an exponential error growth which can affect significantly even differential positioning accuracies, especially for large station separations.

The Navigation Message is a 50 bit per second data bit stream modulated on the GPS signals (both frequencies). The data message is contained within a data frame that is 1500 bits long. Each subframe contains GPS system time, the S to P code handover information and a number of check flags [Van Dierendonck et al., 1980].

5.2.2 Broadcast Ephemeris Computational Procedure

It is required to determine the satellite position in the CT system as defined in Figure 5.3. First, the satellite position is computed in the RA system (Figure 5.2) in the following steps (Figure 5.4):

(1) Find the true anomaly f_k at time t_k by:

- computing semi-major axis of orbit, a

$$a = (\sqrt{a})^2, \quad (5.1)$$

- computing mean motion, n_o

$$n_o = \sqrt{\frac{\mu}{a^3}}, \quad (5.2)$$

- finding t_k , the time since reference time t_{oe} ,

$$t_k = t - t_{oe}, \quad (5.3)$$

- correcting mean motion, n

$$n = n_o + \Delta n, \quad (5.4)$$

- computing M_k , the mean anomaly at t_k ,

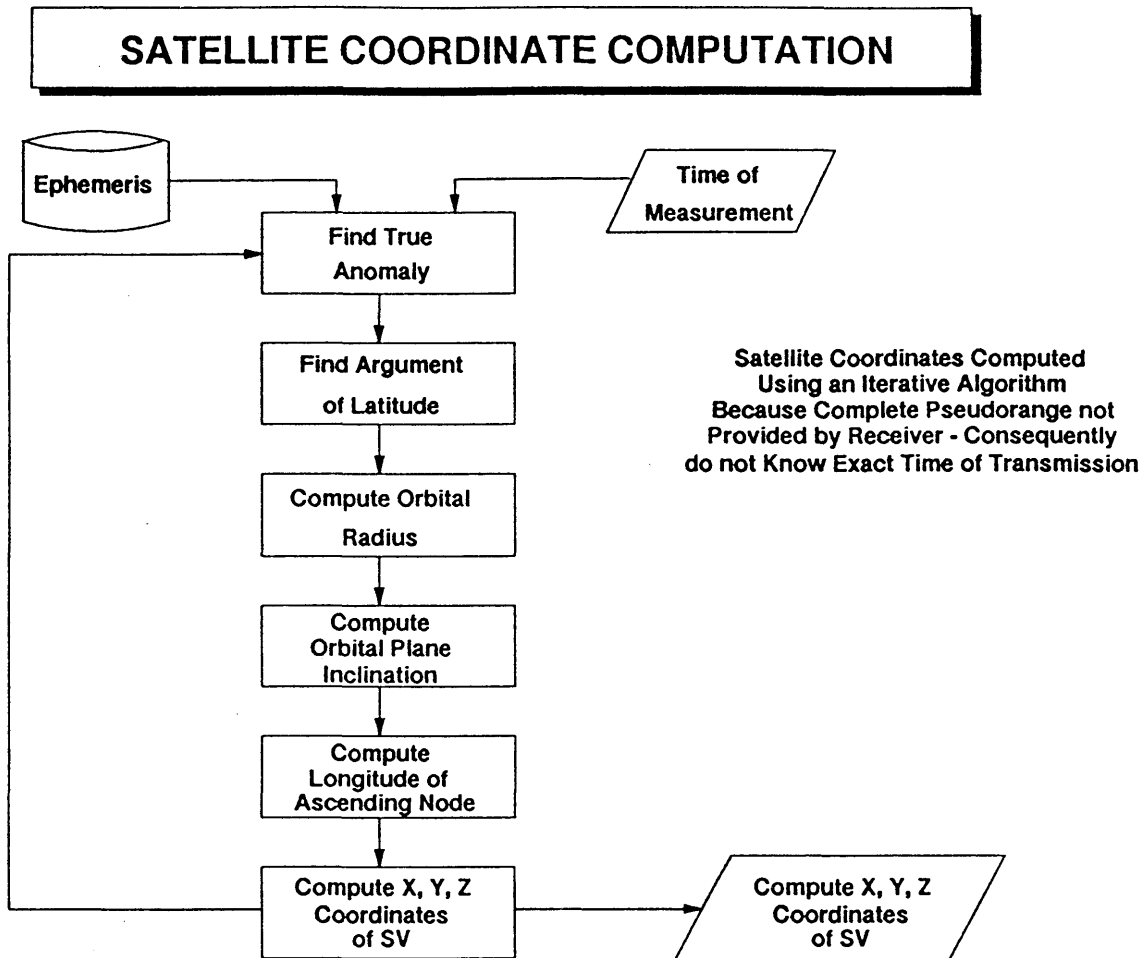


Figure 5.4 Satellite Coordinate Computation

$$M_k = M_o + nt_k , \quad (5.5)$$

- solving Kepler's equation (iteratively or by series expansion) for the eccentric anomaly E_k ,

$$\text{(iteratively)} \quad E_k = M_k + e \sin E_k \quad (5.6)$$

$$\text{(or directly)} \quad E_k = M_k + e \sin M_k + \left(\frac{e^2}{2}\right) \sin 2M_k + \frac{e^3}{8} (3 \sin 3M_k - \sin M_k) , \quad (5.7)$$

- finally computing the true anomaly, f_k

$$\cos f_k = (\cos E_k - e)/(1 - e \cos E_k) , \quad (5.8)$$

$$\sin f_k = \sqrt{1 - e^2} \sin E_k / (1 - e \cos E_k) , \quad (5.9)$$

and solving for the proper quadrant

$$\tan f_k = \frac{\sin f_k}{\cos f_k} , \quad (5.10)$$

or from a series expansion

$$f_k = M_k + 2e \sin M_k + \frac{5}{4}e^2 \sin 2M_k + \frac{e^2}{12} (13 \sin 3M_k - 3 \sin M_k) ; \quad (5.11)$$

(2) Find the argument of latitude u_k , by adding:

- the argument of perigee ω ,
- the true anomaly f_k , and
- the correction terms with coefficients C_{uc} and C_{us} ,

$$\phi_k = f_k + \omega , \quad (5.12)$$

$$\delta u_k = C_{us} \sin 2\phi_k + C_{uc} \cos 2\phi_k , \quad (5.13)$$

$$u_k = \phi_k + \delta u_k ; \quad (5.14)$$

(3) Compute the orbit radius r_k using:

- the expression for elliptical radial distance, and
- the correction terms with coefficients C_{rc} and C_{rs} ,

$$\delta r_k = C_{rc} \cos 2\phi_k + C_{rs} \sin 2\phi_k , \quad (5.15)$$

$$r_k = a(1 - e \cos E_k) + \delta r_k ; \quad (5.16)$$

(4) Compute the orbital plane inclination i_k , using:

- the inclination i_o , at reference time t_{oe} ,

- the linear change in inclination \dot{i} since reference time, and
- the correction terms with coefficients C_{ic} and C_{is} ,

$$\delta i_k = \dot{i} t_k + C_{ic} \cos 2\phi_k + C_{is} \sin 2\phi_k , \quad (5.17)$$

$$i_k = i_o + \delta i_k ; \quad (5.18)$$

- (5) Compute the longitude of the ascending node Ω_k , by adding:

- the right Ascension parameter, Ω_o (broadcast),
- the change in Greenwich Apparent Sidereal Time (GAST) between the beginning of the week and the reference time t_{oe} , and
- the change in longitude of the ascending node since the reference time t_{oe} plus the transmission time,

$$\Omega_k = \Omega_o + (\dot{\Omega} - \dot{\Omega}_e) t_k - \dot{\Omega}_e (t_{oe} + \Delta t) ; \quad (5.19)$$

- (6) Compute the orbital plane positions by:

$$x'_k = r_k \cos u_k , \quad (5.20)$$

$$y'_k = r_k \sin u_k ; \quad (5.21)$$

- (7) Compute the CT system coordinates, x, y, z of the satellite, by applying the three rotations (through u_k, i_k , and Ω_k) described previously,

$$x_k = x'_k \cos \Omega_k - y'_k \cos i_k \sin \Omega_k , \quad (5.22)$$

$$y_k = x'_k \sin \Omega_k + y'_k \cos i_k \cos \Omega_k , \quad (5.23)$$

$$z_k = y'_k \sin i_k , \quad (5.24)$$

where

t is GPS system time of transmission, i.e., GPS time of reception corrected for transit time (range/speed of light),

$\mu = 3.986005 \cdot 10^{14} \text{ m}^3/\text{sec}^2$ WGS 84 value of the Earth's universal gravitational parameter, and

$\dot{\Omega}_e = 7.292115 \cdot 10^{-5} \text{ rad/sec}$ WGS 84 value of the Earth's rotation rate.

Furthermore, t_k must be the actual time difference between the time t and the epoch time t_{oc} , and must account for beginning or end of week crossovers, i.e. if t_k is greater than 302,400, subtract 604,800 from t_k . If t_k is less than 302,400 add 302,400 to t_k .

5.2.3 Computation of Satellite Velocity

The following formulas detail the computation of the satellite velocity from the broadcast ephemerides [Cannon, 1991b]. The satellite velocity is required when the phase rate observations are being used.

Computation of Satellite Velocity in Orbital Plane

Recall from eqns (5.20) and (5.21) that satellite coordinates in the orbital plane are given as

$$x'_k = r_k \cos u_k , \quad (5.25)$$

$$y'_k = r_k \sin u_k . \quad (5.26)$$

Therefore, the satellite velocity in the orbital plane can be expressed as

$$\frac{dx'_k}{dt} = \cos u \frac{dr}{dt} - r \sin u \frac{du}{dt} , \quad (5.27)$$

$$\frac{dy'_k}{dt} = \sin u \frac{dr}{dt} + r \cos u \frac{du}{dt} , \quad (5.28)$$

where the denominator, dt , is the derivative with respect to time.

(1) Initial Computation of $\frac{dr}{dt}$:

By expanding eqn (5.16)

$$r = a(1 - e \cos E) + C_{rc} \cos 2\phi + C_{rs} \sin 2\phi , \quad (5.29)$$

$$r = a \frac{(1 - e^2)}{1 + e \cos f} + C_{rc} \cos 2\phi + C_{rs} \sin 2\phi . \quad (5.30)$$

Therefore,

$$\frac{dr}{dt} = \frac{ae(1 - e^2)}{(1 + e \cos f)^2} \sin f \frac{df}{dt} + 2 \frac{d\phi}{dt} (C_{rs} \cos 2\phi - C_{rc} \sin 2\phi) . \quad (5.31)$$

(2) Computation of $\frac{df}{dt}$:

Rearranging eqns (5.8), (5.9) and (5.10) yields

$$f = \tan^{-1} \left(\frac{\sqrt{1 - e^2} \sin E}{\cos E - e} \right) . \quad (5.32)$$

The derivative can then be computed as

$$\frac{df}{dt} = \frac{n(1 + e \cos f)^2}{\sqrt{1 - e^2}(1 - e^2)} . \quad (5.33)$$

(3) Computation of $\frac{d\phi}{dt}$:

Recall eqn (5.12)

$$\phi = f + \omega . \quad (5.34)$$

The derivative can then be computed as (assuming $\frac{d\omega}{dt} = 0$)

$$\frac{d\phi}{dt} \approx \frac{df}{dt} = \frac{n(1 + e \cos f)^2}{\sqrt{1 - e^2}(1 - e^2)} . \quad (5.35)$$

(4) Final Computation of $\frac{dr}{dt}$:

Using Eqns. (5.33) and (5.35), the rate of change of the orbital radius, $\frac{dr}{dt}$, can be computed as (Eqn. (5.31))

$$\frac{dr}{dt} = \frac{ane \sin f}{\sqrt{1-e^2}} + 2 \frac{n(1+e \cos f)^2}{\sqrt{1-e^2}(1-e^2)} (C_{rs} \cos 2\phi - C_{rc} \sin 2\phi) . \quad (5.36)$$

(5) Computation of $\frac{du}{dt}$ (from Eqns. (5.27) and (5.28)) :

Recall eqns (5.13) and (5.14)

$$u = \phi + C_{uc} \cos 2\phi + C_{us} \sin 2\phi . \quad (5.37)$$

Therefore, the derivative can be expressed as

$$\begin{aligned} \frac{du}{dt} &= \frac{d\phi}{dt} + 2 \frac{d\phi}{dt} (C_{us} \cos 2\phi - C_{uc} \sin 2\phi) \\ &= \frac{n(1+e \cos f)^2}{\sqrt{1-e^2}(1-e^2)} (1 + 2(C_{us} \cos 2\phi - C_{uc} \sin 2\phi)) , \end{aligned} \quad (5.38)$$

where the all terms have been previously defined.

Using eqns (5.36) and (5.38), the satellite velocity in the orbital plane can be computed, as defined in eqns (5.27) and (5.28).

Computation of Satellite Velocity in CT System

In order to compute the velocity in the CT system, a transformation must be made. The position transformation from eqns (5.22), (5.23) and (5.24) are given first and then the velocity transformation is derived.

Position Transformation:

$$x_k = x'_k \cos \Omega_k - y'_k \sin \Omega_k , \quad (5.39)$$

$$y_k = x'_k \sin \Omega_k + y'_k \cos i_k \cos \Omega_k , \quad (5.40)$$

$$z_k = y'_k \sin i_k . \quad (5.41)$$

Expanding on the inclination and ascending node terms give

$$\Omega_k = \Omega_o + (\dot{\Omega} - \dot{\Omega}_e)t_k - \dot{\Omega}_e (t_{oe} + \Delta t) , \quad (5.42)$$

$$i = i_o + C_{ic} \cos 2\phi + C_{is} \sin 2\phi + \frac{di}{dt} (t_k - (t_{oe} + \Delta t)) , \quad (5.43)$$

where

$\frac{di}{dt}$ is the broadcast inclination rate.

Velocity Transformation:

$$\begin{aligned} \dot{x} = \cos \Omega_k \frac{dx'}{dt} - x' \sin \Omega_k \frac{d\Omega_k}{dt} - \sin i \sin \Omega_k \frac{dy'}{dt} + y' \sin i \sin \Omega_k \frac{di}{dt} - \\ y \cos i \cos \Omega_k \frac{d\Omega_k}{dt} , \end{aligned} \quad (5.44)$$

$$\dot{y} = \left(\frac{dx'}{dt} - y' \cos i \frac{d\Omega_k}{dt} \right) \cos \Omega_k - \left(x' \frac{d\Omega_k}{dt} + \cos i \frac{dy'}{dt} - y' \sin i \frac{di'}{dt} \right) \sin \Omega_k , \quad (5.45)$$

$$\begin{aligned} \dot{y} = \sin \Omega_k \frac{dx'}{dt} + x' \cos \Omega_k \frac{d\Omega_k}{dt} + \cos i \cos \Omega_k \frac{dy'}{dt} - y' \sin i \cos \Omega_k \frac{di}{dt} - \\ y \cos i \sin \Omega_k \frac{d\Omega_k}{dt} , \end{aligned} \quad (5.46)$$

$$\dot{z} = \left(\frac{dx'}{dt} - y' \cos i \frac{d\Omega_k}{dt} \right) \sin \Omega_k + \left(x' \frac{d\Omega_k}{dt} + \cos i \frac{dy'}{dt} - y' \sin i \frac{di'}{dt} \right) \cos \Omega_k , \quad (5.47)$$

$$\dot{z} = \sin i \frac{dy'}{dt} + y' \cos i \frac{di'}{dt} , \quad (5.48)$$

where

$$\frac{d\Omega_k}{dt} = \dot{\Omega} - \dot{\Omega}_e , \quad (5.49)$$

and

$$\frac{di'}{dt} = \frac{di}{dt} + 2 \frac{d\phi}{dt} (C_{is} \cos 2\phi - C_{ie} \sin 2\phi) . \quad (5.50)$$

5.3 Observation Reductions

5.3.1 Computation of Distance and Elevation to Satellite

Given the coordinates of the receiver (x_r, y_r, z_r) and the satellites coordinates (x_s, y_s, z_s) we wish to compute the spatial distance r_{rs} , the azimuth α_{rs} and the zenith angle z_{rs} .

We begin by computing

$$\vec{r}_{rsG} = \begin{bmatrix} \Delta x_{rs} \\ \Delta y_{rs} \\ \Delta z_{rs} \end{bmatrix} = \begin{bmatrix} x_s \\ y_s \\ z_s \end{bmatrix} - \begin{bmatrix} x_r \\ y_r \\ z_r \end{bmatrix} . \quad (5.51)$$

Taking the inverse problem of Geodetic (or CT) to Local geodetic (LG) we have [Krakiwsky and Wells, 1971]:

$$\vec{r}_{rsLG} = P_2 R_2(\phi_r - 90^\circ) R_3(\lambda_r - 180^\circ) \vec{r}_{rsG} , \quad (5.52)$$

where R_3 and R_2 are rotation matrices and P_2 is a permutation matrix.

Substituting and expanding gives

$$\Delta x_{rsLG} = -\Delta x_{rsG} \sin \phi_r \cos \lambda_r - \Delta y_{rsG} \sin \phi_r \sin \lambda_r + \Delta z_{rsG} \cos \phi_r , \quad (5.53)$$

$$\Delta y_{rsLG} = -\Delta x_{rsG} \sin \lambda_r + \Delta y_{rsG} \cos \lambda_r , \quad (5.54)$$

$$\Delta z_{rsLG} = \Delta x_{rsG} \cos \phi_r \cos \lambda_r + \Delta y_{rsG} \cos \phi_r \sin \lambda_r + \Delta z_{rsG} \sin \phi_r . \quad (5.55)$$

The equations for distance, azimuth and zenith angle are given as

$$r_{rs} = (\Delta x^2 + \Delta y^2 + \Delta z^2)^{1/2} , \quad (5.56)$$

$$\alpha_{rs} = \tan^{-1} \left[\frac{\Delta y_{rs}}{\Delta x_{rs}} \right] , \quad (5.57)$$

$$z_{rs} = \cos^{-1} \left[\frac{\Delta z_{rs}}{r_{rs}} \right] , \quad (5.58)$$

where the elevation angle, $EL = 90^\circ - z_{rs}$.

5.3.2 Clock Corrections

The measurement transmission time (needed for satellite coordinate computations) can be computed from raw data as follows:

$$t_{SV} = t_{received} - \frac{P}{c} , \quad (5.59)$$

where

- t_{SV} is the raw transmission time - GPS time frame (sec),
- $t_{received}$ is the raw received time - receiver time frame (sec),
- P is the pseudorange observation corrected for the ionosphere and troposphere (m), and
- c is the speed of light ($m \text{ sec}^{-1}$).

The satellite clock polynomial correction term, Δt_{SV} , is used to correct for satellite clock drift and is of the form:

$$\Delta t_{SV} = a_0 + a_1(t - t_{oc}) + a_2(t - t_{oc})^2 , \quad (5.60)$$

where

- t_{oc} is the reference epoch (sec),
- t is the measurement transmission time (sec),

- a_0 is the satellite clock time offset (sec),
 a_1 is the fractional frequency offset (sec sec⁻¹), and
 a_2 is the fractional frequency drift (sec sec⁻²).

This clock correction is applied as follows:

$$t_{corrected} = t_{SV} - \Delta t_{SV} \quad , \quad (5.61)$$

where

- $t_{corrected}$ is the corrected measurement transmission time (sec),
 t_{SV} is the raw measurement transmission time (sec), and
 Δt_{SV} is the satellite clock correction (sec).

In the first equation defining Δt_{SV} , t_{SV} can be used for t (since $t_{corrected}$ is not available).

In addition to the above, there is also a correction for the relativistic effect. The expression for this effect is (ICD-200A)

$$\Delta t_r(t) = (-4.443 \cdot 10^{-10}) e \sqrt{A} \sin E(t) \quad . \quad (5.62)$$

The total satellite clock correction then becomes

$$t_{corrected} = t_{SV} - \Delta t_{SV} - \Delta t_r \quad . \quad (5.63)$$

Finally, corrections to the observations are as follows:

Pseudorange:

$$P_{corrected} = P_{measured} + c [\Delta t_{SV} + \Delta t_r] \quad . \quad (5.64)$$

Phase:

$$\Phi_{corrected} = \Phi_{measured} + c [\Delta t_{SV} + \Delta t_r] \quad . \quad (5.65)$$

Phase Rate:

$$\dot{\Phi}_{corrected} = \dot{\Phi}_{measured} + c [a_1 + 2 \cdot a_2 (t_k - t_{oc})] \quad . \quad (5.66)$$

In the Eqns. (5.65) and (5.66), the raw phase and phase rates have been scaled to metres using the wavelength.

5.3.3 Ionospheric Modelling

The ionospheric delay at GPS frequencies (1575.42 MHz) can reach more than 300 nanoseconds (100 m). For single frequency GPS users, the eight coefficients broadcast in the Satellite Navigation Message provide a correction of approximately 50% of the ionospheric range correction at mid-latitudes. These coefficients are based on a best fit of the diurnal (ie. daily) maximum values of the monthly average Total Electron Count (TEC). Any deviations of these values will be residual error to a single frequency GPS user. The performance of the model is poorer at high and equatorial latitudes.

The model is based on a cosine representation of the diurnal curve in which the amplitude and period vary according to user latitude. It is simplified in order to minimize the time required to compute the correction.

The effect of the ionosphere is to delay the pseudorange, thus the correction must be subtracted as follows:

$$P_{corrected} = P_{measured} - d_{ion} , \quad (5.67)$$

where P represents pseudorange and d_{ion} , the ionospheric correction. Note that the effect of the ionosphere on carrier phase measurements is to advance the signal, thus the correction must be added, namely:

$$\Phi_{corrected} = \Phi_{measured} + d_{ion} , \quad (5.68)$$

$$\dot{\Phi}_{corrected} = \dot{\Phi}_{measured} + \dot{d}_{ion} . \quad (5.69)$$

The algorithm as given in [ICD-GPS-200] is as follows:

Given : user approximate coordinates ϕ_u, λ_u , elevation (EL) and azimuth (AZ) to the GPS satellite for which the ionospheric delay is being calculated. Also given are the coefficients α_n, β_n transmitted as part of the satellite message.

Note : all angles are in units of semi-circles; time is in seconds.

- (1) Calculate Earth centered latitude

$$\Psi = \frac{0.0137}{EL + 0.11} - 0.022 \quad . \quad (5.70)$$

- (2) Compute sub-ionospheric latitude

$$\begin{aligned} \phi_I &= \phi_u + \Psi \cos AZ, & \text{if } |\phi_u| < 0.416 \quad , \\ \phi_I &= 0.416, & \text{if } |\phi_u| > 0.416 \quad . \end{aligned} \quad (5.71)$$

- (3) Compute sub-ionospheric longitude

$$\lambda_I = \lambda_u + \frac{\Psi \sin AZ}{\cos \phi_I} \quad . \quad (5.72)$$

- (4) Find geomagnetic latitude

$$\phi_m = \phi_I + 0.064 \cos(\lambda_I - 1.617) \quad . \quad (5.73)$$

- (5) Find local time

$$\begin{aligned} t &= 4.32 \cdot 10^4 \lambda_I + \text{GPS time (sec)} \quad , & (5.74) \\ \text{if } t &> 86,400, \text{ use } t = t - 86,400 \quad , \\ \text{if } t &< 0, \text{ use } t = t + 86,400 \quad . \end{aligned}$$

- (6) Compute slant factor

$$F = 1.0 + 16.0(0.53 - EL)^3 \quad . \quad (5.75)$$

- (7) Compute ionospheric time delay

$$d_{ion} = c F \left[5*10^{-9} + \left(\sum_{n=0}^3 \alpha_n \phi_m^n \right) \left(1.0 - \frac{x^2}{2} - \frac{x^4}{24} \right) \right] . \quad (5.76)$$

where

$$x = 2\pi \frac{(t - 50,400)}{\sum_{n=0}^3 \beta_n \phi_m^n} . \quad (5.77)$$

Corrections to the phase rate are generally not applied since the rate of change of the correction is fairly slow (longer term effect).

5.3.4 Tropospheric Modelling

The tropospheric corrections are made as follows:

Pseudorange:

$$\dot{P}_{corrected} = P_{measured} - d_{trop} , \quad (5.78)$$

Phase:

$$\Phi_{corrected} = \Phi_{measured} - d_{trop} , \quad (5.79)$$

Phase Rate:

$$\dot{\Phi}_{corrected} = \dot{\Phi}_{measured} - \dot{d}_{trop} , \quad (5.80)$$

where P represents pseudorange and d_{trop} , the tropospheric correction.

In geodetic applications, normally surface meteorological measurements are used. For this vehicle application, either standard values will be used or after testing, it may be found that this correction may be neglected for this particular application.

The modified Hopfield model for tropospheric corrections [Hopfield, 1971] can be used to calculate the tropospheric effect. It is given by [Wells, 1974] using standard atmospheric constants of:

- temperature = 5.85° C,
- pressure 1020 mbar, and
- relative humidity = 50%.

The result is

$$d_{trop} = \frac{k_d}{\sin(EL^2 + 6.25)^{1/2}} + \frac{k_w}{\sin(EL^2 + 2.25)^{1/2}} , \quad (5.81)$$

where

$$k_d = 1.552 \cdot 10^{-5} \frac{P}{TP} ((148.72TP - 488.3552) - h_{stm}) , \quad (5.82)$$

$$k_w = 7.46512 \cdot 10^{-2} \frac{e}{TP^2} (11000 - h_{stm}) , \quad (5.83)$$

- TP* is the temperature in Kelvins,
P is the pressure in mbar,
EL is the elevation angle to the satellite in degrees,
e is the water vapour pressure in mbar, and
h_{stm} is the height of the station above the geoid in metres.

Corrections to the phase rate are generally not applied since the rate of change of the correction is fairly slow (longer term effect).

5.4 Carrier Smoothed Code Measurement

The combination of the carrier phase measurement and the code (pseudorange) measurement produces a smoother ranging measurement due to the fact that the noise on the carrier's phase is a few millimetres while the noise on the pseudorange is a few metres ($\sigma_e = 5m$) [Wells et al., 1986]. By smoothing the pseudorange with range differences computed from the carrier phase (over time), relative positioning accuracy increases significantly. The effects of combining the carrier with the code are not as great in single point

mode as differential, since the error budget is mainly dominated by orbital and atmospheric errors. It does tend to smooth out receiver noise and increase short term relative accuracy. When using differential carrier smoothed range corrections, accuracy can improve to the one to three metre level [Cannon, 1990].

The concept of carrier smoothed code is to use the very accurate range differences (over time) derived from the carrier phase data to complement the instantaneous pseudorange measurements [Hatch, 1982, 1986; Lachapelle et al, 1986]. The use of the carrier phase data leads to the problem of cycle ambiguity resolution, however, it is not considered in the context of this document. In the following analysis it is assumed that no cycle slips have occurred.

At the first epoch of data reduction (or after a cycle slip has occurred), the pseudorange is used to initialize the solution, since the carrier phase is used only as range differences and thus is added at subsequent epoches. At time t_k the measurement for a satellite is [Cannon, 1990]:

$$\hat{P}_k = P_k \quad , \quad (5.84)$$

where

\hat{P}_k is the smoothed measurement at $t_k(m)$, and

P_k is the measured pseudorange at $t_k(m)$.

Each pseudorange is initialized and re-initialized in this manner.

At the next epoch, again the measured pseudorange is used to compute the estimated measurement, however a carrier phase derived range difference is also used. The two measurements can be combined as follows:

$$\hat{P}_2 = \frac{1}{2}P_2 + \frac{1}{2}\{\hat{P}_1 + (\Phi_2 - \Phi_1)\} \quad , \quad (5.85)$$

where

Φ is the measured carrier phase measurement (m).

From eqn (5.85) it can be seen that the smoothed measurement at t_k is a function of the measured pseudorange at t_k , and the predicted range at t_k using the smoothed range at t_{k-1} and the range difference between t_{k-1} and t_k computed from the carrier phase measurements. At epoch t_k , both components have equal weight, however, as subsequent epochs are computed, the weight on the predicted range will increase.

When implementing this technique and the phase is in cycles, caution must be exercised whether a plus or minus sign is applied to the wavelength when converting the phase to metres. This can vary from one receiver manufacturer to another.

A more generalized formulation for carrier smoothed pseudoranges is given below [Cannon, 1990]:

$$\hat{P}_k = \frac{1}{k}P_k + \frac{k-1}{k}\{\hat{P}_{k-1} + (\Phi_k - \Phi_{k-1})\} . \quad (5.86)$$

From eqn (5.86), it can be seen that the contribution of the pseudorange will become miniscule after a period of time. An alternative method proposed by Lachapelle et al. [1986] uses a counter to determine the weight as follows:

$$\hat{P}_k = W_1P_k + W_2\{\hat{P}_{k-1} + (\Phi_k - \Phi_{k-1})\} , \quad (5.87)$$

where

W_1 is the weight of the pseudorange measurement and conversely, and

W_2 (i.e. $1 - W_1$) is the weight of the carrier phase.

In Lachapelle et al. [1986], a "sliding weight" is used. For example, at t_k , the weight assigned to the pseudorange is 1.0 (i.e. $W_1 = 1.0$). At t_{k+1} , the weight assigned to the pseudorange is 0.99 (i.e. $W_1 = 0.99$), while the weight on the carrier phase is increased to 0.01 (i.e. $W_2 = 0.99$). At subsequent epochs where no cycle slips have occurred, the weight on the pseudorange is decreased by 0.01 each epoch and increased by 0.01 on the carrier phase. After 99 epochs, the smoothed pseudorange would be computed as follows:

$$\hat{P}_k = 0.01P_k + 0.99\{\hat{P}_{k-1} + (\Phi_k - \Phi_{k-1})\} \quad (5.88)$$

After this point in time, these weights can be maintained. If reduced any further the effect of the pseudorange would be totally neglected. From studies conducted by Lachapelle et al. [1986], about 100 measurements is the time required to average the noise in the pseudorange to give an unbiased differential measurement.

For a least squares adjustment or Kalman filter, the standard deviation of the input measurements must be a realistic representation of the true accuracy in order to maintain the reliability of the results. One scheme to derive the standard deviation of a smoothed pseudorange measurement is (assume noise only)

$$\sigma_\epsilon^2 = W_{pr}\sigma_{\epsilon_{pr}}^2 + W_{phase}\sigma_{\epsilon_{phase}}^2, \quad (5.89)$$

where

W_{pr} is the weight of the measured pseudorange,

$\sigma_{\epsilon_{pr}}^2$ is the noise of the pseudorange (m^2),

W_{phase} is the weight of the carrier phase, and

$\sigma_{\epsilon_{phase}}^2$ is the noise of the carrier phase (m^2).

The following graph shows various smoothed pseudorange standard deviations over time assuming raw pseudorange noise standard deviations of seven, five, three and one metre.

As can be seen in the graphs, after 95 observations, the standard deviation of the smoothed pseudorange rapidly converges to the noise level assumed for the carrier phase difference.

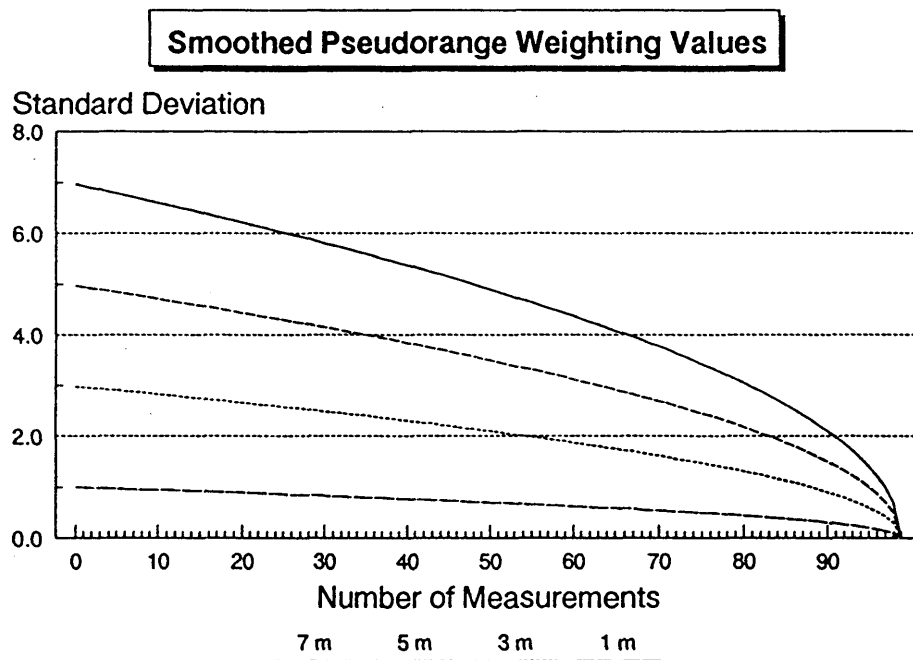


Figure 5.5

5.4.1 Effect of the Ionosphere on Carrier Smoothing

The effect of the ionosphere on the carrier phase and pseudorange are of the same magnitude but opposite in sign. The ionosphere tends to retard the pseudorange, while it advances the carrier phase. This affects the integration of the two measurements since it is assumed in eqn (5.85) that they are identical except for their noise characteristics. If not taken into account, the ionosphere causes a drift in the smoothed pseudorange. A study on

this is reported in Loomis et al. [1989].

In order to reduce the divergence of the code and the carrier, two smoothing filters are operated in parallel [Cannon, 1990]. The first filter is reset after 200 epochs as shown in Figure 5.6 and then the second filter is used to produce the smoothed measurements. This moving window technique reduces the length of time a particular filter is implemented. The assumption here is that there is no divergence between code and carrier during the 200 epochs.

At initialization and after cycle slips, the two ramps are started at the same time. After 100 epochs, the first filter is reset and the second filter is used for 100 more epochs. By this time (epoch 200), the second filter is reset and the first ramp is used again. The 200 epoch length is important since this implies that each filter is used after 100 epochs, the amount of epochs needed to reduce the weight of the smoothed pseudorange to about 10 cm.

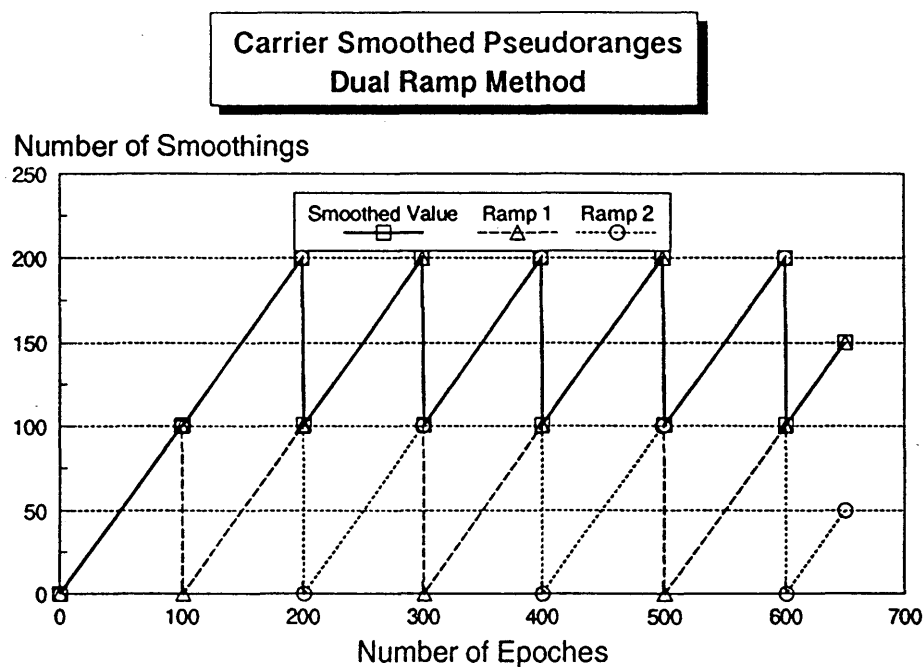


Figure 5.6

5.5 Observation Weighting

The variance of a pseudorange measurement can be expressed as a function of the pseudorange errors. Detailing these errors gives the variance, σ_p^2 , as

$$\sigma_p^2 \approx \sigma_\epsilon^2 + \sigma_{\delta trop}^2 + \sigma_{\delta ion}^2 + \sigma_{\delta \epsilon}^2 + \sigma_{\delta dt}^2, \quad (5.90)$$

where

σ_ϵ^2 is the measurement noise,

$\sigma_{\delta trop}^2$ is the residual unmodelled troposphere,

$\sigma_{\delta ion}^2$ is the residual unmodelled ionosphere,

$\sigma_{\delta dt}^2$ is the residual satellite clock error, and

$\sigma_{\delta \epsilon}^2$ is the orbital error.

Clearly from the above equation, the observation variance is dependent on the magnitude of the residual errors, especially the troposphere and ionosphere. The nominal measurement noise is dependent on vehicle dynamics (i.e. on receiver bandwidth) but will not play a significant role in changing the measurement variance. When carrier smoothing is done, the measurement noise decreases, due to the low noise, on the carrier phase. Therefore, the actual measurement noise, σ_ϵ^2 , is a function of the relative weights on the code and the carrier, i.e.,

$$\sigma_\epsilon^2 = W_{pr} \sigma_{\epsilon_{pr}}^2 + W_{phase} \sigma_{\epsilon_{phase}}^2. \quad (5.91)$$

Typical C/A code accuracies in dynamic mode are about 2 to 3 m and the carrier noise is about 1 cm [Cannon, 1991b].

Orbital and satellite clock errors are a function of whether the pseudorange is differentially corrected. If it is not, then the errors would typically be 15 m for Block I and 30 m for Block II. In differential mode, these errors are virtually eliminated, but a nominal error of say 1 m will be used (e.g. 5 ppm over 200 km).

The ionospheric and tropospheric effects increase dramatically as the satellite elevation decreases. In order to maintain a better reliability of the results, measurements are de-weighted as they drop in elevation. In the case of the ionospheric effect, the residual unmodelled ionospheric error as a function of elevation is given by Martin, [1980] as

$$\sigma_{\delta ion}^2 = \{ \Delta K csc (EL^2 + 20^2)^{1/2} \}^2, \quad (5.92)$$

where

ΔK is the fractional value of reduced ionospheric delay ($0.5m < \Delta K < 5m$), and

EL is the satellite elevation in degrees.

The value of ΔK can be varied according to ionospheric activity. Similarly, the residual unmodelled tropospheric error as a function of elevation is given by Martin, [1980], namely:

$$\sigma_{\delta trop}^2 = \left\{ \Delta C \exp\left(-\frac{0.034}{T}h\right) csc(EL) \right\}^2, \quad (5.93)$$

where

ΔC is the residual compensation magnitude ($\Delta C \approx 0.1m$),

T is the temperature (K°), and

h is the vehicle altitude (m).

Once these two variances have been computed, they are used along with the other variances to form the elevation-dependent pseudorange variance.

The variance of a phase rate measurement, $\sigma_{\dot{\phi}}^2$, can be expressed as

$$\sigma_{\dot{\Phi}}^2 \approx \sigma_e^2 + \sigma_{\text{trop}}^2 + \sigma_{\text{ion}}^2 + \sigma_{\text{oc}}^2 + \sigma_{\text{dt}}^2 , \quad (5.94)$$

where the dot (.) represents a derivative with respect to time. Rather than derive a complicated model for the measurement variance which is dependent on satellite elevation, an empirical variance can be used depending on the observing scenario, e.g. as shown in Table 5.1

Table 5.1 Standard Deviation of Phase Rate Measurements (after Cannon, 1991b)

Scenario	Std. Dev. (cm s ⁻¹)
Single Point, Block I	6
Single Point, Block II	10
Differential, Block I	3
Differential, Block II	6

5.6 Cycle Slip Detection in the Carrier Phase Data

In order to maintain positioning accuracy and reliability, carrier phase cycle slips must be detected. Several methods for detecting cycle slips are discussed in the following Sections.

5.6.1 Phase Velocity Method

The phase at some epoch t_k can be predicted using the phase measurement at t_k and t_{k-1} as follows [Cannon, 1990]:

$$\hat{\Phi}_k = \Phi_{k-1} + \frac{\dot{\Phi}_k + \dot{\Phi}_{k-1}}{2} \Delta t , \quad (5.95)$$

where

$\hat{\Phi}_k$ is the predicted phase measurement at t_k ,

- Φ_{k-1} is the phase measurement at t_{k-1} ,
- $\dot{\Phi}_k$ is the phase rate measurement at t_k ,
- $\dot{\Phi}_{k-1}$ is the phase rate measurement at t_{k-1} , and
- Δt is equal to $t_k - t_{k-1}$.

Eqn (5.95) assumes that the phase rates are available as part of the measurement record and that the phase acceleration is constant over the interval, Δt . If the phase rates are not available, the actual phase measurement could be modelled over time to determine the phase rate. The above equation also assumes that the phase rate and phase measurements are independent such that a cycle slip in the carrier phase will not affect the phase rate measurement. If they are not independent, Eqn (5.95) could be modified to the form

$$\hat{\Phi}_k = \Phi_{k-1} + \dot{\Phi}_{k-1} \Delta t \quad (5.96)$$

in which no t_k appear other than t_k itself. Clearly this will reduce the accuracy of the prediction since the phase velocity is assumed constant over the interval, Δt .

Once the phase measurement is predicted, it can be differenced with the measured phase at that epoch, and then compared to a tolerance value as shown in the following equation.

$$|\hat{\Phi}_k - \Phi_k| < \text{tolerance} ? \quad (5.97)$$

If the absolute value of the difference is greater than the selected tolerance, cycle slips are detected, otherwise the measurement is accepted as error-free. The selection of the tolerance value is critical as this determines the cycle slip capability. Clearly, the value should be as small as possible so no cycle slips will creep into the solution and thus bias the results. However, if the value is selected too small, there is a risk that cycle slips will be detected when in fact they did not occur. Therefore, a balance between acceptable cycle

allowance and positioning accuracy requirements must be determined. Empirical testing is used to determine the tolerance value. Vehicle dynamics along with receiver data rate are the two most important factors affecting the selection of the tolerance.

5.6.2 Pseudorange Method

Another method to test for cycle slip occurrence is to compare the range difference derived from the pseudorange with the range difference derived from the carrier phase as follows:

$$|(\Phi_k - \Phi_{k-1}) - (P_{k+1} - P_k)| < \text{tolerance} ? \quad (5.98)$$

In this case the selection of the tolerance is based solely on the noise of the pseudorange measurement. Since it is approximately one to two meters, the tolerance would be 15 - 30 cycles (3σ). This method also requires empirical testing to determine a tolerance value. It must be noted that the noise on the pseudorange measurement increases with vehicle dynamics due to the increased code tracking bandwidth. Also, since multipath affects pseudoranges much more than the carrier phase, deviations between the data types may not necessarily be due to cycle slips.

5.6.3 Treatment of Cycle Slips

Once the cycle slips have been detected, the smoothing process must be re-initialized. In other words eqn (5.84) must be invoked to reset the smoothing procedure on the satellite in which the slip occurred. Positioning accuracy decreases when cycle slips occur, hence accuracy will tend toward pure pseudorange accuracy. A discontinuity in the positioning accuracy results, but is not that significant if a number of satellites are being tracked.

5.7 Pseudorange and Carrier Phase Measurements

The Magnavox MX 4200 and GPS Engine have two independent tracking loops - one code loop which yields pseudorange measurements (P), and one carrier loop which yields

carrier phase measurements (Φ) [Chamberlain and Chuang, 1991]. These two observables are complementary, in that pseudoranges give absolute information on the position of the observer (x, y, z) but these measurements are noisy ($\sigma_p = 5m$) [Wells et al., 1986]. On the other hand, the carrier phase measurements only give relative information; change in phase (change in range or integrated Doppler) over time ($\delta\Phi$) yields information on change in vehicle position, while phase rate ($\delta\dot{\Phi}$) yields information on the velocity ($\dot{x}, \dot{y}, \dot{z}$).

The carrier is intrinsically stable [Huang and Brown, 1990] and accurate ($\sigma_\Phi = 7mm$) [Wells et al., 1986] and can help to improve the accuracy of the solution. It is, however, plagued by the problem of cycle slips when loss of lock occurs during tracking of the beat frequency. This problem results in discontinuities (jumps) of the determined position change. Clearly, a system devised to combine ρ and Φ must be robust and fault tolerant. Below we aim to achieve this objective, but, first we give the detailed models for GPS pseudorange P , phase Φ , phase difference $\delta\Phi$, and phase rate $\delta\dot{\Phi}$.

5.7.1 Range Model

Cartesian Formulation:

The range model (Figure 5.7) for the basic unit of one tracking station and one satellite j at time epoch t_k is [Wells et al., 1986]

$$P_k^j = \rho_k^j + c(dt_k - dT_k)^j + d_{ion_k}^j + d_{trop_k}^j + d\varrho_k^j, \quad (5.99)$$

where P_k^j is the pseudorange measurement to satellite j at t_k and

$$\rho_k^j = |\vec{r}_k^j - \vec{R}_k| = [(x_k^j - x_k)^2 + (y_k^j - y_k)^2 + (z_k^j - z_k)^2]^{1/2} \quad (5.100)$$

where

Pseudorange Model

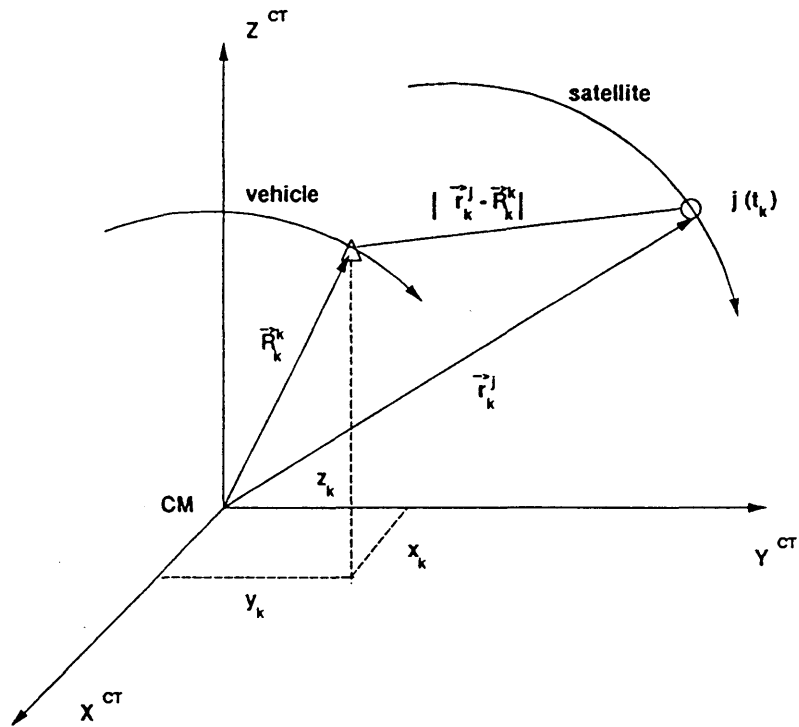


Figure 5.7.

- ρ_k^j is the tracking station-satellite range expressed as a function of the known satellite Cartesian coordinates $\vec{r}_k^j = [x_k^j \ y_k^j \ z_k^j]^T$ and the unknown tracking station coordinates $\vec{R}_k = [x_k \ y_k \ z_k]^T$ at time t_k ,
- dt is the offset of the satellite clock from GPS time,
- dT is the offset of the receiver clock from GPS time,
- $d_{ion_k}^j$ is the ionospheric correction to be applied to the P_k^j ,
- $d_{trop_k}^j$ is the tropospheric correction to be applied to P_k^j , and

dQ_k^j is the equivalent range error arising from orbital parameter inaccuracies.

With respect to orbital errors, nothing can be done with this quantity when observing from only one station, however, it can be determined and applied as a correction when observations are made in conjunction with a receiver at a fixed-known point or dQ_k^j may be determined from an Active Control Point (ACP) and broadcast to users.

The linearized version of eqn (5.99) is [Lachapelle et al., 1986]

$$l_k^e + v_k^e = A_k^e x_k \quad , \quad C_k^e \quad (5.101)$$

where

l_k^e is the vector of range observations to satellites, and

A is the design matrix.

A_k^e corresponds to $j=1, 2, \dots, s$ satellites and is observed as

$$A_k^e = \begin{bmatrix} \frac{(x_k^1 - x_k)}{Q_k^1} & \frac{(y_k^1 - y_k)}{Q_k^1} & \frac{(z_k^1 - z_k)}{Q_k^1} & 1 \\ \frac{(x_k^2 - x_k)}{Q_k^2} & \frac{(y_k^2 - y_k)}{Q_k^2} & \frac{(z_k^2 - z_k)}{Q_k^2} & 1 \\ \cdot & \cdot & \cdot & \cdot \\ \cdot & \cdot & \cdot & \cdot \\ \cdot & \cdot & \cdot & \cdot \\ \frac{(x_k^s - x_k)}{Q_k^s} & \frac{(y_k^s - y_k)}{Q_k^s} & \frac{(z_k^s - z_k)}{Q_k^s} & 1 \end{bmatrix} \quad , \quad (5.102)$$

the vector of unknowns is

$$x_k = [x_k \quad y_k \quad z_k \quad dT_k]^T \quad , \quad (5.103)$$

and v_k^e is the vector of range residuals.

The linearized model (eqn (5.101)) can be put in the following differential form if approximate values (x_k^o, y_k^o, z_k^o) of the vehicles coordinates are used, namely:

$$v_k^o = A_k^o \delta x_k + w_k \quad , \quad (5.104)$$

where

$$w_k = \begin{bmatrix} (Q_k^1)^o - Q_k^1 \\ (Q_k^2)^o - Q_k^2 \\ \cdot \\ \cdot \\ (Q_k^s)^o - Q_k^s \end{bmatrix} \quad (5.105)$$

is the misclosure vector and is evaluated as the difference between the approximate range (computed as a function of the approximate vehicle coordinates (x_k^o, y_k^o, z_k^o) and the satellite coordinates) and the observed range; and

$$\delta x_k = [\delta x_k \quad \delta y_k \quad \delta z_k \quad \delta dT_k]^T \quad (5.106)$$

is the unknown vector of corrections $(\delta x_k, \delta y_k, \delta z_k)$ to the approximate vehicle coordinates.

Geodetic Formulation:

In order to work in the geodetic system, it is a requirement to transform the Cartesian x, y, z coordinates into the geodetic curvilinear ϕ, λ, h coordinates. The transformation can be accomplished by the following equations:

$$e^2 = \frac{a^2 - b^2}{a^2} \quad , \quad (5.107)$$

$$N = \frac{a}{(1 - e^2 \sin^2 \phi)^{1/2}} \quad , \quad (5.108)$$

$$x_r = (N + h) \cos \phi \cos \lambda \quad , \quad (5.109)$$

$$y_r = (N + h) \cos \phi \sin \lambda \quad , \quad (5.110)$$

$$z_r = (N(1 - e^2) + h) \sin \phi \quad , \quad (5.111)$$

where

- a is the semi-major axis of the WGS84 ellipsoid,
- b is the semi-minor axis of the WGS84 ellipsoid,
- e is the eccentricity of the WGS84 ellipsoid,
- N is the radius of curvature in the prime vertical,
- ϕ is the latitude,
- λ is the longitude, and
- h is the ellipsoid height.

Equation (5.100) can be rewritten as

$$\rho_k^j = \left((x_k^j - x_k(\phi, \lambda, h))^2 + (y_k^j - y_k(\phi, \lambda, h))^2 + (z_k^j - z_k(\phi, \lambda, h))^2 \right)^{1/2} \quad . \quad (5.112)$$

Linearizing the above equations (see eqn 5.101) with respect to ϕ, λ, h yields

$$\delta \rho_k^j = \frac{\partial \rho_k^j}{\partial \phi_k} \delta \phi_k + \frac{\partial \rho_k^j}{\partial \lambda_k} \delta \lambda_k + \frac{\partial \rho_k^j}{\partial h_k} \delta h_k \quad . \quad (5.113)$$

Using the chain rule, the partial derivatives of the pseudorange measurement with respect to the users position in ϕ, λ, h coordinate system are the following:

$$\frac{\partial \rho_k^j}{\partial \phi_k} = \frac{\partial \rho_k^j}{\partial x_k} \frac{\partial x_k}{\partial \phi_k} + \frac{\partial \rho_k^j}{\partial y_k} \frac{\partial y_k}{\partial \phi_k} + \frac{\partial \rho_k^j}{\partial z_k} \frac{\partial z_k}{\partial \phi_k} \quad , \quad (5.114)$$

$$\frac{\partial \rho_k^j}{\partial \lambda_k} = \frac{\partial \rho_k^j}{\partial x_k} \frac{\partial x_k}{\partial \lambda_k} + \frac{\partial \rho_k^j}{\partial y_k} \frac{\partial y_k}{\partial \lambda_k} + \frac{\partial \rho_k^j}{\partial z_k} \frac{\partial z_k}{\partial \lambda_k} \quad , \quad \text{and} \quad (5.115)$$

$$\frac{\partial \rho_k^j}{\partial h_k} = \frac{\partial \rho_k^j}{\partial x_k} \frac{\partial x_k}{\partial h_k} + \frac{\partial \rho_k^j}{\partial y_k} \frac{\partial y_k}{\partial h_k} + \frac{\partial \rho_k^j}{\partial z_k} \frac{\partial z_k}{\partial h_k} \quad . \quad (5.116)$$

From the above equations

$$\frac{\partial \varrho_k^j}{\partial x_k} = -\frac{(x_k^j - x_k)}{\varrho_k^j} , \quad (5.117)$$

$$\frac{\partial \varrho_k^j}{\partial y_k} = -\frac{(y_k^j - y_k)}{\varrho_k^j} , \quad (5.118)$$

$$\frac{\partial \varrho_k^j}{\partial z_k} = -\frac{(z_k^j - z_k)}{\varrho_k^j} , \quad (5.119)$$

where x_k, y_k, z_k are computed as a function of ϕ, λ, h .

From equations (5.114) to (5.116) we have

$$\frac{\partial N}{\partial \phi} = \frac{ae^2 \sin(2\phi)}{2(1 - e^2 \sin^2 \phi)^{3/2}} , \quad (5.120)$$

$$\frac{\partial x_k}{\partial \phi} = \frac{\partial N}{\partial \phi} \cos \phi \cos \lambda - (N + h) \sin \phi \cos \lambda , \quad (5.121)$$

$$\frac{\partial y_k}{\partial \phi} = \frac{\partial N}{\partial \phi} \cos \phi \sin \lambda - (N + h) \sin \phi \sin \lambda , \quad (5.122)$$

$$\frac{\partial z_k}{\partial \phi} = \frac{\partial N}{\partial \phi} (1 - e^2) \sin \phi + (N(1 - e^2) + h) \cos \phi , \quad (5.123)$$

$$\frac{\partial x_k}{\partial \lambda} = -(N + h) \cos \phi \sin \lambda , \quad (5.124)$$

$$\frac{\partial y_k}{\partial \lambda} = (N + h) \cos \phi \cos \lambda , \quad (5.125)$$

$$\frac{\partial z_k}{\partial \lambda} = 0 , \quad (5.126)$$

$$\frac{\partial x_k}{\partial h} = \cos \phi \cos \lambda \quad , \quad (5.127)$$

$$\frac{\partial y_k}{\partial h} = \cos \phi \sin \lambda \quad , \quad \text{and} \quad (5.128)$$

$$\frac{\partial z_k}{\partial h} = \sin \phi \quad . \quad (5.129)$$

N is often treated as being a constant resulting in the following:

$$\frac{\partial \rho_k^j}{\partial \phi_k} = a_k^j = (N+h) \sin \phi \cos \lambda \frac{(x_k^j - x_k)}{\rho_k^j} + (N+h) \sin \phi \sin \lambda \frac{(y_k^j - y_k)}{\rho_k^j} - \frac{(N(1-e^2)+h) \cos \phi (z_k^j - z_k)}{\rho_k^j} \quad , \quad (5.130)$$

$$\frac{\partial \rho_k^j}{\partial \lambda_k} = b_k^j = (N+h) \cos \phi \sin \lambda \frac{(x_k^j - x_k)}{\rho_k^j} - (N+h) \cos \phi \cos \lambda \frac{(y_k^j - y_k)}{\rho_k^j} \quad , \quad (5.131)$$

$$\frac{\partial \rho_k^j}{\partial h_k} = c_k^j = -\cos \phi \cos \lambda \frac{(x_k^j - x_k)}{\rho_k^j} - \cos \phi \sin \lambda \frac{(y_k^j - y_k)}{\rho_k^j} - \sin \phi \frac{(z_k^j - z_k)}{\rho_k^j} \quad . \quad (5.132)$$

the design matrix corresponding to $j=1, 2, \dots, s$ satellites observed is

$$A_k^o = \begin{bmatrix} a_k^1 & b_k^1 & c_k^1 & 1 \\ a_k^2 & b_k^2 & c_k^2 & 1 \\ \cdot & \cdot & \cdot & \cdot \\ \cdot & \cdot & \cdot & \cdot \\ \cdot & \cdot & \cdot & \cdot \\ a_k^s & b_k^s & c_k^s & 1 \end{bmatrix} \quad , \quad (5.133)$$

the vector of unknowns is

$$x_k = [\phi_k \quad \lambda_k \quad h_k \quad dT_k]^T \quad , \quad (5.134)$$

and v_k^o is the vector of range residuals.

The linearized model (eqn (5.101)) can be put in the following differential form if approximate values $(\phi_k^o, \lambda_k^o, h_k^o)$ of the vehicles coordinates are used, namely:

$$v_k^o = A_k^o \delta x_k + w_k \quad , \quad (5.135)$$

where

$$w_k = \begin{bmatrix} (\rho_k^1)^o - \rho_k^1 \\ (\rho_k^2)^o - \rho_k^2 \\ \cdot \\ \cdot \\ (\rho_k^s)^o - \rho_k^s \end{bmatrix} \quad (5.136)$$

is the misclosure vector and is evaluated as the difference between the approximate range (computed as a function of the approximate vehicle coordinates $(\phi_k^o, \lambda_k^o, h_k^o)$ and the satellite coordinates) and the observed range; and

$$\delta x_k = [\delta\phi_k \quad \delta\lambda_k \quad \delta h_k \quad \delta dT_k]^T \quad (5.137)$$

is the unknown vector of corrections $(\delta\phi_k, \delta\lambda_k, \delta h_k)$ to the approximate vehicle coordinates.

5.7.2 Phase and Phase Difference Models

Cartesian Formulation:

The carrier phase model in question corresponds to the phase (Φ) difference (δ) over a short time period ($\delta\Phi$). The latter observable is determined from the Doppler effect and corresponds to the range difference between time epoch t_{k-1} and t_k (Figure 5.8).

The first model encountered enroute to the phase difference ($\delta\Phi$) and phase rate ($\delta\dot{\Phi}$) model is the instantaneous phase (Φ) model. For the j^{th} satellite observed from a moving vehicle at time t_k , we have the following mathematical model for the instantaneous (non differenced) phase Φ_k^j [Wells et al., 1986]:

Phase Difference Model

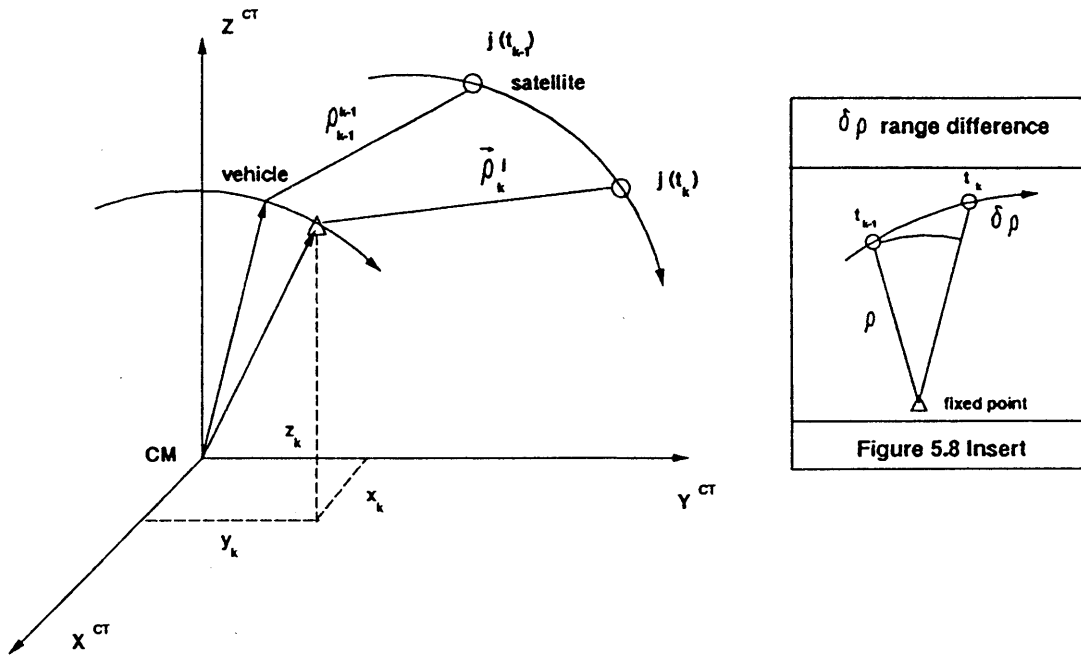


Figure 5.8.

$$\Phi_k^j = \varrho_k^j + dT_k + \lambda N^j - d_{ion_k}^j + d_{trop_k}^j + \delta \varrho_k^j \quad , \quad (5.138)$$

where

λN^j is the newly introduced quantity of the unknown integer wave lengths that have occurred before "lock-on" and they have to be solved for and added to the partially observed phase since "lock on",

dT_k is the unknown clock error to be solved for,

$d_{ion_k}^j$ is the ionospheric correction to the phase (note the sign),

$d_{trop_k}^j$ is the tropospheric correction to the phase,

$\delta\mathcal{Q}_k^j$ is again the problematic range equivalent orbit error, and

\mathcal{Q}_k^j is the function (eqn (5.100)) that contains the unknown vehicle coordinates.

The corresponding linearized model is

$$\mathbf{l}_k^\Phi + \mathbf{v}_k^\Phi = \mathbf{A}_k^\Phi \mathbf{x}_k \quad , \quad \mathbf{C}_k^\Phi \quad (5.139)$$

where

\mathbf{l}_k^Φ is the vector of phase observables,

\mathbf{v}_k^Φ is the vector of phase residuals,

\mathbf{A}_k^Φ is the design matrix and is equivalent to that for ranges (eqn 5.102) except for the presence of the ambiguity unknown; and

\mathbf{C}_k^Φ is the covariance matrix for the Φ_k^j .

For the objective at hand, namely, combining GPS ranges and phase measurements for kinematic point positioning, it is more expedient to avoid the ambiguity unknown of the phase measurements because of the impossibility to solve for them while observing from a single moving point. A more useful model, in this context, is that for time differenced phase ($\delta\Phi$) namely:

$$\delta\Phi_{k-1,k}^j = \delta\mathcal{Q}_{k-1,k}^j + \delta\Delta T_{k-1,k} + \delta d_{ion_{k-1,k}}^j + \delta d_{trop_{k-1,k}}^j + \delta\mathcal{Q}_{k-1,k}^j \quad , \quad (5.140)$$

where

$$\delta\mathcal{Q}_{k-1,k}^j = \left[(x_k^j - x_{k-1}^j)^2 + (y_k^j - y_{k-1}^j)^2 + (z_k^j - z_{k-1}^j)^2 \right]^{1/2} - \left[(x_{k-1}^j - x_{k-2}^j)^2 + (y_{k-1}^j - y_{k-2}^j)^2 + (z_{k-1}^j - z_{k-2}^j)^2 \right]^{1/2} \quad (5.141)$$

is the function which contains the known satellite coordinates for the j^{th} satellite and the unknown vehicle coordinates at t_{k-1} and t_k , and $\delta dT_{k-1,k}$ is the unknown receiver clock drift over t_{k-1} and t_k , while the two refraction corrections are applied apriori over the time interval t_{k-1}, t_k .

The linearization of the model (eqn (5.140)) yields the following matrix equation for the time differenced phase observable:

$$l_{k-1,k}^{\delta\Phi} + v_{k-1,k}^{\delta\Phi} = A_{k-1,k}^{\delta\Phi} x_{k-1,k} \quad , \quad C_{k-1,k}^{\delta\Phi} \quad (5.142)$$

where

$l_{k-1,k}^{\delta\Phi}$ is the vector of phase difference observables,

$v_{k-1,k}^{\delta\Phi}$ is the residual vector, and

$C_{k-1,k}^{\delta\Phi}$ is the corresponding covariance matrix of the $\delta\Phi$.

The design matrix is given as follows:

$$A_{k-1,k}^{\delta\Phi} = \left[\begin{array}{ccc|ccc|c} -\Delta x_{k-1}^1 & -\Delta y_{k-1}^1 & -\Delta z_{k-1}^1 & -\Delta x_k^1 & -\Delta y_k^1 & -\Delta z_k^1 & 1 \\ \frac{Q_{k-1}^1}{Q_{k-1}^1} & \frac{Q_{k-1}^1}{Q_{k-1}^1} & \frac{Q_{k-1}^1}{Q_{k-1}^1} & \frac{Q_k^1}{Q_k^1} & \frac{Q_k^1}{Q_k^1} & \frac{Q_k^1}{Q_k^1} & \\ -\Delta x_{k-1}^2 & -\Delta y_{k-1}^2 & -\Delta z_{k-1}^2 & -\Delta x_k^2 & -\Delta y_k^2 & -\Delta z_k^2 & 1 \\ \frac{Q_{k-1}^2}{Q_{k-1}^2} & \frac{Q_{k-1}^2}{Q_{k-1}^2} & \frac{Q_{k-1}^2}{Q_{k-1}^2} & \frac{Q_k^2}{Q_k^2} & \frac{Q_k^2}{Q_k^2} & \frac{Q_k^2}{Q_k^2} & \\ \cdot & \cdot & \cdot & \cdot & \cdot & \cdot & \cdot \\ \cdot & \cdot & \cdot & \cdot & \cdot & \cdot & \cdot \\ \cdot & \cdot & \cdot & \cdot & \cdot & \cdot & \cdot \\ -\Delta x_{k-1}^s & -\Delta y_{k-1}^s & -\Delta z_{k-1}^s & -\Delta x_k^s & -\Delta y_k^s & -\Delta z_k^s & 1 \\ \frac{Q_{k-1}^s}{Q_{k-1}^s} & \frac{Q_{k-1}^s}{Q_{k-1}^s} & \frac{Q_{k-1}^s}{Q_{k-1}^s} & \frac{Q_k^s}{Q_k^s} & \frac{Q_k^s}{Q_k^s} & \frac{Q_k^s}{Q_k^s} & \end{array} \right] , \quad (5.143)$$

where Δ is the difference between satellite and tracking station coordinates, while the vector of unknowns

$$x_{k-1,k} = [x_{k-1} \quad y_{k-1} \quad z_{k-1} \quad x_k \quad y_k \quad z_k \quad \delta dT_{k-1,k}]^T \quad . \quad (5.144)$$

Note that phase difference information yields only position information, and a nuisance parameter for unknown clock drift must be present. Combining the above model with the pseudorange model will be one of the possibilities when making a decision of how to combine GPS observables. The model can be transformed into a differential form as in eqn (5.104).

Geodetic Formulation:

Expressing eqn (5.141) in geodetic coordinates yields:

$$\delta Q_{k-1,k}^j = \left[(x_k^j - x(\phi, \lambda, h)_k)^2 + (y_k^j - y(\phi, \lambda, h)_k)^2 + (z_k^j - z(\phi, \lambda, h)_k)^2 \right]^{1/2} - \left[(x_{k-1}^j - x(\phi, \lambda, h)_{k-1})^2 + (y_{k-1}^j - y(\phi, \lambda, h)_{k-1})^2 + (z_{k-1}^j - z(\phi, \lambda, h)_{k-1})^2 \right]^{1/2}, \quad (5.145)$$

and is the function which contains the known satellite coordinates for the j^{th} satellite and the unknown vehicle coordinates at t_{k-1} and t_k , $\delta dt_{k-1,k}$ is the unknown receiver clock drift over t_{k-1} and t_k , while the two refraction corrections are applied a priori over the time interval t_{k-1}, t_k .

The design matrix corresponding to $j=1, 2, \dots, s$ satellites observed is

$$A_k^e = \begin{bmatrix} a_k^1 & b_k^1 & c_k^1 & | & d_k^1 & e_k^1 & f_k^1 & | & 1 \\ a_k^2 & b_k^2 & c_k^2 & | & d_k^2 & e_k^2 & f_k^2 & | & 1 \\ \cdot & \cdot & \cdot & | & \cdot & \cdot & \cdot & | & \cdot \\ \cdot & \cdot & \cdot & | & \cdot & \cdot & \cdot & | & \cdot \\ \cdot & \cdot & \cdot & | & \cdot & \cdot & \cdot & | & \cdot \\ a_k^s & b_k^s & c_k^s & | & d_k^s & e_k^s & f_k^s & | & 1 \end{bmatrix}, \quad (5.146)$$

where

$$a_k^j = (N+h) \sin \phi \cos \lambda \frac{(x_{k-1}^j - x_{k-1})}{Q_{k-1}^j} + (N+h) \sin \phi \sin \lambda \frac{(y_{k-1}^j - y_{k-1})}{Q_{k-1}^j} - (N(1-e^2)+h) \cos \phi \frac{(z_{k-1}^j - z_{k-1})}{Q_{k-1}^j}, \quad (5.147)$$

$$b_k^j = (N+h) \cos \phi \sin \lambda \frac{(x_{k-1}^j - x_{k-1})}{\varrho_{k-1}^j} - (N+h) \cos \phi \cos \lambda \frac{(y_{k-1}^j - y_{k-1})}{\varrho_{k-1}^j}, \quad (5.148)$$

$$c_k^j = \cos \phi \cos \lambda \frac{(x_{k-1}^j - x_{k-1})}{\varrho_{k-1}^j} + \cos \phi \sin \lambda \frac{(y_{k-1}^j - y_{k-1})}{\varrho_{k-1}^j} + \sin \phi \frac{(z_{k-1}^j - z_{k-1})}{\varrho_{k-1}^j}, \quad (5.149)$$

$$d_k^j = (N+h) \sin \phi \cos \lambda \frac{(x_k^j - x_k)}{\varrho_k^j} + (N+h) \sin \phi \sin \lambda \frac{(y_k^j - y_k)}{\varrho_k^j} - (N(1-e^2) + h) \cos \phi \frac{(z_k^j - z_k)}{\varrho_k^j}, \quad (5.150)$$

$$e_k^j = (N+h) \cos \phi \sin \lambda \frac{(x_k^j - x_k)}{\varrho_k^j} - (N+h) \cos \phi \cos \lambda \frac{(y_k^j - y_k)}{\varrho_k^j}, \quad (5.151)$$

$$f_k^j = \cos \phi \cos \lambda \frac{(x_k^j - x_k)}{\varrho_k^j} + \cos \phi \sin \lambda \frac{(y_k^j - y_k)}{\varrho_k^j} + \sin \phi \frac{(z_k^j - z_k)}{\varrho_k^j}. \quad (5.152)$$

The vector of unknowns is

$$x_{k-1,k} = [\phi_{k-1} \quad \lambda_{k-1} \quad h_{k-1} \quad \phi_k \quad \lambda_k \quad h_k \quad dT_{k-1,k}]^T. \quad (5.153)$$

5.7.3 Phase Rate Model

Cartesian Formulation:

The phase rate model ($\delta\dot{\Phi} \equiv \dot{\varrho}$) is considered next, because it is this observable that gives information on the position (x,y,z) of the vehicle but mainly on its velocity $(\dot{x}, \dot{y}, \dot{z})$ (Figure 5.9). For kinematic applications, this is an important observable. Some receivers yield this observable directly (e.g., the TI 4100 [Schwarz et al., 1989]) while with other receivers, one has to construct $\delta\dot{\Phi}$ from phase difference $\delta\Phi$ measurements simply by forming the difference $\Phi_k - \Phi_{k-1}$ and dividing by $\Delta t_{k-1,k} = t_k - t_{k-1}$ (e.g., the MX4200 [Chamberlain and Chuang, 1991]).

Phase Rate Model

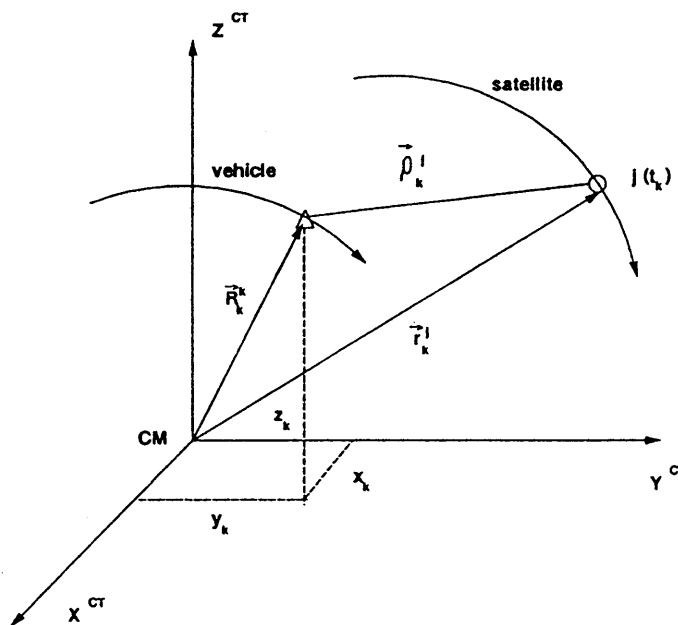


Figure 5.9.

The phase rate model [e.g. Schwarz et al., 1989; Chamberlain and Chuang, 1991] is obtained by differentiating the range model (eqn (5.99)) with respect to time, namely:

$$\dot{\varrho} = \frac{d\varrho}{dt} + c \frac{dT}{dt} = \frac{\partial \varrho}{\partial \vec{\varrho}} \frac{\partial \vec{\varrho}}{\partial t} + c d\dot{T} \quad (5.154)$$

by the chain rule of total and partial derivatives,

where

$$\vec{\varrho} = \vec{\varrho}_k^j = \vec{r}_k^j - \vec{R}_k = \begin{bmatrix} x_k^j - x_k \\ y_k^j - y_k \\ z_k^j - z_k \end{bmatrix} = \begin{bmatrix} \Delta x_k^j \\ \Delta y_k^j \\ \Delta z_k^j \end{bmatrix} . \quad (5.155)$$

The second partial derivative in eqn (5.154) is evaluated as follows [Schwarz et al., 1987; Harris, 1988]:

$$\frac{\partial \underline{Q}}{\partial t} = \begin{bmatrix} \frac{\partial x_k^j}{\partial t} - \frac{\partial x_k}{\partial t} \\ \frac{\partial y_k^j}{\partial t} - \frac{\partial y_k}{\partial t} \\ \frac{\partial z_k^j}{\partial t} - \frac{\partial z_k}{\partial t} \end{bmatrix} = \begin{bmatrix} \dot{x}_k^j - \dot{x}_k \\ \dot{y}_k^j - \dot{y}_k \\ \dot{z}_k^j - \dot{z}_k \end{bmatrix} = \begin{bmatrix} \Delta \dot{x}_k^j \\ \Delta \dot{y}_k^j \\ \Delta \dot{z}_k^j \end{bmatrix}, \quad (5.156)$$

which is clearly the difference in the respective Cartesian velocity components of the vehicle and satellite at t_k .

The first total derivative is

$$\frac{\partial \underline{Q}}{\partial \underline{Q}} = \begin{bmatrix} \frac{\partial \underline{Q}}{\partial \Delta x} & \frac{\partial \underline{Q}}{\partial \Delta y} & \frac{\partial \underline{Q}}{\partial \Delta z} \end{bmatrix}, \quad (5.157)$$

recall eqn (5.100)

$$\rho_k^j = [(x_k^j - x_k)^2 + (y_k^j - y_k)^2 + (z_k^j - z_k)^2]^{1/2} \quad (5.158)$$

$$\rho_k^j = [(\Delta x_k)^2 + (\Delta y_k)^2 + (\Delta z_k)^2]^{1/2} \quad (5.159)$$

$$\frac{\partial \underline{Q}}{\partial \underline{Q}} = \begin{bmatrix} \frac{\Delta x_k^j}{\rho_k^j} & \frac{\Delta y_k^j}{\rho_k^j} & \frac{\Delta z_k^j}{\rho_k^j} \end{bmatrix}, \quad (5.160)$$

$$\frac{\partial \underline{Q}}{\partial \underline{Q}} = \begin{bmatrix} \frac{x_k^j - x_k}{\rho_k^j} & \frac{y_k^j - y_k}{\rho_k^j} & \frac{z_k^j - z_k}{\rho_k^j} \end{bmatrix}. \quad (5.161)$$

Substituting the results (eqns (5.156) and (5.159) into (5.154)) yields the following phase rate model:

$$\dot{\rho}_k^j = \frac{d\rho}{dt} = \frac{\Delta x_k^j}{\rho_k^j} \Delta \dot{x}_k^j + \frac{\Delta y_k^j}{\rho_k^j} \Delta \dot{y}_k^j + \frac{\Delta z_k^j}{\rho_k^j} \Delta \dot{z}_k^j + c \delta \dot{T}, \quad (5.162)$$

$$= \left(\frac{x_k^j - x_k}{\rho_k^j} \right) (\dot{x}_k^j - \dot{x}_k) + \left(\frac{y_k^j - y_k}{\rho_k^j} \right) (\dot{y}_k^j - \dot{y}_k) + \left(\frac{z_k^j - z_k}{\rho_k^j} \right) (\dot{z}_k^j - \dot{z}_k) + c \delta \dot{T}, \quad (5.163)$$

rearranging

$$= \left(\frac{\partial \rho_k^j}{\partial x_k} \right) (\dot{x}_k - \dot{x}_k^j) + \left(\frac{\partial \rho_k^j}{\partial y_k} \right) (\dot{y}_k - \dot{y}_k^j) + \left(\frac{\partial \rho_k^j}{\partial z_k} \right) (\dot{z}_k - \dot{z}_k^j) + c \delta \dot{T} \quad , \quad (5.164)$$

where the position unknown parameters x_k, y_k, z_k are contained in the first half of each expression (eqn 5.164) via eqn (5.161), while the velocity unknown parameters $\dot{x}_k, \dot{y}_k, \dot{z}_k$ are contained in the second half of the expressions (eqn 5.164) via eqn (5.156). Note, the remaining unknown parameter $c \delta \dot{T}$ is the clock rate and is a nuisance parameter to be estimated.

The above model is, however, non-linear, and thus needs to be linearized. Using a Taylor series and taking the partial derivatives with respect to the above six position related unknowns, we get the following linear phase rate model:

$$\delta \dot{\rho}_k^j = \frac{\partial \dot{\rho}_k^j}{\partial x_k} \delta x_k + \frac{\partial \dot{\rho}_k^j}{\partial y_k} \delta y_k + \frac{\partial \dot{\rho}_k^j}{\partial z_k} \delta z_k + \frac{\partial \dot{\rho}_k^j}{\partial \dot{x}_k} \delta \dot{x}_k + \frac{\partial \dot{\rho}_k^j}{\partial \dot{y}_k} \delta \dot{y}_k + \frac{\partial \dot{\rho}_k^j}{\partial \dot{z}_k} \delta \dot{z}_k \quad , \quad (5.165)$$

where

$$\frac{\partial \dot{\rho}_k^j}{\partial x_k} = a_k^j = \frac{\partial^2 \rho_k^j}{\partial x_k^2} (\dot{x}_k - \dot{x}_k^j) + \frac{\partial^2 \rho_k^j}{\partial x_k \partial y_k} (\dot{y}_k - \dot{y}_k^j) + \frac{\partial^2 \rho_k^j}{\partial x_k \partial z_k} (\dot{z}_k - \dot{z}_k^j) \quad , \quad (5.166)$$

$$\frac{\partial \dot{\rho}_k^j}{\partial y_k} = b_k^j = \frac{\partial^2 \rho_k^j}{\partial y_k \partial x_k} (\dot{x}_k - \dot{x}_k^j) + \frac{\partial^2 \rho_k^j}{\partial y_k^2} (\dot{y}_k - \dot{y}_k^j) + \frac{\partial^2 \rho_k^j}{\partial y_k \partial z_k} (\dot{z}_k - \dot{z}_k^j) \quad , \quad (5.167)$$

$$\frac{\partial \dot{\rho}_k^j}{\partial z_k} = c_k^j = \frac{\partial^2 \rho_k^j}{\partial z_k \partial x_k} (\dot{x}_k - \dot{x}_k^j) + \frac{\partial^2 \rho_k^j}{\partial z_k \partial y_k} (\dot{y}_k - \dot{y}_k^j) + \frac{\partial^2 \rho_k^j}{\partial z_k^2} (\dot{z}_k - \dot{z}_k^j) \quad , \quad (5.168)$$

where in turn

$$\frac{\partial^2 \rho_k^j}{\partial x_k^2} = \frac{1}{\rho_k^j} - \frac{(\Delta x_k^j)^2}{(\rho_k^j)^3} \quad , \quad (5.169)$$

$$\frac{\partial^2 \varrho_k^j}{\partial y_k^2} = \frac{1}{\varrho_k^j} - \frac{(\Delta y_k^j)^2}{(\varrho_k^j)^3}, \quad (5.170)$$

$$\frac{\partial^2 \varrho_k^j}{\partial z_k^2} = \frac{1}{\varrho_k^j} - \frac{(\Delta z_k^j)^2}{(\varrho_k^j)^3}, \quad (5.171)$$

$$\frac{\partial^2 \varrho_k^j}{\partial x \partial y} = -\frac{\Delta x_k^j \Delta y_k^j}{(\varrho_k^j)^3}, \quad (5.172)$$

$$\frac{\partial^2 \varrho_k^j}{\partial x \partial z} = -\frac{\Delta x_k^j \Delta z_k^j}{(\varrho_k^j)^3}, \quad (5.173)$$

$$\frac{\partial^2 \varrho_k^j}{\partial y \partial z} = -\frac{\Delta y_k^j \Delta z_k^j}{(\varrho_k^j)^3}. \quad (5.174)$$

The phase rate model for several satellites $j = 1, s$ in matrix form is

$$\dot{l}_k^{\circ} + v_k^{\circ} = A_k^{\circ} x_k \quad , \quad C_k^{\circ} \quad (5.175)$$

where

\dot{l}_k° is the vector of phase rate observables,

v_k° is the corresponding residual vector, and

C_k° is the corresponding covariance matrix.

The design matrix is given as follows:

$$A_k^{\dot{Q}} = \begin{bmatrix} a_k^1 & b_k^1 & c_k^1 & | & -\frac{\Delta x_k^1}{Q_k^1} & -\frac{\Delta y_k^1}{Q_k^1} & -\frac{\Delta z_k^1}{Q_k^1} & | & 1 \\ a_k^2 & b_k^2 & c_k^2 & | & \frac{\Delta x_k^2}{Q_k^2} & -\frac{\Delta y_k^2}{Q_k^2} & -\frac{\Delta z_k^2}{Q_k^2} & | & 1 \\ \cdot & \cdot & \cdot & | & \cdot & \cdot & \cdot & | & \cdot \\ \cdot & \cdot & \cdot & | & \cdot & \cdot & \cdot & | & \cdot \\ \vdots & \cdot & \cdot & | & \cdot & \cdot & \cdot & | & \cdot \\ a_k^s & b_k^s & c_k^s & | & -\frac{\Delta x_k^s}{Q_k^s} & -\frac{\Delta y_k^s}{Q_k^s} & -\frac{\Delta z_k^s}{Q_k^s} & | & 1 \end{bmatrix}, \quad (5.176)$$

and the unknown vector is:

$$x_k = [x_k \ y_k \ z_k \ \dot{x}_k \ \dot{y}_k \ \dot{z}_k \ d\dot{T}]^T. \quad (5.177)$$

The model can be transformed into a differential form as in eqn (5.104).

Geodetic Formulation:

Recall from eqn (5.164) that

$$\dot{Q} = \left(\frac{\partial Q}{\partial x_k} \right) (\dot{x}_k - \dot{x}_k^j) + \left(\frac{\partial Q}{\partial y_k} \right) (\dot{y}_k - \dot{y}_k^j) + \left(\frac{\partial Q}{\partial z_k} \right) (\dot{z}_k - \dot{z}_k^j), \quad (5.178)$$

which is written in terms of geodetic coordinates is

$$\dot{Q} = \frac{\partial Q}{\partial x_{k(\phi, \lambda, h)}} \Delta \dot{x} + \frac{\partial Q}{\partial y_{k(\phi, \lambda, h)}} \Delta \dot{y} + \frac{\partial Q}{\partial z_{k(\phi, \lambda, h)}} \Delta \dot{z}. \quad (5.179)$$

The above model is, however, non-linear, and thus needs to be linearized. Using a Taylor series and taking the partial derivatives with respect to the above six position related unknowns, we get the following linear phase rate model:

$$\delta \dot{Q} = \frac{\partial \dot{Q}}{\partial \phi_k} \delta \phi + \frac{\partial \dot{Q}}{\partial \lambda_k} \delta \lambda + \frac{\partial \dot{Q}}{\partial h_k} \delta h + \frac{\partial \dot{Q}}{\partial V_N} \delta V_N + \frac{\partial \dot{Q}}{\partial V_E} \delta V_E + \frac{\partial \dot{Q}}{\partial V_U} \delta V_U, \quad (5.180)$$

where

$$\frac{\partial \dot{Q}}{\partial \phi} = \frac{\partial \dot{Q}}{\partial x} \frac{\partial x}{\partial \phi} + \frac{\partial \dot{Q}}{\partial y} \frac{\partial y}{\partial \phi} + \frac{\partial \dot{Q}}{\partial z} \frac{\partial z}{\partial \phi} , \quad (5.181)$$

$$\frac{\partial \dot{Q}}{\partial \lambda} = \frac{\partial \dot{Q}}{\partial x} \frac{\partial x}{\partial \lambda} + \frac{\partial \dot{Q}}{\partial y} \frac{\partial y}{\partial \lambda} + \frac{\partial \dot{Q}}{\partial z} \frac{\partial z}{\partial \lambda} , \quad (5.182)$$

$$\frac{\partial \dot{Q}}{\partial h} = \frac{\partial \dot{Q}}{\partial x} \frac{\partial x}{\partial h} + \frac{\partial \dot{Q}}{\partial y} \frac{\partial y}{\partial h} + \frac{\partial \dot{Q}}{\partial z} \frac{\partial z}{\partial h} , \quad (5.183)$$

$$\frac{\partial \dot{Q}}{\partial V_N} = \frac{\partial Q}{\partial \phi} \frac{1}{R} , \quad (5.184)$$

$$\frac{\partial \dot{Q}}{\partial V_E} = \frac{\partial Q}{\partial \lambda} \frac{1}{R \cos \phi} , \quad (5.185)$$

$$\frac{\partial \dot{Q}}{\partial V_U} = \frac{\partial Q}{\partial h} , \quad (5.186)$$

and

$$\frac{\partial \dot{Q}}{\partial x_k} = \frac{\partial^2 Q'_k}{\partial x_k^2} (x_k - x'_k) + \frac{\partial^2 Q'_k}{\partial x \partial y} (y_k - y'_k) + \frac{\partial^2 Q'_k}{\partial x \partial z} (z_k - z'_k) , \quad (5.187)$$

$$\frac{\partial \dot{Q}}{\partial y_k} = \frac{\partial^2 Q'_k}{\partial y \partial x} (x_k - x'_k) + \frac{\partial^2 Q'_k}{\partial y^2} (y_k - y'_k) + \frac{\partial^2 Q'_k}{\partial y \partial z} (z_k - z'_k) , \quad (5.188)$$

$$\frac{\partial \dot{Q}}{\partial z_k} = \frac{\partial^2 Q'_k}{\partial z \partial x} (x_k - x'_k) + \frac{\partial^2 Q'_k}{\partial z \partial y} (y_k - y'_k) + \frac{\partial^2 Q'_k}{\partial z^2} (z_k - z'_k) , \quad (5.189)$$

where in turn

$$\frac{\partial^2 Q'_k}{\partial x_k^2} = \frac{1}{Q'_k} - \frac{(\Delta x'_k)^2}{(Q'_k)^3} , \quad (5.190)$$

$$\frac{\partial^2 Q'_k}{\partial y_k^2} = \frac{1}{Q'_k} - \frac{(\Delta y'_k)^2}{(Q'_k)^3} , \quad (5.191)$$

$$\frac{\partial^2 \rho_k^j}{\partial z_k^2} = \frac{1}{\rho_k^j} - \frac{(\Delta z_k^j)^2}{(\rho_k^j)^3} , \quad (5.192)$$

$$\frac{\partial^2 \rho_k^j}{\partial x \partial y} = -\frac{\Delta x_k^j \Delta y_k^j}{(\rho_k^j)^3} , \quad (5.193)$$

$$\frac{\partial^2 \rho_k^j}{\partial x \partial z} = -\frac{\Delta x_k^j \Delta z_k^j}{(\rho_k^j)^3} , \quad (5.194)$$

$$\frac{\partial^2 \rho_k^j}{\partial y \partial z} = -\frac{\Delta y_k^j \Delta z_k^j}{(\rho_k^j)^3} . \quad (5.195)$$

$$\frac{\partial x_k}{\partial \phi} = -(N + h) \sin \phi \cos \lambda , \quad (5.196)$$

$$\frac{\partial y_k}{\partial \phi} = -(N + h) \sin \phi \sin \lambda , \quad (5.197)$$

$$\frac{\partial z_k}{\partial \phi} = (N(1 - e^2) + h) \cos \phi , \quad (5.198)$$

$$\frac{\partial x_k}{\partial \lambda} = -(N + h) \cos \phi \sin \lambda , \quad (5.199)$$

$$\frac{\partial y_k}{\partial \lambda} = (N + h) \cos \phi \cos \lambda , \quad (5.200)$$

$$\frac{\partial z_k}{\partial \lambda} = 0 , \quad (5.201)$$

$$\frac{\partial x_k}{\partial h} = \cos \phi \cos \lambda , \quad (5.202)$$

$$\frac{\partial y_k}{\partial h} = \cos \phi \sin \lambda , \quad \text{and} \quad (5.203)$$

$$\frac{\partial z_k}{\partial h} = \sin \phi \quad . \quad (5.204)$$

The phase rate model for several satellites $j = 1, s$ in matrix form is

$$\dot{l}_k^e + v_k^e = A_k^e x_k \quad , \quad C_k^e \quad (5.205)$$

where

\dot{l}_k^e is the vector of phase rate observables,

v_k^e is the corresponding residual vector, and

C_k^e is the corresponding covariance matrix.

The design matrix is given as follows:

$$A_k^e = \begin{bmatrix} \frac{\partial \dot{Q}^1}{\partial \phi_k} & \frac{\partial \dot{Q}^1}{\partial \lambda_k} & \frac{\partial \dot{Q}^1}{\partial h_k} & | & \frac{\partial \dot{Q}^1}{\partial V_N} & \frac{\partial \dot{Q}^1}{\partial V_E} & \frac{\partial \dot{Q}^1}{\partial V_U} & | & 1 \\ \frac{\partial \dot{Q}^2}{\partial \phi_k} & \frac{\partial \dot{Q}^2}{\partial \lambda_k} & \frac{\partial \dot{Q}^2}{\partial h_k} & | & \frac{\partial \dot{Q}^2}{\partial V_N} & \frac{\partial \dot{Q}^2}{\partial V_E} & \frac{\partial \dot{Q}^2}{\partial V_U} & | & 1 \\ \cdot & \cdot & \cdot & | & \cdot & \cdot & \cdot & | & \cdot \\ \cdot & \cdot & \cdot & | & \cdot & \cdot & \cdot & | & \cdot \\ \cdot & \cdot & \cdot & | & \cdot & \cdot & \cdot & | & \cdot \\ \frac{\partial \dot{Q}^s}{\partial \phi_k} & \frac{\partial \dot{Q}^s}{\partial \lambda_k} & \frac{\partial \dot{Q}^s}{\partial h_k} & | & \frac{\partial \dot{Q}^s}{\partial V_N} & \frac{\partial \dot{Q}^s}{\partial V_E} & \frac{\partial \dot{Q}^s}{\partial V_U} & | & 1 \end{bmatrix} \quad , \quad (5.206)$$

and the unknown vector is:

$$x_k = [\phi_k \quad \lambda_k \quad h_k \quad V_{Nk} \quad V_{Ek} \quad V_{Uk} \quad d\dot{T}]^T \quad . \quad (5.207)$$

The model can be transformed into a differential form as in eqn (5.104).

5.8 Complementary GPS Observables

The following models were presented above:

- (1) pseudorange (ρ),

- (2) instantaneous phase (Φ),
- (3) phase difference ($\delta\Phi$), and
- (4) phase rate ($\delta\dot{\Phi}$ or $\dot{\rho}$).

In the Magnavox (MX4200) receiver there are essentially only two independent observables - the code ranging loop and the carrier phase loop, which means that only two of the above four models can be used. Using more would be committing the sin of using some derived observable which was not independent information, thus, we will limit our choices to only two.

The following two models have been chosen:

- (1) The range model ρ (eqn 5.101) which will be smoothed by differential phases ($\delta\Phi$) or range differences according to the procedure established by Hatch [1982], Lachapelle et al [1986], and Chamberlain and Chuang [1991]. Recall the vector of unknowns was given by eqn (5.103) as follows:

$$\mathbf{x}_k = [x_k \quad y_k \quad z_k \quad dT_k] \quad . \quad (5.208)$$

- (2) The phase rate model ($\delta\dot{\Phi}$ or $\dot{\rho}$; eqn (5.175)) involves the construction of $\delta\dot{\Phi}$ by differencing two instantaneous phase measurements $\Phi_k - \Phi_{k-1}$ and dividing by $\Delta t = t_k - t_{k-1}$ according to Chamberlain and Chuang [1991]. Recall the vector of unknowns was given by eqn (5.177) as follows:

$$\mathbf{x}_k = [x_k \quad y_k \quad z_k \quad \dot{x}_k \quad \dot{y}_k \quad \dot{z}_k \quad d\dot{T}_k] \quad . \quad (5.209)$$

Note that the phase difference $\delta\Phi$ is used twice. Upon closer examination we see that this is not the case. It is used only as an aid in reducing the size of the noise in the range data and it is believed that this usage is of only a second order effect from the point of view "independentness of observables". The second use of $\delta\Phi$ is to construct phase rate observables $\delta\dot{\Phi}$ and is clearly a first order usage of the information.

The above choice of two models clearly points to the possibility of joining the two by forming a hyper system as follows:

$$l_k^* + v_k^* = A_k^* x_k^* \quad , \quad C_k^m \quad , \quad (5.210)$$

where the observables are represented by the following:

$$l_k^* = \begin{bmatrix} l_k^o \\ l_k^{\dot{o}} \end{bmatrix} \quad , \quad v_k^* = \begin{bmatrix} v_k^o \\ v_k^{\dot{o}} \end{bmatrix} \quad , \quad C_k^m = \begin{bmatrix} C_k^o & | & 0 \\ - & - & - \\ 0 & | & C_k^{\dot{o}} \end{bmatrix} \quad , \quad (5.211)$$

and the design matrix and unknown vector are

$$A^* = \begin{bmatrix} A_k^o & | & 0 \\ - & | & - \\ A_k & | & \dot{A}_k \end{bmatrix} \quad , \quad (5.212)$$

$$x_k = [x_k \quad y_k \quad z_k \quad cdT \quad \dot{x}_k \quad \dot{y}_k \quad \dot{z}_k \quad d\dot{T}]^T \quad . \quad (5.213)$$

Note in the above, the design matrices A_k and \dot{A}_k are subsets of the matrix A_k^o corresponding respectively to the subset of unknown parameters $(x_k \quad y_k \quad z_k \quad dT)$ and $(\dot{x}_k \quad \dot{y}_k \quad \dot{z}_k \quad d\dot{T})$.

In other words, using the hyper system eqn (5.210) in a set of Kalman filter equations as the measurement update, would result in what is called a centralized filter approach. Using them separate with their own filters is the decentralized-federated filter approach, and these separate (parallel) filter processes would be fused from time to time to yield a

combined solution. At the other end of the spectrum we could de-couple the two models by dropping the $(x_k \ y_k \ z_k)$ components from the phase rate model and only solving for $(\dot{x}_k \ \dot{y}_k \ \dot{z}_k)$ as is performed by Magnavox [Chamberlain and Chuang, 1991].

5.9 Kinematic State Space Model

In this section the theory given in Chapter 4 regarding kinematic modelling of the vehicle's motion is implemented. At this juncture it is suffice to say that in addition to the knowledge of the vehicle's path as traced out by the measurements (e.g. dead reckoning or GPS carrier phase), there is other independent information that we can introduce into the process about the kinematics of a vehicle's motion. This information arises from the fact that the motion of a land vehicle on a road is not some discrete - discontinuous motion; more realistically it is reasonably well behaved over the short term (e.g. a few seconds). In other words one can only turn so sharply and over short time intervals, thus, a constant velocity can be assumed. Care must be taken to keep the time interval Δt of the kinematic process small enough so that a constant velocity model can be assumed. This simplifies matters considerably.

Using the starting point of Gelb [1974] and Brown [1973], Schwarz et al. [1989] employs the following differential equations to describe the vehicle's motion (eqn (4.6)):

$$\dot{x} = Fx + Gu \quad , \quad (5.214)$$

where

- x is the state vector (position, velocity, time biases)
- \dot{x} is the time derivative of x ,
- F is the dynamics matrix, and
- Gu is the driving noise due to the kinematic model imperfections and vehicle dynamics such as assuming constant velocity of Δt when in fact it is not.

To describe the motion of a land vehicle in an on road situation, a first order Gauss Markov process is used and satisfies the differential equation of the following type [Wong, 1987; Schwarz et al., 1989]:

$$\dot{x} = -\alpha x + w \quad , \quad (5.215)$$

where the newly introduced quantities are

- α is the inverse of the correlation length, and
 w is the white process noise.

The interpretation of the correlation length is such that if α is large (short correlation length), then x is allowed to have a large change from one measurement epoch $k-1$ to the next k . On the other hand, a small α indicates a strong correlation between successive epochs ($k-1, k$) and thus x will have a small change.

In considering the combination of pseudoranges and phase rates, the Gauss Markov process becomes the following:

$$\begin{bmatrix} \dot{x}_k \\ \dot{y}_k \\ \dot{z}_k \\ - \\ \ddot{x}_k \\ \ddot{y}_k \\ \ddot{z}_k \\ - \\ d\dot{T} \\ d\ddot{T} \end{bmatrix} = \begin{bmatrix} 0 & 0 & 0 & | & 1 & 0 & 0 & | & 0 & 0 \\ 0 & 0 & 0 & | & 0 & 1 & 0 & | & 0 & 0 \\ 0 & 0 & 0 & | & 0 & 0 & 1 & | & 0 & 0 \\ - & - & - & | & - & - & - & | & - & - \\ 0 & 0 & 0 & | & -\alpha_1 & 0 & 0 & | & 0 & 0 \\ 0 & 0 & 0 & | & 0 & -\alpha_2 & 0 & | & 0 & 0 \\ 0 & 0 & 0 & | & 0 & 0 & -\alpha_3 & | & 0 & 0 \\ - & - & - & | & - & - & - & | & - & - \\ 0 & 0 & 0 & | & 0 & 0 & 0 & | & 0 & 1 \\ 0 & 0 & 0 & | & 0 & 0 & 0 & | & 0 & -\alpha_5 \end{bmatrix} \begin{bmatrix} x_k \\ y_k \\ z_k \\ - \\ \dot{x}_k \\ \dot{y}_k \\ \dot{z}_k \\ - \\ cdtT \\ cd\dot{T} \end{bmatrix} + \begin{bmatrix} 0 \\ 0 \\ 0 \\ - \\ u_1 \\ u_2 \\ u_3 \\ - \\ u_4 \\ u_5 \end{bmatrix} \quad (5.216)$$

$$\dot{x} = Fx + u \quad . \quad (5.217)$$

In order to combine the above Gauss Markov process with the GPS measurements, the transition matrix Φ and covariance matrix $C_{k-1,k}^u$ of the white process noise is needed.

Assuming F is constant over Δt (not measurement update but dynamic process interval - usually less than the former), a good approximation of the transition matrix is given by (eqn (4.15)), namely:

$$\Phi = I + F\Delta t . \quad (5.218)$$

The eight state transition matrix becomes

$$\Phi_8(\Delta t) = \begin{bmatrix} 1 & 0 & 0 & | & \Delta t & 0 & 0 & | & 0 & 0 \\ 0 & 1 & 0 & | & 0 & \Delta t & 0 & | & 0 & 0 \\ 0 & 0 & 1 & | & 0 & 0 & \Delta t & | & 0 & 0 \\ - & - & - & | & - & - & - & | & - & - \\ 0 & 0 & 0 & | & -\alpha_1 & 0 & 0 & | & 0 & 0 \\ 0 & 0 & 0 & | & 0 & -\alpha_2 & 0 & | & 0 & 0 \\ 0 & 0 & 0 & | & 0 & 0 & -\alpha_3 & | & 0 & 0 \\ - & - & - & | & - & - & - & | & - & - \\ 0 & 0 & 0 & | & 0 & 0 & 0 & | & 1 & \Delta t \\ 0 & 0 & 0 & | & 0 & 0 & 0 & | & 0 & -\alpha_5 \end{bmatrix} . \quad (5.219)$$

Brown [1983] describes a Gauss Markov (Figure 5.10) process which incorporates an auto-correlation to describe $\alpha = i = 1, 5$ in the above, namely

$$R_x(\tau)_i = \sigma^2 e^{-\alpha_i \tau} , \quad (5.220)$$

where σ^2 is the process variance and α_i is the inverse of the correlation length (e.g. sec^{-1}).

The eight state transition matrix becomes

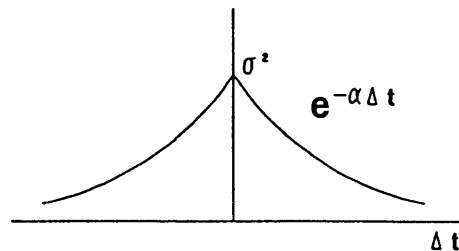


Figure 5.10. Exponential Auto-correlation Function [Brown, 1983; Wong, 1987;]

$$\Phi_8(\Delta t) = \begin{bmatrix} 1 & & & | & \Delta t & & & | & & & \\ & 1 & & | & & \Delta t & & | & & & \\ & & 1 & | & & & \Delta t & | & & & \\ - & - & - & | & - & - & - & | & - & - & \\ & & & | & e^{-\alpha_1 \Delta t} & & & | & & & \\ & & & | & & e^{-\alpha_2 \Delta t} & & | & & & \\ & & & | & & & e^{-\alpha_3 \Delta t} & | & & & \\ - & - & - & | & - & - & - & | & - & - & \\ & & & | & & & & | & 1 & \Delta t & \\ & & & | & & & & | & 0 & e^{-\alpha_5 \Delta t} & \end{bmatrix}, \quad (5.221)$$

where Δt is in units sec and α_i in sec^{-1} . Cannon [1990] interprets the above elements as follows:

- (1) a long Δt results in less correlation;
- (2) the correlation length α_i defines the shape of the curve so that when it is small, the corresponding state vector element will be allowed to change from one epoch to the other; and
- (3) clearly when α_i is large, there will be a strong correlation from one epoch to the other.

These concepts are now applied to the selection of $\alpha_i, i = 1, 5$. For the three velocities, the values for α_1, α_2 and α_3 , may be quite small (e.g. few sec^{-1}). Also, if \dot{x}_k, \dot{y}_k , and \dot{z}_k are resolved into horizontal velocities V_N and V_E , then they should get a different value than that for the vertical velocity \dot{h} . Note the correlation length for the clock affect dT is constant at 1 (7,7 element) but changes every Δt (7,8 element). The clock drift, on the other hand, has a fairly long wave length, thus its correlation length α_5^{-1} should be large (e.g. minutes or hours - depending upon clock stability).

CHAPTER 6

DEAD RECKONING AND MASTER FILTER

The navigation module for land based vehicle positioning contains a dead reckoning component which provides

- (a) velocity estimates to complement the Global Positioning System (GPS), and
- (b) a relative positioning feature via the master filter.

The module's coordinate system is the three dimensional geodetic curvilinear coordinate frame. The navigation equations to compute the change in position are given in Appendix B.

Dead reckoning is a term used in kinematic positioning describing the maintenance of one's position by observing changes in position relative to a known starting point. These relative changes in position are computed using incremental velocities over small epochs of time. A curvilinear driven path is thus approximated by a series of connected vectors in a linear piecewise manner. The accuracy of this approximation is maintained by using small time intervals (eg. 0.2 sec).

6.1 Dead Reckoning Sensors

Sensors are generally divided into heading and distance categories. Contained in Table 6.1 is a comparison of the various heading sensors.

Table 6.1 Heading Sensors (after Hojo et al., [1990])

Types	Sensors	Accuracy	Advantages	Disadvantages
Rate Gyro Type	Vibratory rate gyro	$0.1^\circ \text{sec}^{-1}$	Small size. Long life. Low cost.	Errors caused by vibration. Temperature sensitive.
	Spinning rate gyro	$0.03^\circ \text{sec}^{-1}$	High accuracy.	Short life.
	Gas rate gyro	$0.15^\circ \text{sec}^{-1}$	Vibration proof.	Long start up time.
	Fiber optical gyro	$0.001^\circ \text{sec}^{-1}$	Very high accuracy.	Very expensive.
Absolute Course	Flux gate compass	$2 - 4^\circ$	Absolute course. Small size. Low cost.	Course offset. Sensitive to external objects.
	Gyro compass	$2 - 4^\circ$	Absolute course. Not sensitive to external objects.	Large size. Long start up time. Expensive.

Contained in Table 6.2 is a comparison of the various distance sensors. The values in the accuracy column are a percentage of distance travelled.

Table 6.2 Distance Sensors (after Hojo et al., [1990])

Types	Sensors	Accuracy	Advantages	Disadvantages
Wheel Revolution Type	Hall effect	0.3 to 2%	High sensitivity at high and low speeds.	None.
	Light shield	0.3 to 2%	None.	Limitation of sensor position.
	Generator	0.3 to 2%	Simple.	Low sensitivity at low speed.
Speed Type	Doppler radar	1 %	Remote sensor.	Errors caused by road surface's irregularity and vehicles motion.
	Space filter	3 %	Remote sensor.	Errors caused by road surface's irregularity and vehicles motion.

The types of sensors tested in the dead reckoning component along with their direct and derived output are contained in Table 6.3.

Table 6.3 Sensors and Their Output

Sensor	Direct Output	Derived Output
Three odometers	Pulse count left wheel. Pulse count right wheel.	Relative change in azimuth. Forward or reverse motion distance travelled (centre line of vehicle).
Single odometer	Pulse count from transmission.	Forward or reverse motion. Distance travelled (centre line of vehicle).
Fluxgate compass	x and y voltages (0-4 volts).	Absolute geodetic azimuth.
Rate gyro	Rate of change about axis (0-5 volts).	Rate of change in geodetic azimuth.
Inclinometer	Pitch and roll of vehicle.	Tilt w.r.t. horizontal.

The following dead reckoning sensors were tested and analyzed:

- (1) Etak fluxgate compass;
- (2) Etak turn rate sensor and inclinometer;
- (3) GYROSTARTM rate gyro;
- (4) Etak wheel sensors; and
- (5) White transmission odometer.

These sensors along with the associated mathematical models are treated in the following sections.

6.2 Distance Filter

6.2.1 Differential Odometry

Three odometers are mounted on two wheels of the non-driven wheel pair providing distance travelled, heading change (i.e. change in azimuth) by differential odometry, and forward-reverse motion detection.

Distances are computed by observing the number of pulses detected from targets affixed to, and equally spaced around each wheel, and, by multiplying these pulse counts by a calibration value representing pulse counts per distance travelled. A pulse is generated each time a magnet passes the magnetometer. Changes in the magnet spacing changes the quantization values. An example of this type of sensor is shown in Figure 6.1.

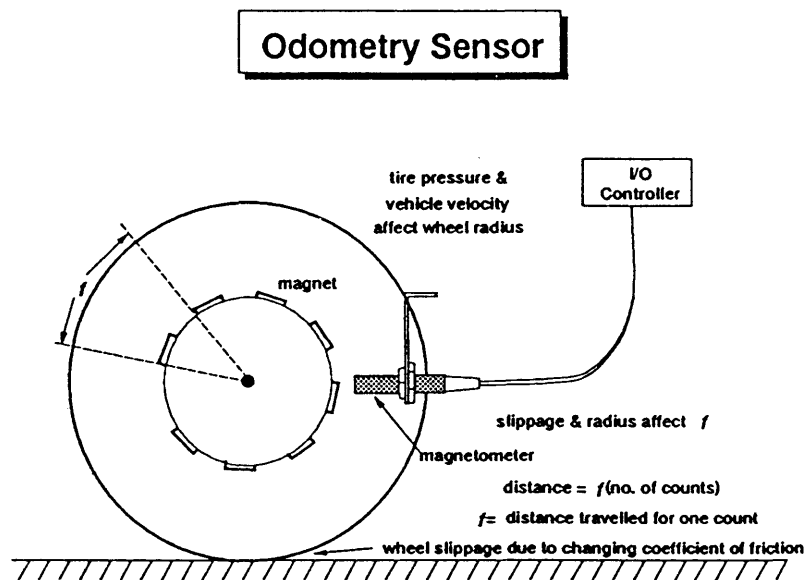


Figure 6.1

The Etak wheel sensors evaluated were similar in nature except rather than magnetic clips, there is a magnetic strip with holes approximately every 3 cm. This magnetic strip is installed where the bead of the tire meets the rim. Quantization error is significantly less with the Etak strip as compared to the sensor shown in Figure 6.1. It is also constant except at the point where the ends of the strip join together.

Heading change from differential odometers is observed by differencing the two odometer distance measurements across the TRACK [Harris, 1989]. The concept is made clear by realizing that through the act of turning, while in motion, an automobile's outer wheel travels a further distance than its inner wheel. This difference can be represented as

a function of the change in azimuth corresponding directly to the turn itself (Figure 6.2). When the odometers are mounted on the rear wheels, the TRACK remains constant, however, it changes on the front wheels as a function of the steering angle.

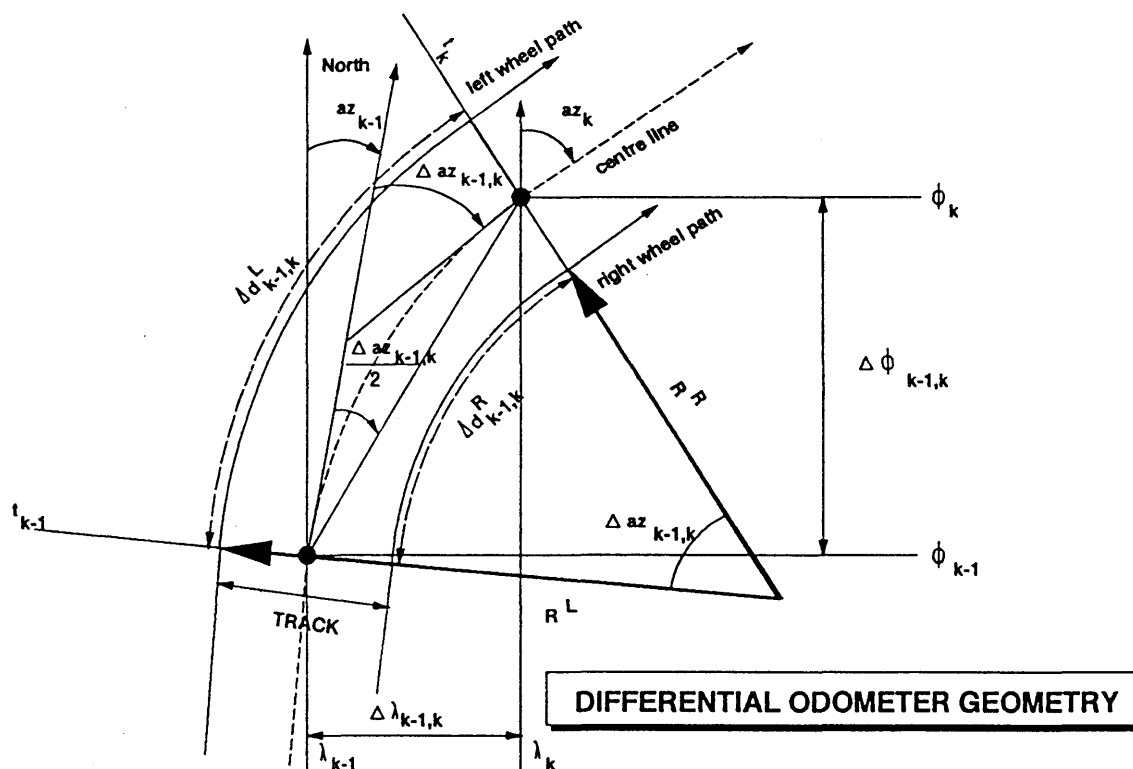


Figure 6.2 (after Harris [1989])

The notation in Figure 6.2 is defined as follows:

- t_k is the time of epoch k (sec),
- t_{k-1} is the time of epoch $k-1$ (sec),
- TRACK** is the distance between the treads of a wheel pair in rest on the road surface (m),
- az is the geodetic azimuth (rad),
- $\Delta az_{k,k-1}$ is the change of azimuth (rad sec⁻¹),
- R^R is the radius of right wheel path (m),

- L^L is the radius of left wheel path (m),
 $\Delta d_{k-1,k}^R$ is the distance travelled by the right wheel (m), and
 $\Delta d_{k-1,k}^L$ is the distance travelled by the left wheel (m).

Normally, the heading of the automobile is aligned to the forward pointing direction of the automobile; undetected reverse motion will obviously introduce dead reckoning error. To detect forward and reverse motion, two odometers are mounted on the same wheel, 90° out of phase from one another. Upon vehicle movement, the leading odometer with respect to signal reception will reveal whether the vehicle is travelling forward or backward. Mathematically, this detection is used to change the azimuth heading by 180° during the reverse motion or alternatively to use a negative speed. The distance travelled over the epoch is determined from

$$\Delta d = \frac{\Delta d_L + \Delta d_R}{2} \left(1 - \frac{1}{24} \Delta az_m^2 \right) , \quad (6.1)$$

where

$$az_m = (az_{k-1} + az_k) / 2 = az_{k-1} + \Delta az / 2 . \quad (6.2)$$

Odometer observables Δd^L and Δd^R are assumed equally weighted and thus are meaned in eqn (6.1). The third odometer is reserved for forward/reverse motion detection only.

Both equations are clearly a linear representation of a change in ϕ and λ over an interval . They do not model the true curvilinear path of the vehicle but rather approximate this path with a series of arcs (Figure 6.2). For this reason, it is necessary to decrease the interval t_{k-1} to t_k to minimize errors resulting from the chord approximation of the arc.

Δaz is determined by the pair of odometers as follows:

$$\Delta az_{DR} = \frac{\Delta d^L - \Delta d^R}{TRACK} . \quad (6.3)$$

It should be noted that in the situation where the vehicle is a rear wheel drive, the odometers will be mounted on the front wheels. The TRACK between the front wheels varies as a function of the steering angle and the wheel base of the vehicle.

The variance of the differential odometer change in azimuth is a function of the left and right wheel odometer sensors and TRACK. Thus the variance associated with the change in azimuth from the differential odometers is

$$\sigma_{\Delta\alpha}^2 = \frac{\sigma_{\Delta d^L}^2 + \sigma_{\Delta d^R}^2}{TRACK^2} + \left(\frac{\Delta d^L - \Delta d^R}{TRACK} \right)^2 \sigma_{TRACK}^2, \quad (6.4)$$

with

$$\Delta d^{R,L} = (n_{R,L} + \Delta n) f_{R,L}, \quad (6.5)$$

where

$n_{L,R}$ is the integer odometer count picked off at the end of a specified time interval (At the end of an interval, a fraction of a count is not reset to zero but saved and transmitted to the next interval.),

Δn is a real random number of the open interval $-1 < \Delta n < +1$, and it has an expectation (mean) of zero, and

$f_{R,L}$ is the factor to convert measured pulses into distance travelled.

The variance for $\Delta d^{L,R}$ becomes

$$\sigma_{\Delta d^{L,R}}^2 = n_{L,R}^2 \sigma_f^2 + f_{L,R}^2 \sigma_{\Delta n}^2. \quad (6.6)$$

Assuming a rectangular density function for Δn ,

$$\sigma_{\Delta n}^2 = \frac{1}{3} m^2, \quad (6.7)$$

where m equals 1 for the odometer pickoff.

The differential odometers will not be dealt with further as they were not used in the final design. After considerable discussions with potential users of the system, there was reluctance to mount the wheel based sensors. This was mainly due to time required for installation and the required maintenance. For this reason a single transmission connected odometer was selected and is described in the following section. The math models, however, have been designed to readily accommodate differential odometer data, if available.

6.2.2 Single Odometer

Single odometers are typically of the transmission type and mount where the speed odometer cable connects to the transmission. Reverse motion is detected externally by connection to a back-up light switch.

Distances are computed by observing the pulse count detected from speed odometer transmission output, and, by multiplying these pulse counts by a calibration value representing pulse counts per distance travelled. Odometers are typically rated as producing a certain number of pulses per distance travelled. Two models were installed and tested, namely: 4000 pulses per km and 12,000 pulses per km which translates to 0.25 m per pulse and 0.083 m per pulse, respectively.

The output from the odometer is differentiated to produce speed. Modelling as a parametric system

$$l = f(x) , \quad (6.8)$$

yields

$$count_{k,k-1} = (speed \cdot (t_k - t_{k-1})) \cdot f^{-1} , \quad (6.9)$$

where

$count_{k-1,k}$ is the number of pulses accumulated over the epoch $t_k - t_{k-1}$,

$speed$ vehicle speed; + forward, - backward (m sec⁻¹).

The scale factor tends to change quite slowly varying with velocity, tire pressure and the coefficient of friction of the tire to the road.

A two state model is used namely:

$$x = [\text{speed} \quad f]^T . \quad (6.10)$$

The speed is modelled using a Gauss Markov process compensating for using a constant velocity model. The transition matrix is

$$\Phi = \begin{bmatrix} e^{-\alpha\Delta t} & 0 \\ 0 & e^{-\beta\Delta t} \end{bmatrix} , \quad (6.11)$$

where

- Δt is the prediction time (sec),
- α is the inverse of the correlation time for the odometer speed (sec^{-1}) and,
- β is the inverse of the correlation time for the scale factor (sec^{-1}).

The process noise matrix is

$$C^u = \begin{bmatrix} Q_1\Delta t & 0 \\ 0 & Q_2\Delta t \end{bmatrix} , \quad (6.12)$$

where

- Q_1 is the spectral density of the speed, and
- Q_2 is the spectral density of the scale.

The spectral densities are computed as a function of the standard deviations of the states and the correlation times. The shorter the correlation time, the faster the response of the state to changes. Correlation times were determined empirically to reflect vehicle dynamics and sensor characteristics.

$$Q_1 = 2 \cdot \sigma_{\text{speed}}^2 \cdot \alpha , \quad (6.13)$$

$$Q_2 = 2 \cdot \sigma_f^2 \cdot \beta , \quad (6.14)$$

where σ^2 is the variance of the process and α_i^{-1} is the correlation length. Values for these quantities are given in Table 6.4.

Table 6.4 Values for Odometer Filter
Spectral Densities Q_i , variances σ_i^2 and Correlation Length α_i^{-1}

States	σ_i^2	Q_i	α_i^{-1}
Speed	$0.25m^2 sec^{-2}$	$0.1m^2 sec^{-3}$	5 sec
Scale factor	$0.0001m^2 pulse^{-2}$	$1 \times 10^{-8}m^2 pulse^{-2} s^{-1}$	20,000 sec

Linearizing eqn (6.9) yields

$$\delta count = \frac{\partial count}{\partial speed} \delta speed + \frac{\partial count}{\partial f} \delta f . \quad (6.15)$$

The design matrix is

$$A = [(t_k - t_{k-1}) \cdot f^{-1} \quad , \quad speed(t_k - t_{k-1})] , \quad (6.16)$$

and the misclosure is formed from

$$l = count_{obs} - count_{pred} . \quad (6.17)$$

The filter can be updated externally a using constant velocity from GPS filter. The velocity from the GPS filter is propagated into speed and heading and is described in Section 6.5.2. The update equation is simply

$$speed_{GPS} = speed_{predicted} . \quad (6.18)$$

The design matrix for the update is

$$A = [1 \quad 0] . \quad (6.19)$$

6.3 Compass

The geomagnetic field has been the subject of extensive investigation for many centuries. The Earth's magnetic field is equivalent to that of a permanent magnet, lying in a general north - south direction, near the Earth's rotational axis. At the north magnetic pole, the horizontal component of this field is zero, while near the equator, the vertical component is zero. The strength and direction of the magnetic vector at any location is subject to anomalies due to large variations in the content of magnetic minerals contained in near-surface rock.

The geomagnetic field is composed of three components, namely:

- (1) main field, where
 - (a) the origin is internal to the earth;
 - (b) it varies slowly; and
 - (c) accounts for 99 % of the total field.
- (2) external field, where
 - (a) the origin is external to the earth;
 - (b) it varies rapidly, partly period and partly random; and
 - (c) accounts for 1 % of the total field.
- (3) variations in the main field caused by local anomalies.

An electronic compass, which measures the direction of the vehicle in relation to the Earth's magnetic field (Figure 6.3), gives information about the heading. An electronic fluxgate compass contain transducers that convert a magnetic flux into a voltage. The compass heading can be used when other sources of heading information are unavailable or unreliable. GPS derived heading is interrupted or degraded by tall buildings or poor satellite coverage. Gyro heading is relative to an initial heading which may be in error.

The magnetic compass observes angles in reference to the Earth's magnetic field. Thus the angles are measured relative to the Earth's magnetic pole and not to the Earth's spin axis which is the reference required for the reduction to geodetic north.

A magnet takes up a position parallel within the lines of magnetic force of the earth. In a horizontal projection, the lines define the magnetic meridians. In elevation, the lines are inclined downward toward the north in the northern hemisphere, and downward toward the south in the southern hemisphere. The angle between the horizontal and the inclined line is called the angle of inclination. The inclination varies from 0° at or near the equator to 90° at the magnetic poles.

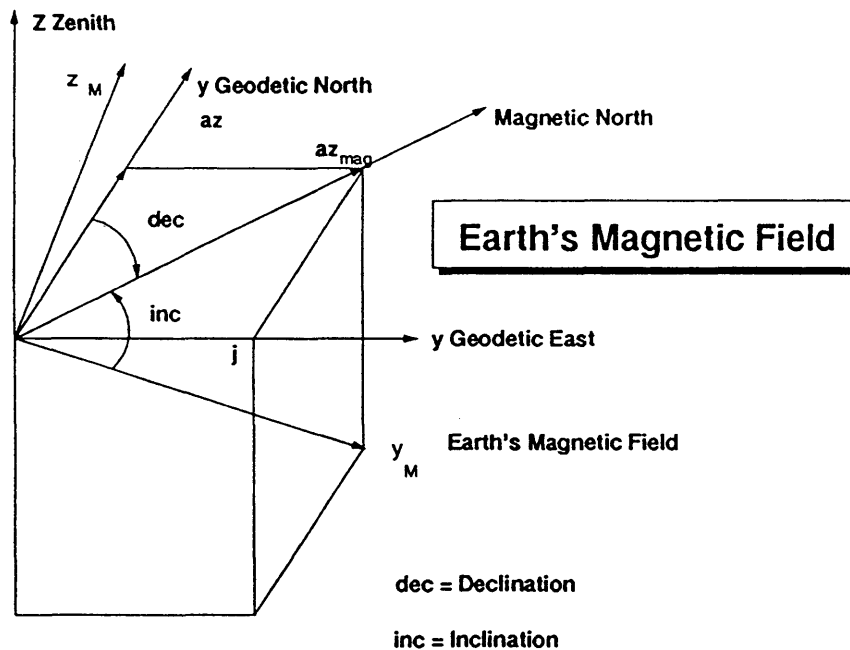


Figure 6.3

The angle between the true meridian and the magnetic meridian is called the magnetic declination or variation. If the magnetic heading is east of true north, the declination is said to be east. Magnetic declination is a non-linear function of both position and time.

The magnetic declination changes more or less systematically in cycles over periods of (1) approximately 300 years, (2) one year, and (3) one day, as follows [Davis et al., 1981]:

- (1) **Secular variation.** The magnetic meridian swings in one direction for about 150 years, then stops and swings in the other direction. The velocity of the shift is greatest during the middle of the swing, the rate of change per year varies irregularly. The rate of changes varies both with geographic area and time. The variation is the one most often referred to and applied as a correction.
- (2) **Annual variation.** This can amount to up to 1' per year and is distinctly different from the above noted variation.
- (3) **Daily variation.** This variation, also called solar-diurnal variation is a periodic swing of the compass occurring each day. Variations can reach up to 8'.
- (4) **Irregular variations.** They are usually caused by magnetic disturbances associated with sunspots. They cannot be predicted but are most likely to occur during magnetic storms and may amount up to 1° to 2°.

Isogonic charts displaying magnetic declination plots over geographic regions are often used to obtain magnetic declination parameters but exist in paper format only. Typically, values are stored in a look-up table (e.g., 1° x 1° grid) or mathematical expression (e.g. spherical harmonic series) is used. In Canada, maps of declination and inclination are available from the Department of Energy, Mines and Resources, Ottawa. The declination and inclination in Calgary ($\phi = 51^\circ N$; $\lambda = 114^\circ W$) are approximately 21° and 74.3°, respectively.

The horizontal component can be computed as

$$az_{mag} = y_M \cos(inc) . \quad (6.20)$$

The vertical component can be computed as

$$mag_z = y_M \sin(inc) . \quad (6.21)$$

For Calgary, the ratio of the vertical to the horizontal component would be

$$\frac{mag_z}{az_{mag}} = \frac{\sin 74.3^\circ}{\cos 74.3^\circ} = 3.6 \quad (6.22)$$

In other words, the vertical component is 3.6 times the strength of the horizontal component. As can be seen, a sensor with a fixed sensor axis encountering uncorrected pitch and roll can have a significant effect on the heading determination.

The electronic compass may contain three transducers for the magnetic field. They measure the components of mag_F , the strength of the terrestrial magnetic field, in three orthogonal directions. The Etak compass contains only the two horizontal axes. Ideally, the outputs would correspond to the sine and cosine of the angle between the compass and the field but the axes are not orthogonal. To relate the compass derived heading to vehicle heading, it is necessary to know the pitch and roll of the axes, the amount of non-orthogonality between the axes, and the effect of the magnetic field inclination angle.

6.3.1 Etak Flux Gate Sensor

A flux gate sensor is a device used for measuring the intensity of an external magnetic field in which the sensor is placed. In general, it comprises a saturable core, a drive winding for driving the core into and out of saturation and one or more sense windings. The sense windings provide, when properly oriented relative to the external magnetic field, a signal proportional to the strength of the external magnetic field [Honey, 1987]. Figure 6.4 contains a block diagram of the Etak flux gate sensor.

The output of the filters provide a signal as follows:

$$X = C_x + B \cos(inc) \sin(H) , \text{ and} \quad (6.23)$$

$$Y = C_y + B \cos(inc) \cos(H) , \quad (6.24)$$

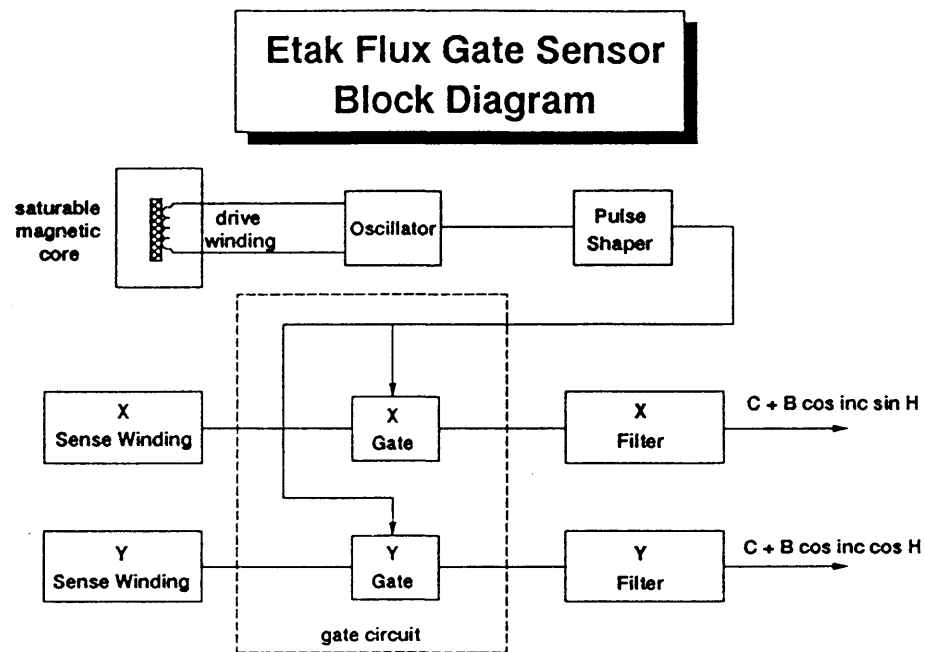


Figure 6.4 (after Honey [1987])

where

X is the output from the X filter of the sense winding (v),

Y is the output from the Y filter of the sense winding (v),

C_x is the X axis offset (v),

C_y is the Y axis offset (v),

H is the heading (angle between sine winding and longitudinal projection of the earth's field),

inc is the inclination angle (angle between the horizon and earth's field, and

B is a constant linearly proportional to the strength of the earth's field.

Often in a local area, the inclination is treated as a constant and becomes part of the scale factor. If the compass is constantly calibrated, the inclination will be computed as part of the scale factor rather than extracting it from look-up tables.

The signal from the fluxgate compass and the rate of heading change from the rate gyro can both provide a measure for the heading of a vehicle. The compass signal supplies an absolute value of the heading relative to magnetic north; the rate gyro supplies a relative value with respect to the initial value of the heading. The signals must thus be made comparable. Both signals are also subject to interference because of the way in which the signals have been obtained. The difference in signal from the rate gyro has a slow drift due to changes in temperature causing a DC offset change and a change in scale factor which translates into drift. The compass signal contains very fast fluctuations due to the magnetic fields of other vehicles, steel bridges, structural metal in buildings and railway lines. The compass signal also has a constant error due the magnetic field of the steel body of the vehicle.

6.3.2 Model

The output of the Etak compass varies with the component of the Earth's magnetic field in the sensitive axes of the sensor. The output is affected by the pitch, roll and heading of the vehicle and also by the inclination angle of the magnetic field. The relationship is depicted in Figure 6.5.

In Figure 6.5, the origin is at the centre of the flux gate compass. The z axis is orthogonal to the normal ellipsoid and Y_N points to geodetic north. The observations must be rotated through a series of coordinate frames to be used in the general navigation equations.

The z axis of the magnetic frame is drawn towards magnetic north, causing the y axis to incline, becoming aligned with the north - south magnetic axis at magnetic north. The maximum line of force lies along the y axis, thus as the magnetic pole is approached, the azimuth determination, which is computed in the horizontal plane, must be scaled by a factor based on the inclination.

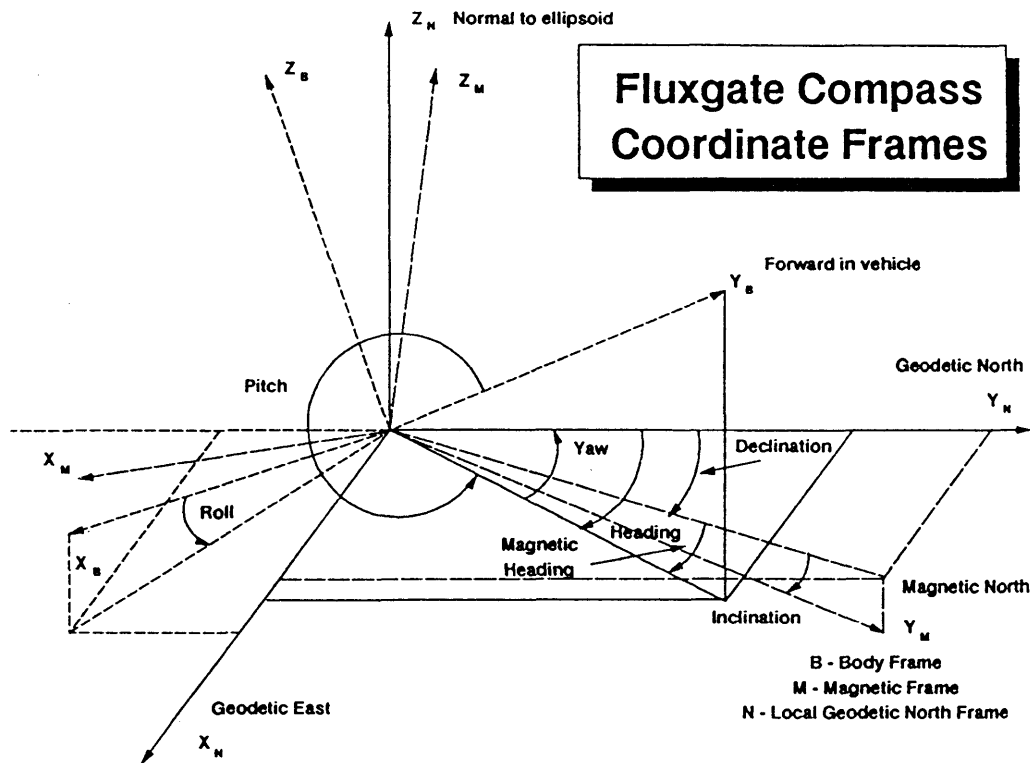


Figure 6.5

The first rotation involves going from the compass coordinate frame to a common point on the body frame. The relationship (Figure 6.6) of the two coordinate frames remains a constant in this case as the sensors are fixed with respect to the body frame.

In all cases the Y axis of the compass has been approximately oriented to the forward direction of motion of the vehicle. The three rotation angles are as follows:

- θ_c is the pitch angle of the compass relative to the body axis (degrees),
- ϕ_c is the roll angle of the compass relative to the body axis (degrees), and
- ψ_c is the yaw angle of the compass relative to the body axis (degrees).

The relationship of the compass coordinate frame to the body frame is as follows:

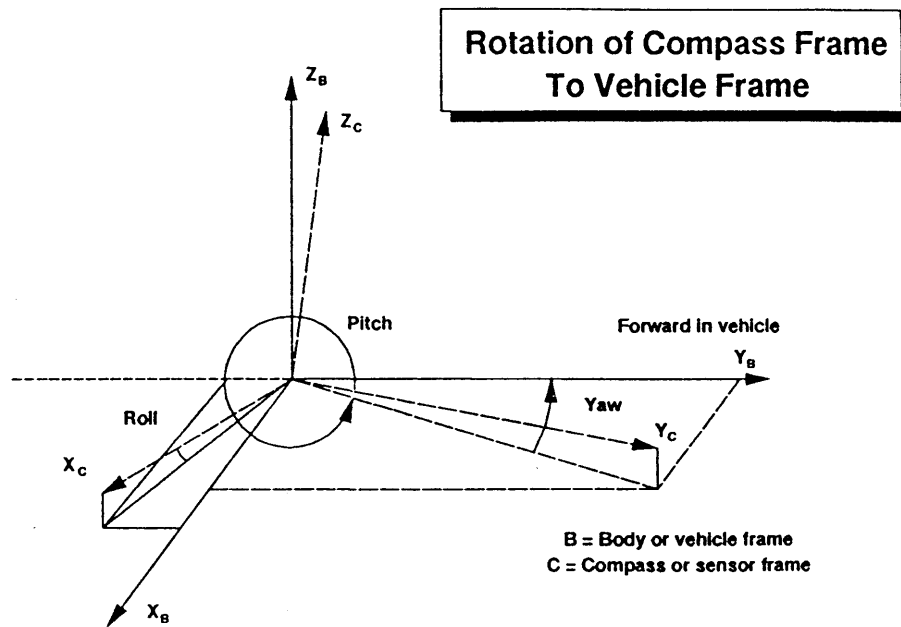


Figure 6.6

$$r_B = R_{BC} r_C , \quad (6.25)$$

$$r_B = R_2(\phi_C) R_1(\theta_C) R_3(\Psi_C) r_C \quad (6.26)$$

where the matrix R is a three dimensional rotation matrix, the quantity in parameters is the angle through which the rotation is to be made, and the subscript (1, 2, 3) denotes the axis (x, y, z) about which the rotation is made.

The relationship of the magnetic coordinate frame to the local level system is as follows:

$$r_N = R_{NM} r_M , \quad (6.27)$$

$$r_N = R_1(\text{inc}) R_3(-\text{dec}) r_M . \quad (6.28)$$

The relationship of the body coordinate frame to the local level system is as follows:

$$r_N = R_{NB} r_B , \quad (6.29)$$

$$r_N = R_1(\phi_B) R_1(\theta_B) R_3(\Psi) r_B , \quad (6.30)$$

where

- θ_B is the pitch angle of the body relative to the local level axis (degrees),
 ϕ_B is the roll angle of the body relative to the local level axis (degrees), and
 Ψ_B is the yaw angle of the body relative to the local level axis (degrees).

The observations from the flux gate sensor are X_C and Y_C of the magnetic field in the sensor frame. The inclination and declination may be treated as known values from a look-up table or solved for as part of the continuous calibration. The requirement is thus to relate the sensor observations in the compass frame to the required local geodetic frame to obtain the required geodetic azimuth. The relationship is expressed as a series of rotations as follows:

$$r_C = R_{CN} r_N , \quad (6.31)$$

which can be expanded to

$$r_C = R_{CB} R_{BN} r_N , \quad (6.32)$$

and expressed in terms of rotation matrices

$$r_C = R_2(-\phi_C) R_1(-\theta_C) R_3(-\Psi_C) R_2(-\phi_B) R_1(-\theta_B) R_3(-\Psi_B) r_N , \quad (6.33)$$

which expressed in terms of the earth's magnetic frame is

$$r_C = R_2(-\phi_C) R_1(-\theta_C) R_3(-\Psi_C) R_2(-\phi_B) R_1(-\theta_B) R_3(-\Psi_B) R_1(inc) R_3(-dec) r_M . \quad (6.34)$$

For simplification and lack of information, the pitch and roll of the sensor will be assumed to be aligned with the body axis leading to

$$r_C = R_3(-\Psi_C) R_2(-\phi_B) R_1(-\theta_B) R_3(-\Psi_B) R_1(\pi/2 - inc) R_3(-dec) r_M . \quad (6.35)$$

If the pitch and roll of the vehicle relative to the local level system are assumed to be zero, or are unavailable, the expression further simplifies to

$$r_C = R_3(-\Psi_C) R_3(-\Psi_B) R_1(inc) R_3(-dec) r_M . \quad (6.36)$$

There is a scaling factor and x, y, z offsets between the magnetic field and the compass measurements. Using eqn (6.36), this can be expressed as

$$r_C = t + b \cdot R_3(-\Psi_C)R_3(-\Psi_B)R_1(inc)R_3(-dec)r_M , \quad (6.37)$$

and after rearranging becomes

$$r_C = t + b \cdot R_3(-\Psi_C - \Psi_B)R_1(inc)R_3(-dec)r_M , \quad (6.38)$$

where

$$t = [C_x \quad C_y \quad C_z]^T , \quad (6.39)$$

and b is a scale factor matrix

$$b = \begin{bmatrix} k_x & 0 & 0 \\ 0 & k_y & 0 \\ 0 & 0 & k_z \end{bmatrix} . \quad (6.40)$$

Multiplication yields

$$x_c = C_x + k_z \cos(inc) \sin(H) , \text{ and} \quad (6.41)$$

$$y_c = C_y + k_z \cos(inc) \cos(H) , \quad (6.42)$$

where

$$H = -\Psi_C - \Psi_B + dec . \quad (6.43)$$

If the inclination is assumed constant for a local area, then $k_z \cos(inc)$ can be treated as constant R and eqns (6.41) and (6.42) can be rewritten as

$$x_c = C_x + R \sin(h) , \text{ and} \quad (6.44)$$

$$y_c = C_y + R \cos(h) , \quad (6.45)$$

$$h = az - \Psi_C , \quad (6.46)$$

where

- X_c, Y_c are the compass x, y readings (volts),
 R is the radius of a circle which the compass readings form (volts),
 α is the heading (degrees),
 Ψ_c is the compass angular offset (degrees), and
 C_x, C_y are the compass axes offset (volts).

The compass observations in an x, y plane tend to lie in an ellipse with an offset as shown in Figure 6.7.

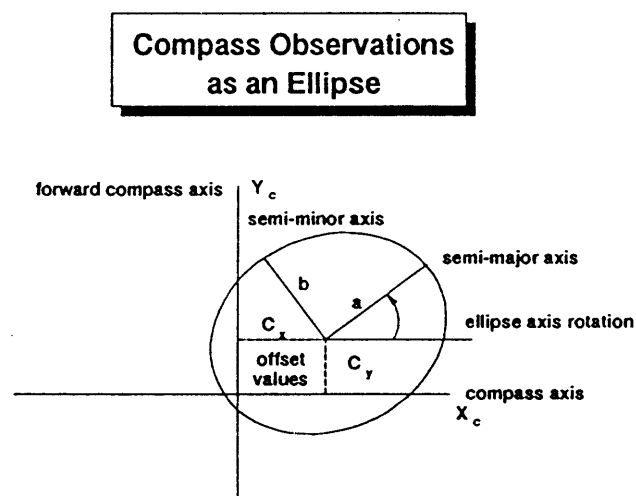


Figure 6.7

where

- a is the semi-major axis of the ellipse,
 b is the semi-minor axis of the ellipse,
 Y_c is the y axis of the compass in the forward direction of the vehicle, and
 X_c is the x axis of the compass.

A best fitting ellipse usually has its axes rotated with respect to the sensor axis. The axes of the ellipse are also non-orthogonal. The shape of the ellipse is dependant upon the magnetic field of the vehicle and external magnetic sources.

In typical vehicle installations the compass is positioned so that the x and y ranges are very close to being equal. In this situation, the observations tend to lie more closely on a circle. The solution for the ellipse becomes very unstable as the two axes become close to being equal. Hence, the observations are often modeled as lying in a circle as shown in Figure 6.8.

Writing eqns (6.44) and (6.45) in terms of a past heading plus a heading rate over an epoch yields

$$x_c = C_x + R \sin(az_{k-1} + az_{k,k-1}(t_k - t_{k-1}) - \Psi_c) , \text{ and} \quad (6.47)$$

$$y_c = C_y + R \cos(az_{k-1} + az_{k,k-1}(t_k - t_{k-1}) - \Psi_c) , \quad (6.48)$$

where

az is the heading rate over the epoch $t_k - t_{k-1}$ (degrees).

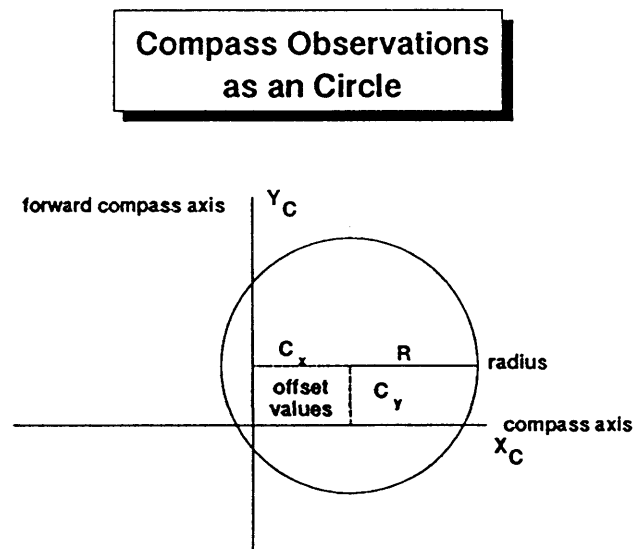


Figure 6.8

Rewriting eqns (6.47) and (6.48) results in

$$\cos(az_k - \Psi_c) = \frac{Y_c - C_y}{R}, \text{ and} \quad (6.49)$$

$$\sin(az_k - \Psi_c) = \frac{X_c - C_x}{R}. \quad (6.50)$$

Combining eqns (6.49) and (6.50) yields

$$az_k = \tan^{-1}\left(\frac{X_c - C_x}{Y_c - C_y}\right) + \Psi_c. \quad (6.51)$$

The filter contains six states with the vector of unknowns written as

$$x = [az \quad \dot{az} \quad R \quad C_x \quad C_y \quad \Psi_c]^T. \quad (6.52)$$

The transition matrix is given as

$$\Phi = \begin{bmatrix} 1 & \Delta t & 0 & 0 & 0 & 0 \\ 0 & e^{-\alpha \Delta t} & 0 & 0 & 0 & 0 \\ 0 & 0 & 1 & 0 & 0 & 0 \\ 0 & 0 & 0 & 1 & 0 & 0 \\ 0 & 0 & 0 & 0 & 1 & 0 \\ 0 & 0 & 0 & 0 & 0 & 1 \end{bmatrix}, \quad (6.53)$$

where

α is the inverse of the correlation time for the heading rate (sec^{-1}), and

Δt is the prediction time (sec).

Only the heading rate is modelled using a Gauss Markov process.

The process noise matrix is given as

$$C^u = \begin{bmatrix} Q_1 \Delta t & 0 & 0 & 0 & 0 & 0 \\ 0 & Q_2 \Delta t & 0 & 0 & 0 & 0 \\ 0 & 0 & Q_3 \Delta t & 0 & 0 & 0 \\ 0 & 0 & 0 & Q_4 \Delta t & 0 & 0 \\ 0 & 0 & 0 & 0 & Q_5 \Delta t & 0 \\ 0 & 0 & 0 & 0 & 0 & Q_6 \Delta t \end{bmatrix}. \quad (6.54)$$

Values for these quantities are given in Table 6.5.

Table 6.5 Values for Compass Filter
Spectral Densities Q_i , variances σ_i^2 and Correlation Length α_i^{-1}

States	σ_i^2	Q_i	α_i^{-1}
Heading		$49deg^2 sec^{-1}$	
Heading Rate	$4deg^2 sec^{-2}$	$8deg^2 sec^{-3}$	$0.5 sec$
Radius		$1 \times 10^{-7} v^2 sec^{-2}$	
Offsets		$1 \times 10^{-6} v^2 sec^{-2}$	
Offset Angle		$1 \times 10^{-6} deg^2 sec^{-1}$	

The heading equation is

$$az_k = az_{k-1} + \dot{a}z_{k,k-1}(t_k - t_{k-1}) \quad (6.53)$$

Linearizing the observations eqns (6.47) and (6.48) leads to

$$\delta X_C^k = \frac{\partial X_c}{\partial az_k} \delta az_k + \frac{\partial X_c}{\partial \dot{a}z} \delta \dot{a}z + \frac{\partial X_c}{\partial R} \delta R + \frac{\partial X_c}{\partial C_x} \delta C_x + \frac{\partial X_c}{\partial C_y} \delta C_y + \frac{\partial X_c}{\partial \Psi_c} \delta \Psi_c, \text{ and} \quad (6.54)$$

$$\delta Y_C^k = \frac{\partial Y_c}{\partial az_k} \delta az_k + \frac{\partial Y_c}{\partial \dot{a}z} \delta \dot{a}z + \frac{\partial Y_c}{\partial R} \delta R + \frac{\partial Y_c}{\partial C_x} \delta C_x + \frac{\partial Y_c}{\partial C_y} \delta C_y + \frac{\partial Y_c}{\partial \Psi_c} \delta \Psi_c. \quad (6.55)$$

The design matrix is as follows:

$$A = \begin{bmatrix} R \cos(h) & R \cdot (t_k - t_{k-1}) \cos(h) & \sin(h) & 1 & 0 & -R \cdot \cos(h) \\ -R \sin(h) & -R \cdot (t_k - t_{k-1}) \sin(h) & \cos(h) & 0 & 1 & R \cdot \sin(h) \end{bmatrix}. \quad (6.56)$$

The misclosure is computed from

$$l = \text{observed} - \text{predicted} \quad (6.57)$$

where

$$l_{X_C} = X_C - C_X - R \sin(az_{k-1} + az_{k,k-1} \cdot (t_k - t_{k-1}) - \Psi_C) , \quad (6.58)$$

$$l_{Y_C} = Y_C - C_Y - R \cos(az_{k-1} + az_{k,k-1} \cdot (t_k - t_{k-1}) - \Psi_C) . \quad (6.59)$$

External updates can be done via two sources, namely;

- (1) Constant heading from GPS filter; and
- (2) Heading rate change of zero when odometer is stopped.

The heading update is as follows:

$$l = az_{obs} - az_{pred} \quad (6.60)$$

and the design matrix is

$$A = [1 \ 0 \ 0 \ 0 \ 0 \ 0] . \quad (6.61)$$

The heading rate update is as follows:

$$l = \dot{az}_{obs} - \dot{az}_{pred} \quad (6.62)$$

and the design matrix is

$$A = [0 \ 1 \ 0 \ 0 \ 0 \ 0] . \quad (6.63)$$

6.4 Rate Gyro

Gyroscopes are angular sensors that output either angular rate or attitude, depending whether they are rate sensing or rate integrating. A low cost rate gyro, that is typically used for land navigation applications outputs a voltage proportional to the rate of angular displacement. The rate gyro has only recently been considered as a heading sensor. In the past, most systems have relied only upon compass based systems, however, they have proved unsatisfactory for most urban applications where there are an abundance of external forces. In terms of navigation errors, the heading has proven to be the most problematic to solve. Odometers consistently provide sufficient accuracy for distance travelled, hence gyro

research and development has received considerable efforts. In evaluating inertial system performance, the gyro has often been the limiting factor [Krakiwsky et al., 1990] and is also one of the most costly items.

The scale factor stability and bias define the accuracy of a gyro. The scale factor stability is the capability of the gyro to accurately sense angular velocities at various rates. Designers strive for output values which are linear over their dynamic range. The vehicle dynamics play a major part in the attainable heading accuracy. For instance, an aircraft undergoing high dynamics would require a much larger dynamic range than vehicles which are travelling generally on paved roads with a reasonably low rate of heading change. Any errors in scale translate into affects on the rotation rate, which when integrated over time affects the heading.

The capability of the gyro to reference all rate measurements to the nominal zero point is characterized by the gyro bias. The bias model varies according to the various sensor designs.

Gyros are basically designed following three principles and are listed in Table 6.6 [Krakiwsky et al., 1990].

The rotor gyro is the most popular and is available at various accuracy levels. The optical gyros are starting to replace rotor gyro applications and will likely become more available over time. The fibre optic gyro has good potential for low cost production and solid state fabrication and is being tested by several Japanese companies such as Sumitomo Electric [Ikeda et al., 1991]. The vibration gyro makes use of the principle that an oscillating inertial body will preserve the plane of vibration in space despite rotation of the base. This gyro can also be produced cheaply and is being built by some Japanese companies such as Murada [Nakamura, 1990].

Table 6.6 Gyro Principles and Designs

Type	Principle	Design	Degrees of Freedom
Rotor	Constancy of Angular Momentum	Rigid Rotors	1 and 2
		Dry Tuned	2
		Nuclear Resonant	1
Optical	Sagnac Effect	Ring Laser	1
		Fibre Optic	1
Vibration	Preservation of Plane Vibration	Hemispherical Resonant	1

For land vehicles travelling in a horizontal plane, only the angular velocity produced during vehicle turning is of interest. For a constant sampling rate, the angular speeds are in proportion to the relative headings. Therefore, gyroscopes can be used in a similar manner to differential odometers to measure the relative headings of the vehicle. Unlike differential odometers, the performance of the gyroscopes is not subject to factors such as a change in effective tire size [Kao, 1991].

The single axis gyros used in land navigation applications are mounted with their z axis approximating the local level z axis as shown in Figure 6.9.

The output from the low cost rate gyros is offset by a voltage that varies with the power supply. The GPS heading is used to determine the constant of proportionality and offset for the rate gyro so that a heading based on the gyro output can be calculated when no GPS heading is available. Two types of rate gyros were tested and are described below.

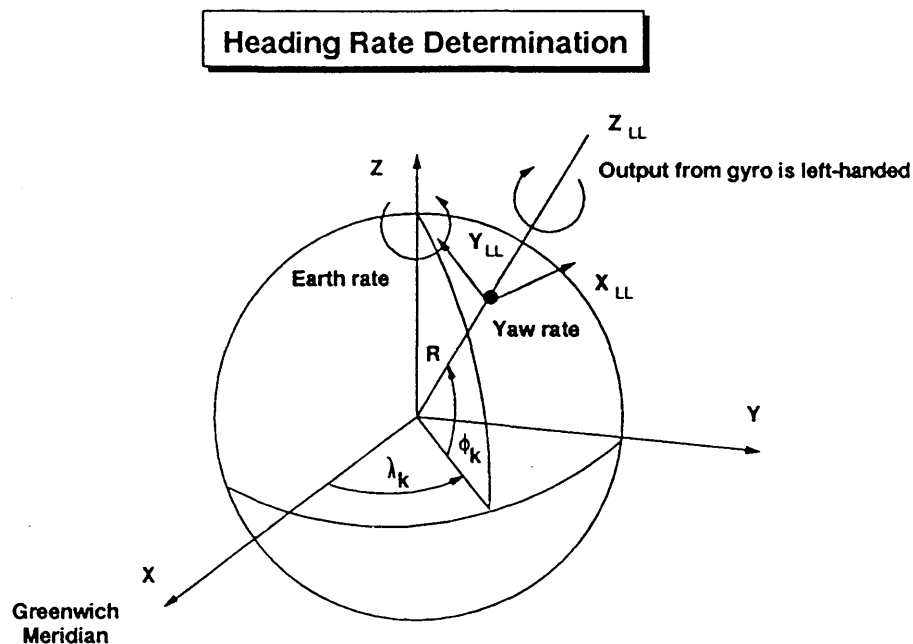


Figure 6.9

6.4.1 Etak Turn Sensor

The Etak turn sensor incorporates two subsystems; a two axis gyroscopic turn-rate sensor, and two-axis fluid inclinometer. The gyroscope is used to measure yaw rate and the inclinometer is used to measure pitch and roll.

The gyro uses a rotating flexible disc. Precessive flex in the disc is measured capacitively. The primary output is a digital pulse train. With the gyro stationary, the pulse train has a quiescent frequency; the deviation from the quiescent is proportional to the yaw rate. Typically the pulse train is time integrated in a counter, the quiescent counts subtracted, and the remainder is yaw. The secondary gyro axis is an analog output voltage.

The inclinometer uses a bottle filled with a dielectric fluid. Capacitive plates sense the position of the fluid. The inclinometer outputs are analog. With the sensor upright, the outputs are nominally half of the supply voltage. Deviations from the quiescent are proportional to the tilt.

The linearity of the yaw rate is $\pm 1\%$ over a $\pm 60^\circ \text{ sec}^{-1}$ allowable range. The yaw drift rate is rated to be less than 10° per minute but is typically 3° to 4° per minute.

6.4.2 Murata GYROSTAR™

The vibration gyroscope employs a mechanical phenomenon in which the coriolis force develops in the direction perpendicular to the vibration when an angular velocity is applied to a vibrating body [Nakamura, 1990].

In practical terms, a free-free-bar or a tuning fork vibrator and a piezoelectric ceramic are pasted together and the vibrator is driven (x axis). When rotational angular velocity (Ω_o) is applied to the central axis (z axis) of the vibrator, the coriolis force develops (y axis) in the direction perpendicular to the vibration direction (x axis) and the rotational angular velocity is detected from the piezoelectric ceramics glued in the y axis direction. The basic principle is shown in Figure 6.10.

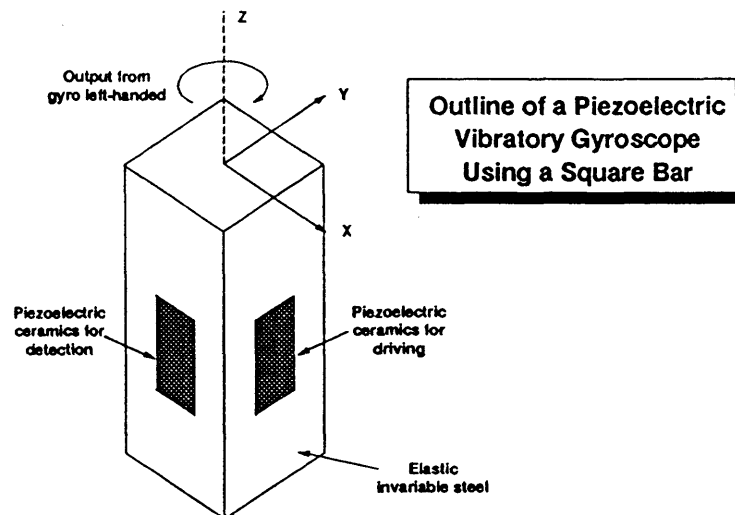


Figure 6.10 (after Nakamura, [1990])

The vibration gyroscopes require high sensitivity to rotational angular velocity; at the same time, the detection voltage at the time of no rotation must be zero or null voltage.

Using the conventional square gyro shown in Figure 6.10, the null voltage is not exactly zero due to the manufacturing inaccuracy of vibrators and the variability of the gluing position.

The GYROSTAR™ rate gyro is in the shape of an equilateral triangle and shown in Figure 6.11. The equilateral triangle prism vibrating unit allows the left and right piezoelectric ceramics to be arranged in the direction of the compound vibration mode. This means that the same ceramics can be used for both excitation and detection, enabling a simple structure and simplified circuit [Nakamura, 1990].

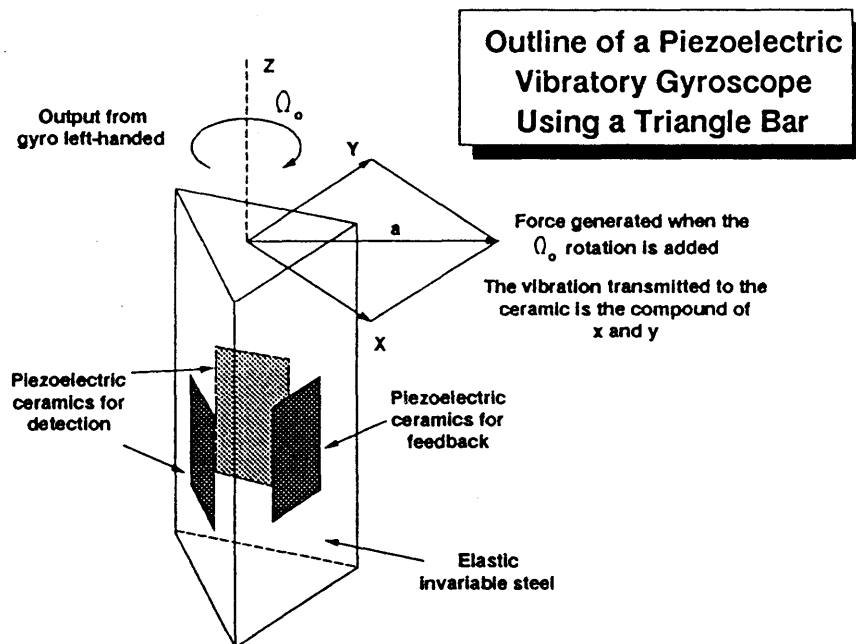


Figure 6.11 (after Nakamura, [1990])

The GYROSTAR™ detects the angular velocity by subtracting the left and right outputs from each other. When there is no rotation (i.e. driving in a straight line), the unwanted vibrations entering due to vertical movement and backward-forward motion are subtracted, so the noise components are reduced, minimizing their effect on the angular detection.

When rotating, the left and right detection values are subtracted from each other (Figure 6.12). In equation form, the detection voltage is

$$2a = (A + a) - (A - a) , \quad (6.64)$$

which yields a relatively large detection output.

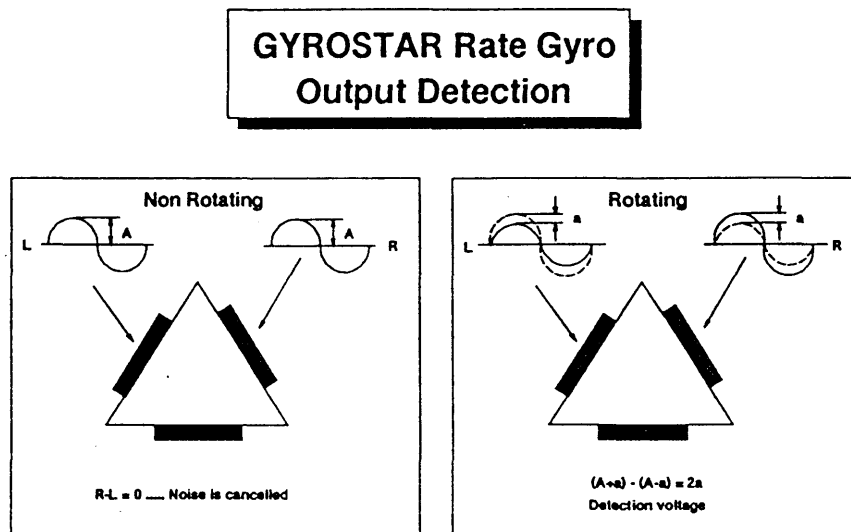


Figure 6.12 [after Nakamura, 1990]

The maximum angular velocity is $\pm 90^\circ \text{ sec}^{-1}$. The scale factor is 22 mV per degree per sec. The reference voltage is 2.5 volts, which represents zero velocity. The linearity is less than 0.1% at maximum angular velocity. The drift rate is less than 0.2% of the maximum angular velocity per hour.

6.4.3 Model

The heading rate equation is given as

$$\dot{az}_k = \dot{az}_{k-1} + \text{drift}(t_k - t_{k-1}) . \quad (6.65)$$

The observation equation is

$$\text{yaw} = 0 \text{ ls} + \frac{1}{\text{scale}} (\dot{az} - \omega_e \sin \phi + \text{drift}(t_k - t_{k-1})) \quad (6.66)$$

where

- o/s is the reference voltage offset (v),
 $y\dot{a}w$ is the angular rate of change from the rate gyro (v sec⁻¹),
 $scale$ is the conversion of volts to deg per sec,
 ω_e is the Earth rotation rate, and
 $drift$ is the drift rate of the gyro (deg per sec).

Linearizing eqn (6.66) results in

$$\delta y\dot{a}w = \frac{\partial y\dot{a}w}{\partial a\dot{z}} \delta a\dot{z} + \frac{\partial y\dot{a}w}{\partial drift} \delta drift + \frac{\partial y\dot{a}w}{\partial o/s} \delta o/s . \quad (6.67)$$

The vector of unknowns is

$$x = [a\dot{z} \quad drift \quad o/s]^T . \quad (6.68)$$

The transition matrix is

$$\Phi = \begin{bmatrix} 1 & \Delta t & 0 \\ 0 & e^{-\alpha \Delta t} & 0 \\ 0 & 0 & e^{-\beta \Delta t} \end{bmatrix} , \quad (6.69)$$

where

- α is the inverse of the correlation time for the drift (sec⁻¹), and
 β is the inverse of the correlation time for the offset (sec⁻¹).

The process noise matrix is

$$C^u = \begin{bmatrix} Q_1 \Delta t & 0 & 0 \\ 0 & Q_2 \Delta t & 0 \\ 0 & 0 & Q_3 \Delta t \end{bmatrix} , \quad (6.70)$$

where

- Q_1 is the spectral density for $a\dot{z}$ (deg² sec⁻³),

Q_2 is $2 \cdot \alpha \cdot \sigma_{drift}^2 (v^2 \text{ sec}^{-3})$, and

Q_3 is $2 \cdot \beta \cdot \sigma_{o/s}^2 (v^2 \text{ sec}^{-1})$.

Values for these quantities are given in Table 6.7.

Table 6.7 Values for Heading Rate Filter
Spectral Densities Q_i , variances σ_i^2 and Correlation Length α_i^{-1}

States	σ_i^2	Q_i	α_i^{-1}
Heading Rate		$0.01 \text{ deg}^2 \text{ sec}^{-3}$	
Drift	$1 \cdot 10^{-6} v^2 \text{ sec}^{-2}$	$8 \cdot 10^{-6} v^2 \text{ sec}^{-3}$	$172,800 \text{ sec}$
Offset	$.0001 v^2$	$8 \cdot 10^{-6} v^2 \text{ sec}^{-1}$	$42,000 \text{ sec}$

The design matrix is

$$A = \begin{bmatrix} 1 & (t_k - t_{k-1}) & \\ \text{scale} & \text{scale} & 1 \end{bmatrix} . \quad (6.71)$$

The misclosure vector is

$$l = yaw - o/s - \frac{1}{\text{scale}} (az - \omega_e \sin \phi + drift (t_k - t_{k-1})) . \quad (6.72)$$

The rate gyro filter can be updated externally from the odometer when a zero velocity condition exists or when there is a constant heading determined from the GPS velocity filter.

The misclosure vector is

$$l = 0.0 - az + drift (t_k - t_{k-1}) . \quad (6.73)$$

The design matrix is

$$A = [1 \quad 0 \quad 0] . \quad (6.74)$$

6.5 Velocity Filters

The heading and heading rates are combined from the various sensor filters into one filter. This heading is then combined with the speed from the odometers to produce velocity components compatible with the master filter. This implementation is described in the following sections.

6.5.1 Heading Filter

The system was designed such that each sensor that produces heading has its own filter for determining heading states and sensor bias. The output from these filters are combined into a two state filter containing heading and heading rate. The vector of unknowns is

$$\mathbf{x} = [az \quad a\dot{z}]^T . \quad (6.75)$$

The transition matrix is

$$\Phi = \begin{bmatrix} e^{-\alpha\Delta t} & 0 \\ 0 & e^{-\beta\Delta t} \end{bmatrix} , \quad (6.76)$$

where

α is the inverse of the correlation time for the heading (sec^{-1}).

β is the inverse of the correlation time for the heading rate (sec^{-1}).

The process noise matrix is

$$\mathbf{C}^u = \begin{bmatrix} Q_1\Delta t & 0 \\ 0 & Q_2\Delta t \end{bmatrix} , \quad (6.77)$$

where

Q_1 is the spectral density for az ($\text{deg}^2 \text{sec}^{-1}$), and

Q_2 is the spectral density for $a\dot{z}$ ($\text{deg}^2 \text{sec}^{-3}$).

Values for these quantities are given in Table 6.8.

Table 6.8 Values for Heading Filter
Spectral Densities Q_i , variances σ_i^2 and Correlation Length α_i^{-1}

States	σ_i^2	Q_i	α_i^{-1}
Heading	4 deg^2	$8 \text{ deg}^2 \text{ sec}^{-1}$	1 sec
Heading Rate	$4 \text{ deg}^2 \text{ sec}^{-2}$	$8 \text{ deg}^2 \text{ sec}^{-2}$	1 sec

Compass Update

The are two observation update equations from the compass, namely:

$$az_{comp} = az_{pred} , \text{ and} \quad (6.78)$$

$$a\dot{z}_{comp} = a\dot{z}_{pred} . \quad (6.79)$$

The design matrix is

$$A = \begin{bmatrix} 1 & 0 \\ 0 & 1 \end{bmatrix} . \quad (6.80)$$

Rate Gyro Update

The is one observation update equation from the rate gyro, namely;

$$a\dot{z}_{gyro} = a\dot{z}_{pred} . \quad (6.81)$$

The design matrix is

$$A = [0 \quad 1] . \quad (6.82)$$

GPS Constant Heading Update

The is one observation equation from the GPS velocity filter, namely;

$$az_{GPS \text{ derived}} = az_{pred} . \quad (6.83)$$

The design matrix is

$$A = [1 \quad 0] . \quad (6.82)$$

The conversion of velocity to speed and heading is given in Section 6.5.2.

Odometer Zero Velocity Update

This is one observation equation coming from the odometer that is used when the velocity is detected as being zero, namely;

$$az_{odo} = az_{pred} = 0.0 \quad . \quad (6.83)$$

In this case the vehicle is deemed to be stopped, thus the heading rate is zero.

The design matrix is

$$A = [0 \quad 1] \quad . \quad (6.84)$$

6.5.2 Propagation of Velocity to Azimuth and Speed

The output from the GPS filter are velocity components. In order to use them in the heading filter they must be converted to speed and heading along with the associated covariance propagation.

The output from the GPS filter is

$$V_N, V_E, \sigma_{VN}^2, \sigma_{VE}^2 \quad ,$$

where

V_N, V_E are the north and east velocity components respectively (m sec^{-1}), and
 $\sigma_{VN}^2, \sigma_{VE}^2$ are the north and east velocity component variances, respectively ($\text{m}^2 \text{sec}^{-2}$).

The required input to the heading filter is

$$az, speed, \sigma_{az}^2, \sigma_{speed}^2 \quad ,$$

where

$az, speed$ are the heading and speed the vehicle is travelling at ($\text{rad}, \text{m sec}^{-1}$), and
 $\sigma_{az}^2, \sigma_{speed}^2$ are the variances respectively ($\text{rad}^2, \text{m}^2 \text{sec}^{-2}$).

The conversion equations are

$$speed = (V_N^2 + V_E^2)^{0.5}, \text{ and} \quad (6.85)$$

$$az = \tan^{-1}\left(\frac{V_E}{V_N}\right). \quad (6.86)$$

The variances are

$$\sigma_{az}^2 = \frac{\cos^2(az) \cdot \sigma_{VE}^2 + \sin^2(az) \cdot \sigma_{VN}^2}{speed^2}, \text{ and} \quad (6.87)$$

$$\sigma_{speed}^2 = \sin^2(az) \cdot \sigma_{VE}^2 + \cos^2(az) \cdot \sigma_{VN}^2. \quad (6.88)$$

6.5.3 Conversion of Speed and Heading to Velocity

The conversion of speed and heading to velocity components is as follows:

$$V_E = \sin(az) \cdot speed, \text{ and} \quad (6.89)$$

$$V_N = \cos(az) \cdot speed. \quad (6.90)$$

The corresponding error propagation is

$$\sigma_{VN}^2 = \frac{V_N^2 \cdot \sigma_{speed}^2}{speed^2} + \frac{V_E^2 \cdot V_N^4 \cdot \sigma_{az}^2}{speed^4 \cdot \cos^4(az)}, \quad (6.91)$$

$$\sigma_{VE}^2 = \frac{V_E^2 \cdot \sigma_{speed}^2}{speed^2} + \frac{V_N^6 \cdot \sigma_{az}^2}{speed^4 \cdot \cos^4(az)}, \text{ and} \quad (6.92)$$

$$\sigma_{VNE}^2 = \frac{V_N \cdot V_E \cdot \sigma_{speed}^2}{speed^2} - \frac{V_E \cdot V_N^5 \cdot \sigma_{az}^2}{speed^4 \cdot \cos^4(az)}. \quad (6.93)$$

6.6 NavTrax™ Master Filter

The master filter was designed to be as generic as possible. Part of the design goal was to be able to add or change sensors without having to significantly modify the master filter,

other than to account for the vehicle dynamics. With this in mind, the master filter consists of three position states (ϕ, λ, h) and three velocity states (V_N, V_E, V_U) . Updates to the filter are also done in terms of position and velocity as follows:

$$\phi_{obs} = \phi_{pred} , \quad (6.94)$$

$$\lambda_{obs} = \lambda_{pred} , \quad (6.95)$$

$$h_{obs} = h_{pred} , \quad (6.96)$$

$$V_{N_{obs}} = V_{N_{pred}} , \quad (6.97)$$

$$V_{E_{obs}} = V_{E_{pred}} , \quad (6.98)$$

$$V_{U_{obs}} = V_{U_{pred}} . \quad (6.99)$$

The vector of unknowns is

$$x = [\phi \quad \lambda \quad h \quad V_n \quad V_E \quad V_U]^T . \quad (6.100)$$

The design matrix for a position update is

$$A_{pos} = \begin{bmatrix} 1 & 0 & 0 & 0 & 0 & 0 \\ 0 & 1 & 0 & 0 & 0 & 0 \\ 0 & 0 & 1 & 0 & 0 & 0 \end{bmatrix} , \quad (6.101)$$

and for a velocity update is

$$A_{pos} = \begin{bmatrix} 0 & 0 & 0 & 1 & 0 & 0 \\ 0 & 0 & 0 & 0 & 1 & 0 \\ 0 & 0 & 0 & 0 & 0 & 1 \end{bmatrix} , \quad (6.102)$$

The transition matrix is given by

$$\Phi = \begin{bmatrix} 1 & 0 & 0 & \frac{\Delta t}{R_m + h} & 0 & 0 \\ 0 & 1 & 0 & 0 & \frac{\Delta t}{(R_m + h) \cos \phi} & 0 \\ 0 & 0 & 1 & 0 & 0 & \Delta t \\ 0 & 0 & 0 & e^{-\alpha \Delta t} & 0 & 0 \\ 0 & 0 & 0 & 0 & e^{-\alpha \Delta t} & 0 \\ 0 & 0 & 0 & 0 & 0 & e^{-\beta \Delta t} \end{bmatrix}, \quad (6.103)$$

where

α is the inverse of the correlation time for the horizontal velocity (sec^{-1}), and

β is the inverse of the correlation time for the vertical velocity (sec^{-1}).

The process noise matrix is

$$C^u = \begin{bmatrix} Q_1 \Delta t & & & & & \\ & Q_2 \Delta t & & & & \\ & & Q_3 \Delta t & & & \\ & & & Q_4 \Delta t & & \\ & & & & Q_5 \Delta t & \\ & & & & & Q_6 \Delta t \end{bmatrix}. \quad (6.104)$$

The above expression may be simplified to

$$C^u = \begin{bmatrix} 0 & & & & & \\ & 0 & & & & \\ & & 0 & & & \\ & & & Q_4 \Delta t & & \\ & & & & Q_5 \Delta t & \\ & & & & & Q_6 \Delta t \end{bmatrix}, \quad (6.105)$$

because the kinematic model deficiencies are only in the vehicle velocities, as the position is not affected by vehicle dynamics [Wong, 1987; Cannon, 1990]. Values for these quantities and they are given in Table 6.9.

Table 6.9 Values for Master Filter
Spectral Densities Q_i , variances σ_i^2 and Correlation Length α_i^{-1}

States	σ_i^2	Q_i	α_i^{-1}
Position (x_k, y_k, z_k)		0	
Horizontal velocity	$1 \text{ m}^2 \text{ sec}^{-2}$	$2 \text{ m}^2 \text{ sec}^{-3}$	1 sec
Vertical velocity	$1 \text{ m}^2 \text{ sec}^{-2}$	$0.1 \text{ m}^2 \text{ s}^{-3}$	20 sec

The process noise must be reduced by the proportionment factor γ_m to account for the additional process noise incurred on the local filters by the federated filter process. The process noise becomes

$$C^u = \begin{bmatrix} 0 & & & & & \\ & 0 & & & & \\ & & 0 & & & \\ & & & Q_4 \Delta t \cdot \gamma_m & & \\ & & & & Q_5 \Delta t \cdot \gamma_m & \\ & & & & & Q_6 \Delta t \cdot \gamma_m \end{bmatrix}, \quad (6.106)$$

where γ_m is a function of the number of local filters and the feedback γ_i .

CHAPTER 7

SENSOR ASSESSMENT

Described in this Chapter are the various tests carried out on the sensors to determine their operating characteristics. The dead reckoning sensors were tested as to their sensitivities to changes in operating temperatures. Some attempt was made to model these changes. The compass was also tested when various devices were operating in the vehicle. The GPS was tested as to its tracking capabilities in an urban environment. All equipment was mounted in a 1990 Ford Aerostar van. Tests were also done to ascertain the best location for sensor installation.

7.1 Dead Reckoning Sensors

The sensors used for navigation must withstand the temperature extremes experienced in a vehicle environment which may range from -40° to $+50^{\circ}$ C. Tests were performed to gauge the sensitivity and linearity of the output of the sensors to temperature change.

The Etak compass and rate gyro and the Murada rate gyro were subjected to temperatures, varying between -40° and $+50^{\circ}$ C, in an environmental chamber. The outputs of the sensors were monitored with a data logging system which has an A/D resolution of 14 bits. The data was recorded once per second. Shown in Figure 7.1 is the temperature profile as a function of time. The rapid temperature changes were enforced to simulate leaving a heated garage in the winter and travelling into cold winter temperatures and vice versa.

The temperature was monitored with an AD590 temperature transducer mounted to the gyros. The transducer has an approximate constant offset error of 0.5° C. The temperature

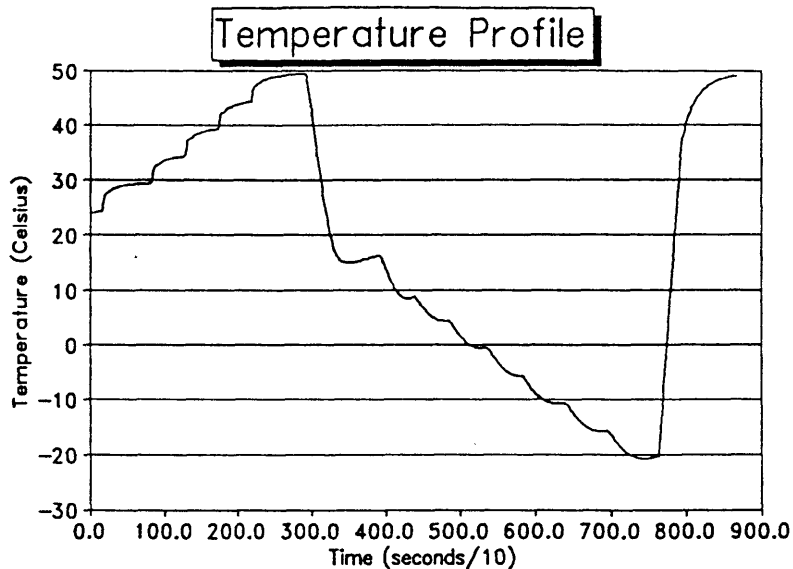


Figure 7.1.

as indicated by the AD590 does not reflect the internal temperature of the sensors but does reflect the ambient temperature in the test chamber. The temperature chamber has heating and cooling capacity. Cooling is provided by carbon dioxide expansion.

The test was begun at room temperature and heat only was applied to bring the temperature up to +50° C in five steps. The chamber was maintained at +50° C for approximately ten minutes until thermal equilibrium was attained. The temperature was then lowered to -20° C in eight steps using cooling only. The temperature was then raised to +50° C in one step. Results of the tests are reported in the following sections.

7.1.1 Compass

The Etak compass x axis output varies with temperature as shown in Figure 7.2. The slanted output is the raw response of the compass to the temperature profile. The straight line is a best fit to this output. The horizontal output has been temperature corrected using the best fit straight line. From the graph, it can be seen that the compass changes due to

temperature can be modelled with some degree of confidence.

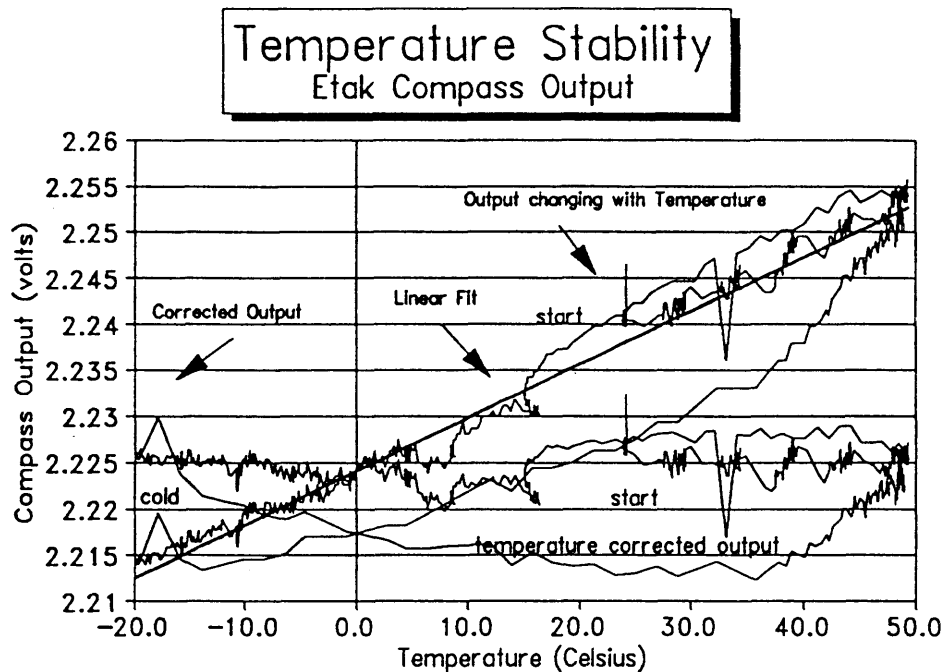


Figure 7.2. Etak Compass Response

Tests were also conducted as to the best place for installation of the compass. The optimal location is in the roof of the vehicle as far as possible from the engine and any electrical motors. The compass is usually mounted such that one of its axis is parallel to the forward motion of the vehicle. The compass should also be located such the magnitude of the x and y ranges are approximately equal. If they are not, the compass output will have to be modelled as an ellipse rather than a circle. The compass generally should not be located near the sides of the vehicle, so as to minimize external effects. It is also critical that the compass be mounted horizontal so tilt effects are not combined with inclination. The location that matches all the above criteria can generally only be determined by empirical testing for each vehicle make and model.

It is well known that compass-derived headings are adversely affected by a variety of unmodelled external magnetic forces, such as driving over a steel girder bridge or other vehicles passing by. In some cases these magnetic disturbances can cause almost instantaneous heading deflections of greater than 90° and at times even 180° . In order to learn about these effects on the compass, raw compass data was gathered under a variety of conditions.

It is the raw X and Y voltages that were analyzed and not the derived headings, since a deflection in the raw values affects the derived heading in different ways depending upon the orientation of the vehicle. The reason for this lies in the fact that headings are computed by evaluating where the raw values are placed on a calibrated circle model. Therefore a shift in raw X or Y can produce no apparent heading error, a large heading error, or somewhere in between, depending upon the placement of the raw values on the circle.

Several test runs were performed with the NavTrax system in order to determine the behavior and characteristics of the compass. The van was in a stationary position for testing the compass output for various vehicle power fluctuations. Data was collected before, during, and after the air conditioner was used at full power. While the air conditioner was running, the electric windows were also operated for a short interval of time.

The results of this test show that the air conditioner can produce a heading deflection of up to 20° in the worst case. This is seen in Figure 7.3 where the Y value changed by 0.04 volts. It has not been determined if the reason for this is that the power to the navigation system is inadequately filtered, or if the air conditioner induces a magnetic field which the compass detects. Note in Figure 7.4 that the X value was only affected minimally. The y axis units are in volts and the x axis is in seconds in both Figures 7.3 and 7.4.

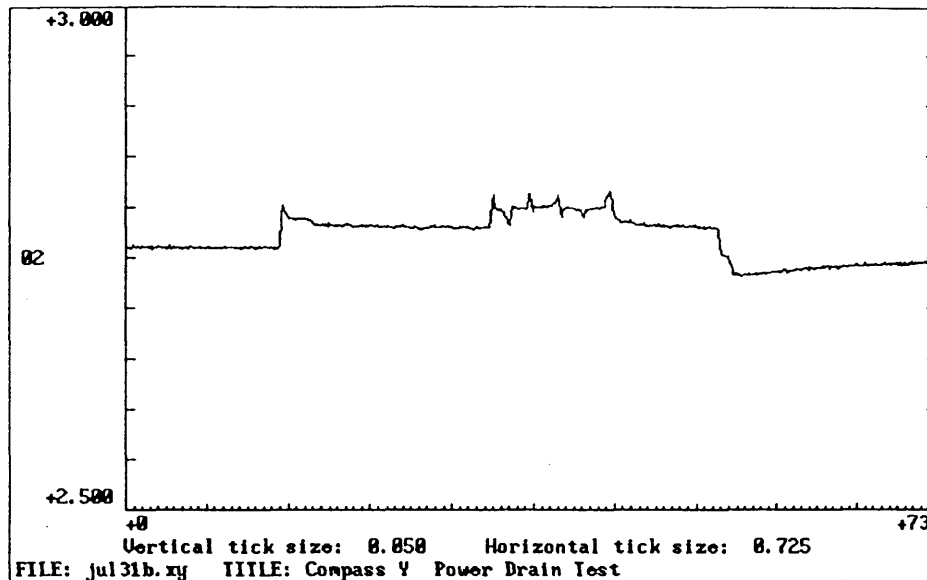


Figure 7.3 Compass Y Power Drain Test

The compass derived headings are extremely sensitive to unmodelled external forces. It seems that concentrations of metal in nearby objects (bridges, other vehicles) cause large instantaneous heading deflections. If the compass is to be used for dead reckoning in a land vehicle, algorithms must be employed to filter out these effects and other blunders.

The vehicle takes on its own magnetic field. The field can be changed instantaneously by events such as hitting a pot hole, slamming a door or putting metal material in the vehicle. It was also found that the number of people in the vehicle changes readings, since the increased weight changes the pitch and roll of the vehicle.

The pitch and roll from the Etak turn sensor, were used to try to account for the tilt of the compass. It was found, nonetheless, that the vehicle tilted the most on turns. The pitch and roll, however, were influenced by the centrifugal forces and could not be used.

At present, a simple misclosure check on the observation prior to input into a local filter is used. The check on the misclosure can be performed using either a preset threshold or the variances for the state being increased by an expansion factor.

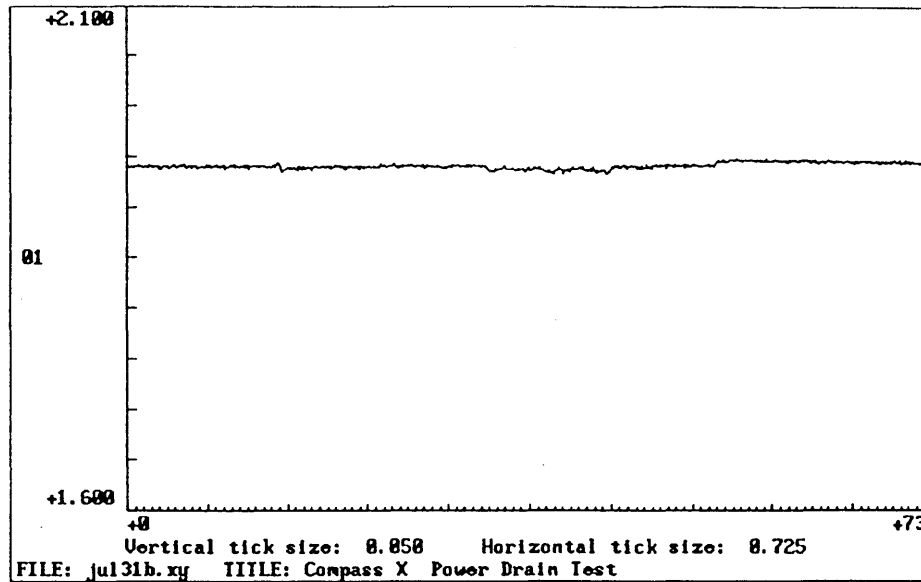


Figure 7.4 Compass X Power Drain Test

7.1.2 Rate Gyro

The rate gyro (GYROSTAR™ by Murata) outputs a voltage proportional to the rate of angular motion. The output is also offset by a voltage that varies with the power supply.

An important characteristic of the rate gyro is its sensitivity to temperature changes. Shown in Figure 7.5 is the output from the GYROSTAR as the temperature was varied in the previously described manner.

Shown in Figure 7.6 is the output from the Etak turn sensor as the temperature was varied in the previously described manner.

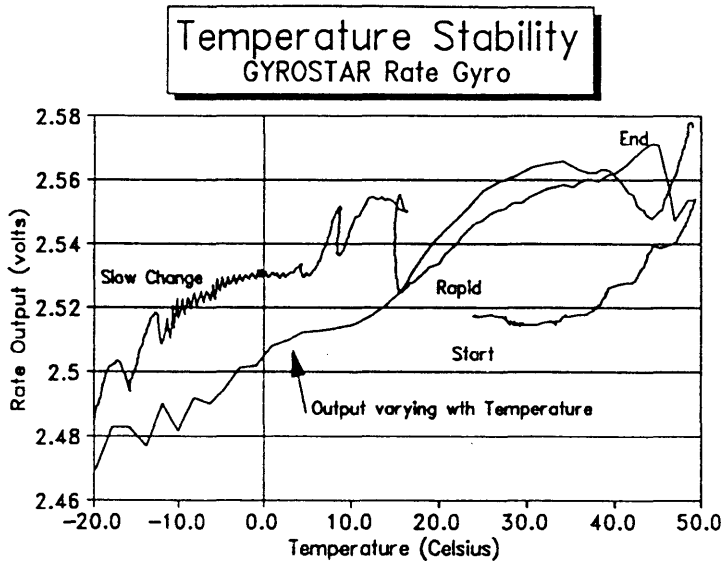


Figure 7.5.

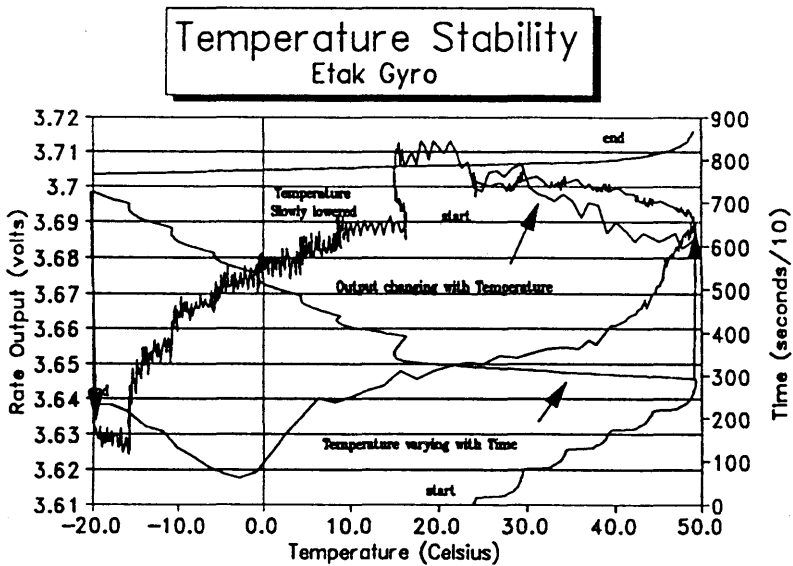


Figure 7.6.

A large hysteresis with change in temperature is exhibited in all of the temperature responses except for the compass. A linear regression analysis will indicate the closest straight line fit but cannot be used to correct the gyro outputs because of the larger hysteresis. If applied, as much error would remain in the corrected gyro outputs as existed prior to correction.

The rate gyro is also affected by vibration in the vehicle and by jolts. It recovers from the jolts, but heading error will occur if the heading rate is used over the period the jolt occurred.

Errors are also caused by not mounting the gyro exactly perpendicular. This has the effect of sensing heading rate change when there is none.

The drift of the gyro is quite small when operated under ideal operating conditions. However, when driving on typical Calgary roads, there are problems. When driving up a straight incline, the compass senses a heading change due the tilt. The rate gyro also experiences a similar effect, though smaller, since the sensitive axis is partly rotated during the transition period in and out of the vertical curves. This problem is compounded on a turn that is super elevated.

7.1.3 Odometer

The White odometer outputs 4000 pulses per kilometre travelled. The odometer is connected to the transmission. When the vehicle rolls ahead or backwards, the odometer outputs pulses proportional to the distance travelled.

The scale factor for converting pulse counts to distance travelled is dependent upon the effective radius of the wheel. This radius can vary as a function of tire pressure and speed. It is also affected by the tread wear of the tires and the type of tires used.

Shown in Figures 7.7 and 7.8 are changes due to variations in velocity and tire pressure. It can be seen that bias ply tires are much more sensitive than radial tires. The type of tires should be taken into account when choosing the filter state parameters. Clearly, the odometer scale is much more sensitive to tire pressure variations in bias ply tires than in radial tires.

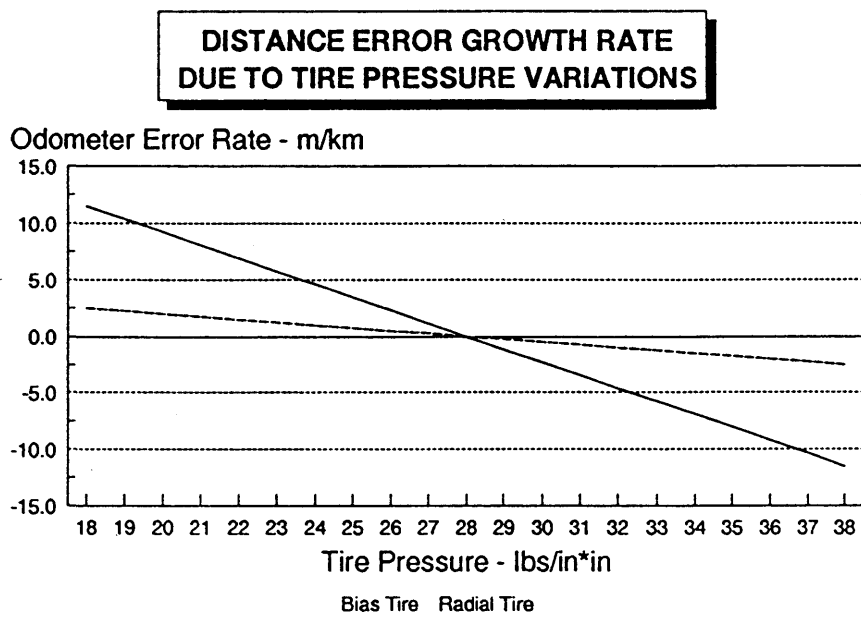


Figure 7.7.

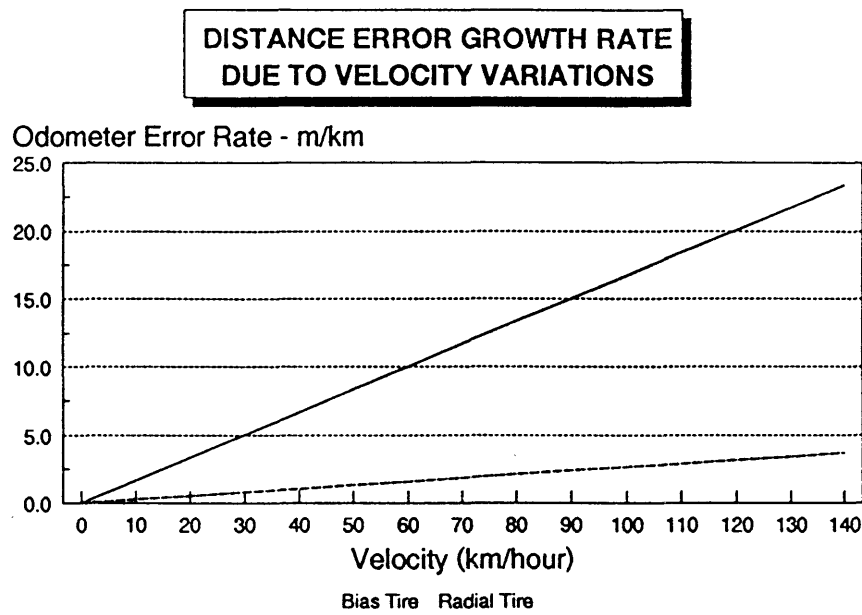


Figure 7.8.

7.2 GPS

Tests were performed within the urban and suburban areas of Calgary to ascertain how often and where positioning was not possible due to GPS signal blockage and multipath [McLellan et al., 1990].

In the City of Calgary, the urban environment containing tall buildings and areas with foliage over the streets comprise less than five percent of the roads. The area containing tall buildings does, however, have a high concentration of traffic, hence, it is still a major concern. Large trees also can cause blockage, but again, account for only a small percentage of the navigatable roads in Calgary.

Illustrated in Figure 7.9 is the single line road network for Calgary's downtown core and the fringe urban areas. Shown are thicker lines defining the GPS (only) satellite derived path of Pulsesearch's test vehicle within the downtown core. During the period of testing,

five satellites were visible above five degrees. While the test vehicle was within the downtown core, a number of positioning outages were experienced which are illustrated by a broken line.

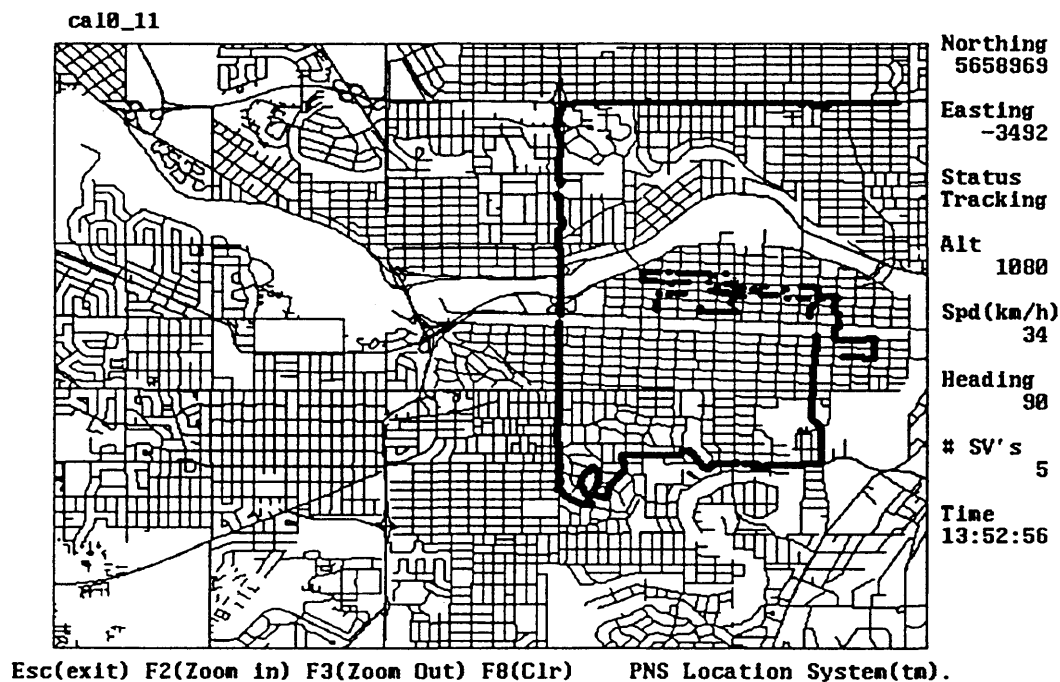


Figure 7.9 Urban Tracking (NavTrax Screen)

These outages ranged from loss of all but one or two GPS satellites to the loss of one critical satellite which degraded the positioning accuracy sufficiently to render the derived position unusable. Typically, within the downtown core the vehicle could track at least three satellites at intersections and combined with a height constrained solution, this was sufficient to determine a horizontal position. Satellite positioning was often lost while driving the block long (about 200 m) urban canyons between the intersections. These urban canyons are bounded by tall buildings constructed close to the roads and the roadways are often crossed by Plus 15 walkways which will effectively block all satellite signals if you are unfortunate enough to stop beneath one. Within the downtown core, positioning was

available approximately 40% to 50% of the time during this one particular run. While this may be sufficient for monitoring vehicle positions on an occasional basis it is less than satisfactory for detailed navigation and route guidance for emergency services.

Illustrated in Figure 7.10 are some typical positioning results within Calgary's fringe urban, suburban and light industrial areas. Part of the test vehicle's path is along a freeway and occasional satellite positioning outages were recorded when the vehicle drove through underpasses. Other outages experienced were due to buildings and trees blocking critical satellites. In this case, GPS navigation was available approximately 99% of the time. Similar outages are shown in the test results given in Chapter 8.

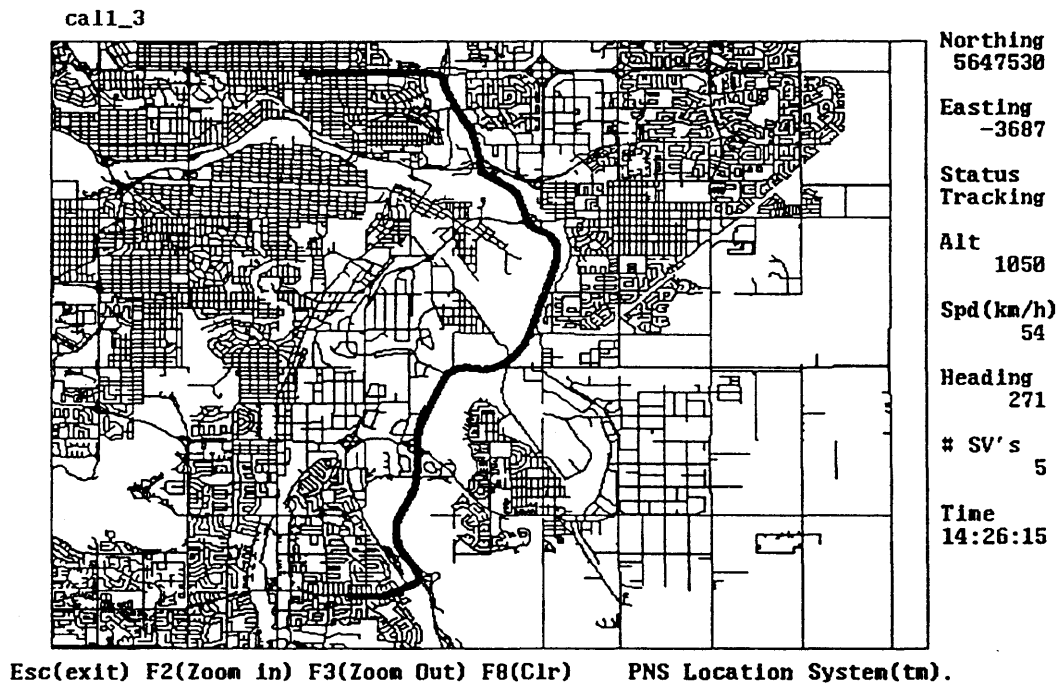


Figure 7.10 Suburban Tracking (NavTrax Screen)

Having tested each sensor separately, the task at hand is to now test the combination of these sensors- namely the NavTrax™ System (Chapter 8).

CHAPTER 8

TEST DESCRIPTION AND RESULTS

Testing of the system was done from several points of view. In the previous section, the individual sensors were tested and analyzed to learn about their characteristics and to establish accuracy values. Given the large number of filters and the quantity of data, a user friendly system was required to test the system and tune the filters without extensive field testing. A setup was also required to test the accuracy of the system, given that the most critical part was in the downtown urban core where satellite visibility was limited.

A single line road network was developed for Calgary and was being tested for dispatching of police vehicles. For the purposes of testing, it was decided to run the navigation software on one computer and then transmit the coordinates to a dispatch display computer in a compatible format. The various states were displayed on the navigation computer while simultaneously the position was displayed on the NavTrax screen. In this way the system accuracy relative to the single line road network could easily be visually accessed. Also, tuning values for the filters could be quickly changed and the results readily available.

The input values (standard deviations on observations, correlation times, spectral densities) were given in the previous chapter for the various filters and were obtained using the software described in Section 8.1. The values are being modified over time as further system experience is gained. The frequency of measurement updates is also being tuned to combine system accuracy and computation through put.

8.1 NavTrax™ Testing

Shown in Figure 8.1 is the initial navigation filter states at cold startup. All quantities have been defined in earlier Chapters. During offline data processing, the system can be "paused" and a snapshot of the system states can be recorded for further analysis.

Five filters are displayed in Figure 8.1, namely:

- (1) Master filter,
- (2) Compass filter,
- (3) DR Heading filter,
- (4) Odometer filter, and
- (5) Gyro filter.

During this test, the states for the GPS solution were taken from the internal MX 4200 Kalman filter. GPS solutions were weighted according to the computed Horizontal Dilution of Precision (HDOP) values.

Observations were tested prior to being added to the local filter (two times standard deviation compared to predicted state). If rejected, they would show up in the "Upd Rejected" appropriate row. For compass observations, if either x or y was rejected, they were both rejected.

The latitude and longitude are in decimal deg, velocity is in m sec^{-1} , heading in deg, heading rate in deg sec^{-1} and speed in m sec^{-1} . The compass biases and the gyro offset are in volts.

Figure 8.2 is a screen capture on the NavTrax display. The display could be zoomed out to include the whole city or zoomed in to a level where the whole screen only covered 10 m. At the smaller scales, only the major roads appear. Various classifications of roads are added in at the larger scales. By using a mouse, and clicking on a road, the street name and address would appear in the side bar.

Test results given include a 32 km test run starting at Southland Drive and MacLeod Trail in the south part of Calgary. The vehicle proceeded to the downtown core and made several crossings of the downtown core. The vehicle then proceeded east on Memorial Drive, south on Deerfoot Trail and then west on Southland Drive to MacLeod Trail.

PNS Navigation Filter						
MASTER FILTER						
	Lat	Lng	Alt	Vn	Ve	Vv
States:	50.963	-114.072	1037	0.00	0.00	0.1
Std Dev:	500	500	10	10.0	10.0	3.0
Upd Rejected:	0	0		0	0	
COMPASS FILTER						
	Heading	H-Rate	Radius	Cx	Cy	AngOff
States:	90.0	0.00	0.34392	2.34197	2.72277	198.1
Std Dev:	30.0	10.00	0.01000	0.01000	0.01000	1.0
Upd Rejected:	0			0	0	
DR HDG FILTER		Heading	H-Rate	ODO FILTER		Speed
States:	90.0	0.00			0.00	4.846
Std Dev:	6.3	0.00			1.00	0.010
Upd Rejected:	0	0			0	
GYRO FILTER		H-Rate	Drift	Offset		
States:	0.00	-0.1808	2.5050			
Std Dev:	0.01	0.0100	0.0100		GPS HDG:	90.0
Upd Rejected:	0				GPS TIME:	157204.0
F1 = Save States F2 = Pause				F10 = Run 4200 Program		

Figure 8.1 Filter Screen (Initial)

The test included speeds from stop and go (0 to 20 km hr⁻¹), urban streets (40 to 70 km hr⁻¹), and freeway speeds (90 to 110 km hr⁻¹). The vehicle passed over steel and concrete bridges and over and under passes. Satellite visibility ranged from six in number in the open areas to none in certain parts of the downtown core.

It should be noted that S/A was turned off during this test. Additional tests were conducted where differential range corrections were transmitted to the MX 4200 in the vehicle. These tests were conducted during the Gulf War, and the range corrections were quite small resulting in a small improvement to the GPS solutions. These tests were conducted on a 34 km baseline located outside the city on rural roads.

Shown in Figures 8.3 and 8.4 are the standard errors (filtered) in latitude and longitude for the total run. These standard errors were calculated as the square root of the corresponding values of the covariance matrix of the state vector. The areas where the growth of the standard

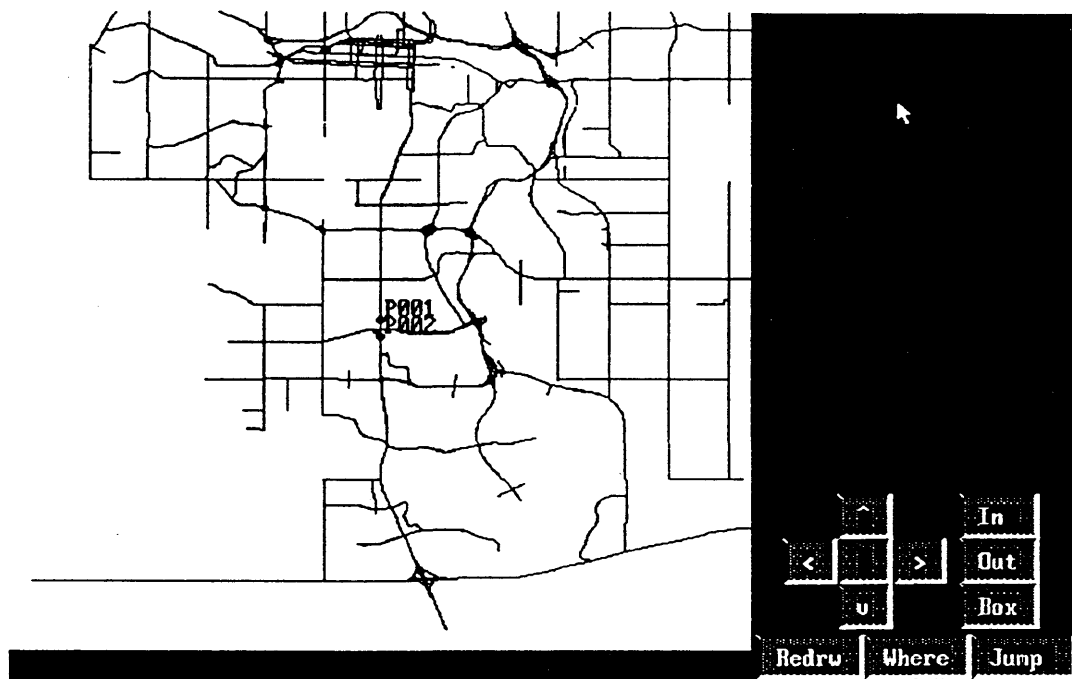


Figure 8.2 Initial NavTrax Screen - Overview

errors increased rapidly, the system was running with dead reckoning only. The system has purposely been tuned with a high noise level on the dead reckoning components to allow the GPS to dominate.

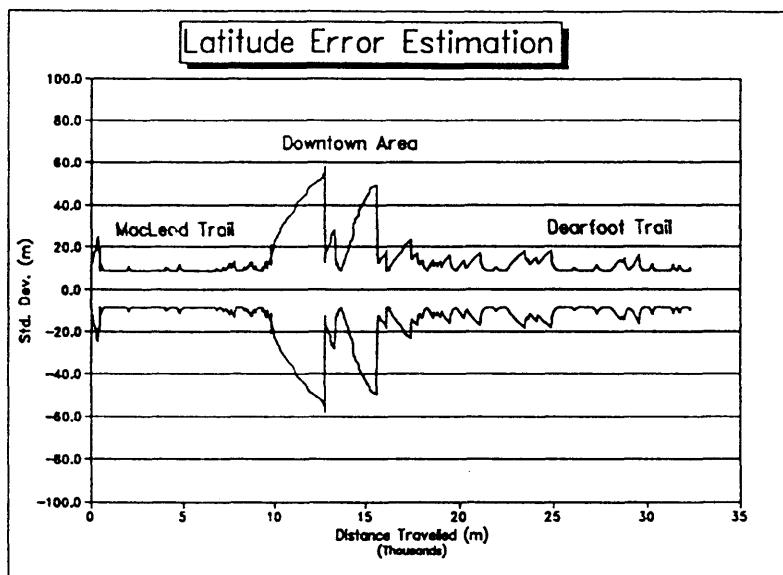


Figure 8.3

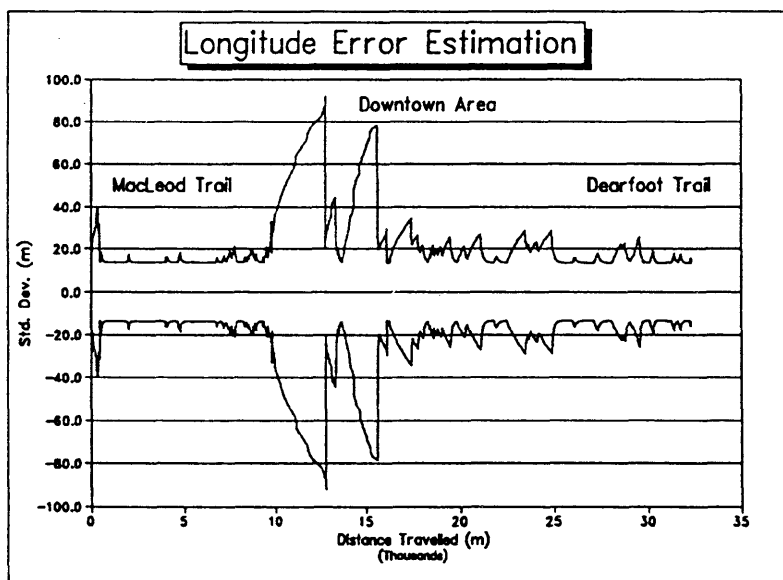


Figure 8.4

Shown in Figure 8.5 is the case of the vehicle proceeding north on MacLeod Trail. Where the vehicle appears to be veering to the right, it was moving from the lane closest to the centre line meridian to the lane on the outside of the road. Clearly, one of the problems

with single line roads is that three to four lanes must be approximated by a single line. Also, in Calgary, the single line road was taken from the center line of the legal property boundaries of the roadway rather than from the actual road surface (between curbs).



Figure 8.5 NavTrax Screen - MacLeod Trail

Shown in Figures 8.6 and 8.7 are the standard errors (filtered) of the latitude and longitude while travelling north on MacLeod Trail to 10 Street S. The GPS bounded the error growth to about 20 m.

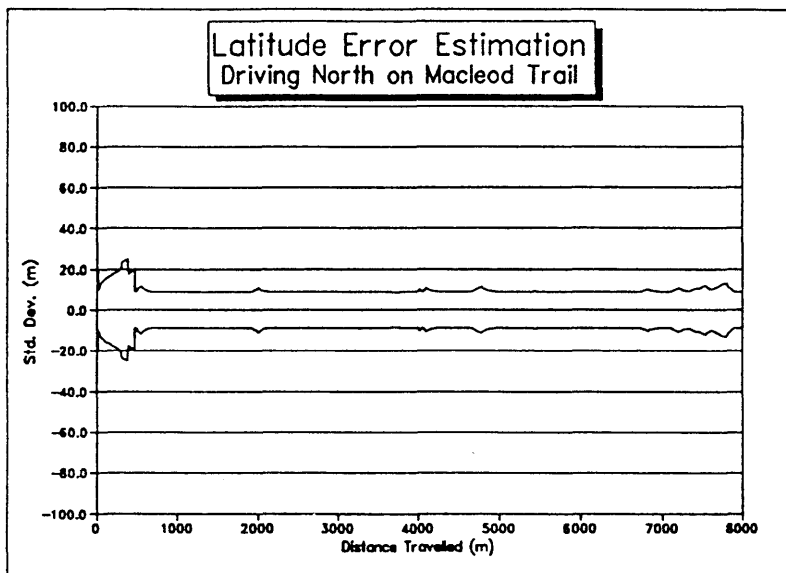


Figure 8.6

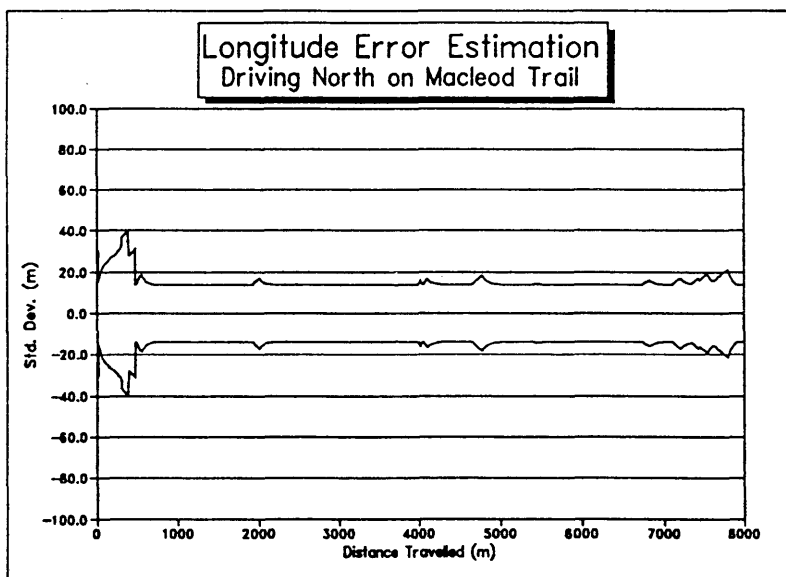


Figure 8.7

Shown in Figure 8.8 is the status of the filters in the downtown part of the run. Note the large number of rejections of compass observations below the calibration parameters (1181, 1629). In early testing, it was thought that the compass observations could simply

be de-weighted and included in the solution. Increasing the standard deviation up to 20 degrees caused a bias in the heading determination, thus the practise of increasing the variance was found to be faulty.

Without disturbances, the compass is accurate to about three to five degrees, however, blunders can cause it to be out as much as 180°. These are easy to detect, however, the real problem is on hills where it may only be out 5° to 10°. A better solution was obtained when a fairly high rejection criteria (< 10°) was applied. The compass can still be beneficial when there are long GPS outages.

PNS Navigation Filter						
MASTER FILTER						
States:	Lat	Lng	Alt	Vn	Ve	Vv
	51.049	-114.074	1098	-0.53	13.38	0.0
Std Dev:	41	66	82	0.50	0.60	0.5
Upd Rejected:	0	0		0	0	
COMPASS FILTER						
States:	Heading	H-Rate	Radius	Cx	Cy	AngOff
	87.6	0.33	0.34666	2.37111	2.73636	198.0
Std Dev:	15.7	2.10	0.00796	0.01174	0.01216	0.7
Upd Rejected:	0			1181	1629	
DR HDG FILTER		Heading	H-Rate	ODO FILTER		Speed
States:		92.3	-0.18			13.40
Std Dev:		2.1	0.05			0.60
Upd Rejected:		0	1			5
GYRO FILTER		H-Rate	Drift	Offset		
States:		-0.18	-0.1832	2.5059		
Std Dev:		0.05	0.0030	0.0010		
Upd Rejected:		1				
				GPS HDG: -9.0		
				GPS TIME: 158326.0		
F1 - Save States F2 - Pause				F10 - Run 4200 Program		

Figure 8.8 Filter Screen - Downtown

Shown in Figure 8.9 is the path of the vehicle in the downtown core. The system had very few GPS updates on this part of the test. Travelling up and down the hills (Cemetery Hill, north of Bow River) affected the compass substantially. As previously stated, the vertical component of the magnetic field in Calgary is about 3.6 times stronger than the horizontal component, hence, any tilt of the compass causes a magnified error in heading. Also the vehicle passed under a railway bridge causing the compass heading to deviate substantially. The rate gyro is also affected by the inclines, though by a much smaller amount.

When the receiver was only able to track three satellites, it went into an altitude hold mode, and constrained the height to the initialization value, which in this case is an average value for the whole city. This caused some of the jumps in position shown in Figure 8.9. The maximum error in position, compared to the single line road map occurred in the downtown area, where there was little or no GPS available. The maximum error detected was about 70 m, which is within the computed accuracy estimate. With the parameters used in the current filters, the computed error growth from the dead reckoning system is about 1.0 to 1.5% of the distance travelled.



Figure 8.9 NavTrax Screen - Downtown

Shown in Figures 8.10 and 8.11 are the standard deviations (filtered) of the latitude and longitude in the downtown core. Intuitively, one would expect that the latitude error would be larger than the longitude, since the direction of travel is primarily east-west. The

larger longitude error is confirmed in Figure 8.9, however. Since the GPS was only operating on three satellites for most of the time in this area, this may be affecting the longitude with a poor HDOP value.

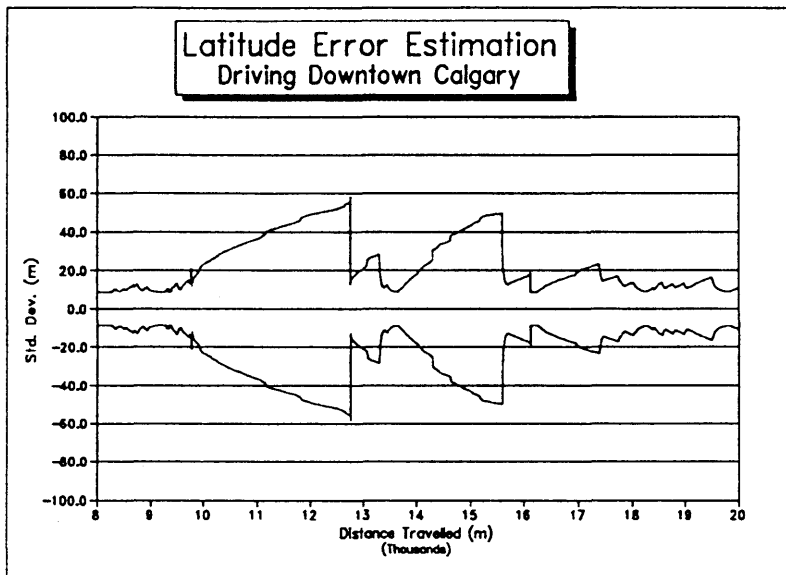


Figure 8.10

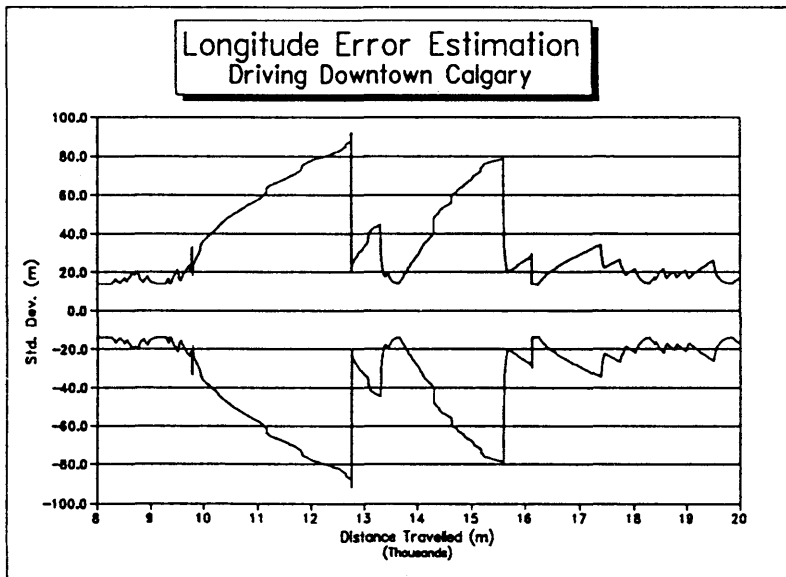


Figure 8.11

Shown in Figures 8.12 and 8.13 are the standard errors (filtered) of the latitude and longitude while travelling east on Memorial drive and then south on Deerfoot Trail. The small spikes are due to short GPS outages.

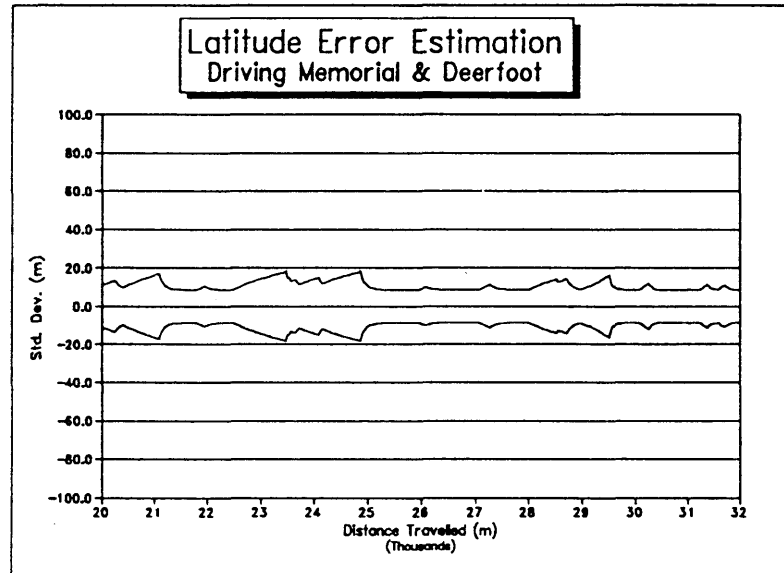


Figure 8.12

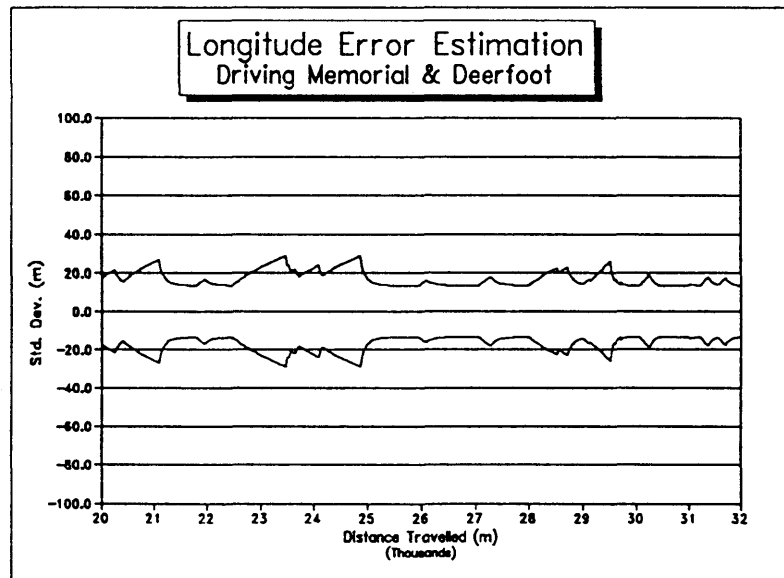


Figure 8.13

8.2 Field Trials In the Calgary Police Department

Field trials of NavTrax™ were conducted in The City of Calgary Police Department during the spring and fall of 1991. A variety of vehicles were selected including a van, an off road vehicle and three cruisers. All were responsible for responding to 911 calls. The van was designated as a supervisor's vehicle and was responsible for about 20 vehicles in its zone. This trial was performed in conjunction with the development of a single line road network data base for Calgary [McLellan et al., 1991], in which about 30,000 nodes (intersections, shape points) and 50,000 links (road links, shape cords) are involved. Accurate geometry (3 to 5 m), full connectivity, address ranges and street names make up this data base.

A UHF private radio system base station was installed at Pulsesearch's office which is capable of reaching vehicles out to about 35 km. There were only a few areas where there were signal outages. A dedicated phone line was installed which relayed the information to the central dispatch centre where all emergency calls are handled. Pulsesearch was also able to eavesdrop on the signal and display information on their own computer for testing purposes. Dataradio modems were used to communicate from the processors to the radio. There are plans to interface with the Motorola MDT system as these are installed in many current police installations.

The test ran independent of the dispatcher's computer system. A display was installed above the dispatcher's normal screen allowing a view of large parts of the City down to the intersection level. A 14 inch screen was used for the test, however, from discussions with the dispatchers, a much larger screen would eventually be required. The dispatchers quickly saw the benefits of having the vehicles displayed on a map, their only comment being that five vehicles was not enough for an accurate evaluation. It was felt that a complete district (about 30 vehicles) would have to be equipped to fully test the system.

At the other end of the spectrum, there were a few skeptical officers, who felt their privacy was being invaded. The system is being presented to the police officers as a tool that can improve their safety in cases of danger. Due to ever increasing budget restraints the police forces must be able to better utilize their existing fleet resources. There is the same type of reluctance that occurred when Computer Aided Dispatch (CAD) systems were initially introduced. These have now been accepted, and similarly Automatic Vehicle Location (AVL) will be the next technology to be introduced.

The accuracy issue was also addressed in this test as to what is needed in order to correctly allocate - dispatch the correct vehicle to an emergency call. Placing the vehicle on the wrong street would not be tolerated, as well, continuous positioning is required at all times. This means that an accuracy value of about 30 m is required and DR sensors are needed to bridge the gap caused by the blockage of GPS signals.

CHAPTER 9

SUMMARY AND CONCLUSIONS

In so far as land navigation related technology is concerned, the following conclusions can be made as a results of the research performed herein:

- (1) The advent of GPS has been the single-most important technological development to help improve the navigation and dispatching of fleets of vehicles.
- (2) Digital communications, inexpensive and high-powered PC's, and road network data bases complete the array of technologies, that, when integrated into a system, can significantly improve the safety and efficiency of mobile operations.
- (3) The price of GPS sensors are decreasing rapidly. Sensor assemblies are now readily available for under \$1,000 in OEM quantities. Manufacturers are claiming that the price will and must drop to the \$100 level for car manufacturers.
- (4) Many of the low cost receivers, however, only provide position information without raw data. Those that do provide raw data only supply pseudoranges with no carrier phase information. Many of the low cost receivers take a substantial time to initialize (3 to 4 minutes) with is unacceptable for emergency response vehicles. Magnavox has been the exception and are providing raw data with the exception of the polarity on the raw carrier phase data.
- (5) Gyro sensors are improving in quality, reducing in size and becoming much cheaper. Differential odometry will be obtainable at the OEM level by taking advantage of anti-lock braking systems (ABS) which are now becoming standard equipment on many new vehicles. The combination of differential odometry with a rate gyro will greatly improve the heading.

- (6) DGPS technology is needed for an array of users including police and fire fighting operations, as well as mobile GIS applications. Many organizations, such as EMR, Coast Guard and Provincial Agencies, are considering setting up their own differential networks. Some manufacturers, such as Trimble and Magnavox, are looking at nation wide services.

Conclusions concerning the NavTrax™ system developed principally by the author, and reported herein are as follows:

- (1) Continuous and economical positioning can be achieved by integrating GPS with dead reckoning devices, this integration is needed for emergency fleet services in areas of GPS signal blockage.
- (2) The key to multi-sensor integration is to decentralize the computation process so that spurious readings can be blocked and removed from entering into the combined solution for position and velocity.
- (3) Trials in Calgary have indicated that dispatching of police vehicles is significantly enhanced through the use of a GPS based positioning system - NavTrax™.
- (4) The best positional accuracy achieved by the NavTrax™ System was when all sensors were functioning and were continuously added to the solution. A standard error of about 20 m is representative of this situation (with SA off).
- (5) The worst positional accuracy occurred in the downtown core where frequent GPS signal blockage occurred. A standard error of up to 80 m was experienced (with SA off), which is a function of the error growth on the dead reckoning system with no external updates.

REFERENCES

- BOMFORD, G. [1971]. *Geodesy*. Oxford.
- BROWN, R.G. [1983]. *Introduction to Random Signal Analysis and Kalman Filtering*. Wiley and Sons, New York.
- CANNON, M.E. [1987]. *Kinematic Positioning Using GPS Pseudorange and Carrier Phase Observations*. Masters Thesis, Publication #20019, Department of Surveying Engineering, The University of Calgary, Calgary, Alberta.
- CANNON, M.E. [1990]. *Analysis of Differential GPS Algorithms*, Pulsesearch Internal Report, May.
- CANNON, M.E. [1991a]. *Airborne GPS/INS with an Application to Aerotriangulation*. Doctoral Thesis, The University of Calgary, Department of Surveying Engineering, Calgary, Alberta.
- CANNON, M.E. [1991b]. *Design of a Real-time Differential GPS System for Multiple Tail Buoy Positioning*, Pulsesearch Internal Report, November.
- CARLSON, N.A. [1988a]. *Information-sharing Approach to Federated Kalman Filtering*, *Proceedings of National Aerospace and Electronics Conference, Naecon, Dayton*.
- CARLSON, N.A. [1988b]. *Federated Filter for Fault-tolerant Integrated Navigation Systems*, *Proceedings of IEEE PLANS88*, Nov 28 to Dec 1, Orlando.
- CHAMBERLAIN, S.M. and J. CHUANG [1991]. *Combined GPS/Glonass data Processing*. A Paper Presented at the ION Technical Meeting, January 22 to 24, Arizona.

- DAWSON, E. and L.R. NEWITT [1984]. Magnetic Declination in Canada from 1750 to 1980. **The Canadian Surveyor**. Vol. 38, No. 1, pp. 35 to 40.
- DAWSON, E., L.R. NEWITT, A. NANDI and D. NAGY [1981]. **A Spherical Harmonic Approach to Mapping the Magnetic Field in Canada for 1980**. Geomagnetic Series No. 21, EMR, Ottawa.
- DAVIS, R.E., F.S. FOOTE, J.M. ANDERSON and E.M. MIKHAIL [1981]. **Surveying Theory and Practise**. McGraw-Hill Book Company.
- DENARO, R.P. [1990]. GPS-Based Automatic Vehicle Location (AVL) and Fleet Management Systems - Robust and Affordable for the 90s. Paper presented at the UK NAV 90, September 18 to 20, Warwick.
- FRENCH, R.L. [1974]. **Method and Apparatus Employing Automatic Route Control System**, US Patent No. 3,845,289, October 29.
- GAO, Y., E.J. KRAKIWSKY and J.F. MCLELLAN [1991]. Comparison and Analysis of Centralized, Decentralized and Federated Filters. Submitted to **Institute of Navigation**.
- GAO, Y., E.J. KRAKIWSKY and J.F. MCLELLAN [1992]. Application of Federated Filter Design to Kinematic GPS Positioning, **Proceedings of IEEE PLANS92**, March 25 to 27, Monterey (in press).
- GELB, A. (Editor) [1974]. **Applied Optimal Estimation**. MIT PRESS.
- HARRIS, C.B., [1988]. **A Kalman Filter for Integrating Navstar GPS Pseudorange and Carrier Phase Observables: A Mathematical Formulation**. Course presentation, ENSU625, GPS: Theory and Applications. The University of Calgary, Department of Surveying Engineering, Calgary, Alberta.

- HARRIS, C.B., [1989]. **Prototype for a Land Based Automatic Vehicle Location and Navigation System**. Masters Dissertation, The University of Calgary, Department of Surveying Engineering, Calgary , Alberta.
- HARUMASA, H., S. KAWASHIMA and N. NAKAMURA [1990]. Land Mobile Receiver, **Proceedings of ION GPS-90**, September 19 to 21, Colorado Springs, pp. 183 to 190.
- HATCH, R.R. [1982]. The Synergism of GPS Code and carrier Measurements, **Proceedings of the Third International Geodetic Symposium on Satellite Doppler Positioning**, Feb. 8 to 12, Las Cruces, Vol II, pp. 1213 to 1232.
- HATCH, R.R. [1986]. Dynamic Differential GPS at the Centimeter Level, **Proceedings of the Fourth International Geodetic Symposium on Satellite Positioning**, April 28 to May 2, Las Cruces, Vol. II, pp 1287 to 1298.
- HONEY, S.K., W.B. ZAVOLI, K.A. MILNES, A.C. PHILLIPS, M.S. WHITE Jr. and G.E. LOUGHMILLER Jr. [1989]. **Vehicle Navigation System and Method**. United States Patent Number 4,796,191, January 3.
- HOPFIELD, H.S. [1971]. Tropospheric Effect on Electromagnetically Measured Range: Prediction Surface Weather Data. **Radio Science**, Vol. 6, No. 3, pp. 357 to 367.
- HUANG, P.C. and R.G. BROWN [1990]. GPS Navigation: Combining Pseudorange with Continuous Carrier Phase Using a Kalman Filter. **Navigation**, Vol. 37, No. 2.
- ICD-GPS-200, [1987]. **Interface Control Document**, Navstar GPS Space Segment/ Navigation User Interface, Rockwell International Corporation.
- IKEDA, H., Y. KOBAYASHI, S. KAWAMURA and H. NOBUTA [1991]. "Sumitomo Electric's Navigation Systems for Private Automobiles", **Vehicle Navigation & Information Systems Conference Proceedings**, October 20 to 23, Dearborn, Vol. I, pp 451 to 462.

- KALMAN, R.E. [1960]. A New Approach to Linear Filtering and Prediction. **Journal of Basic Engineering**, ASME, 82D.
- KAO, W. [1991]. "Integration of GPS and Dead-Reckoning Navigation Systems", **Vehicle Navigation & Information Systems Conference Proceedings**, October 20 to 23, Dearborn, Vol. II, pp 635 to 644.
- KRAKIWSKY, E.J. [1973]. **Conformal Map Projections in Geodesy**. Department of Surveying Engineering, Technical Report No. 37, University of New Brunswick, Fredericton, New Brunswick.
- KRAKIWSKY, E.J. [1990]. **The Method of Least Squares: A Synthesis of Advances**. Department of Surveying Engineering, Technical Report, The University of Calgary, Calgary, Alberta.
- KRAKIWSKY, E.J., G. LACHAPELLE, and K.P. SCHWARZ [1990]. **Assessment of Emerging Technologies for Future Navigation Systems in the Canadian Transportation Sector**. Reports of the Department of Surveying Engineering, No. 60007, The University of Calgary.
- KRAKIWSKY, E.J. [1991]. GPS and Vehicle Location and Navigation Systems. Innovation Column, **GPS World**, Volume 2, No. 5, pp. 50 to 53.
- LACHAPELLE, G., J. HAGGLUND, W. FALKENBERG, P. BELLEMARE, M. CASEY and M. EATON [1986]. "GPS Land Kinematic Experiments, Proceedings of the **Fourth International Geodetic Symposium on Satellite Positioning**, Austin.
- LACHAPELLE, G., T. SPEAKMAN, and B. TOWNSEND [1989]. Performance of Loran-C on the Canadian West Coast. Proceedings of the **18th Annual Technical Symposium**, The Wild Goose Association, pp. 135 to 143.

- LACHAPELLE, G., and B. TOWNSEND [1990]. A Comparative Analysis of Loran-C and GPS for Land Vehicle Navigation in Canada. **Canadian Aeronautics and Space Journal**, CASI, Ottawa, Vol. 36, No. 1, pp. 29 to 35.
- LACHAPELLE, G., and B. TOWNSEND [1991]. En-Route Coverage Validation and Calibration of Loran-C with GPS. **GPS World**, Volume 2, No. 3, pp. 36 to 41.
- LILLEY, R.W., and J.S. EDWARDS [1986]. Loran-C Monitor Correlation Over a 92-mile Baseline in Ohio. **Proceedings of the 15th Annual Technical Symposium**, Wild Goose Association, pp. 36 to 44.
- LOOMIS, P., G. KREMER and J. REYNOLDS [1989]. Correction Algorithms for Differential GPS Reference Stations, **Navigation**, Vol. 36, No. 2.
- MARTIN, E.H. [1980]. GPS User Equipment Error Models, **Global Positioning System, Volume I**, Institute of Navigation, Washington, D.C.
- MCLELLAN, J. F., [1987]. **The Application of Satellite Techniques for Cadastral and Geodetic Surveys**. Report prepared to fulfill requirements for Alberta Land Surveyor's License.
- MCLELLAN, J.F., J.R. ADAMS, M. CROCKER, H. OSHIZAWA, E.J. KRAKIWSKY, and H.A. KARIMI [1989]. Dispatch Automatic Vehicle Location, Navigation and Allocation Systems for the Petroleum and Utility Industries, **Proceedings of the CPA Colloquium V Conference**, October 4 to 6, Calgary.
- MCLELLAN, J.F., J.B. SCHLEPPE, and M.E. CANNON [1990]. Performance of a GPS Board Automatic Vehicle Location System within Urban Canyons, **Proceedings of the Second International GPS Symposium**, September 3 to 7, Ottawa.
- MCLELLAN, J.F., E.J. KRAKIWSKY, and J. SCHLEPPE [1991a]. Application of GPS Positioning to Fleet Management of Mobile Operations. Paper Presented at **ACSE GPS91 Conference**, September 19 to 21, Sacramento.

- MCLELLAN, J.F., E.J. KRAKIWSKY, H. HUFF, E. KITAGAWA and M. GERVAIS [1991b]. "Fleet Management Trials in Western Canada", **Vehicle Navigation & Information Systems Conference Proceedings**, October 20 to 23, Dearborn, Vol. II, pp 797 to 806.
- MCLELLAN, J.F. E.J. KRAKIWSKY, J. SCHLEPPE and P. KNAPP [1992]. The Nav-Trax™ Fleet Management System. **Proceedings of the IEEE PLANS 92**, March 25 to 27, Monterey (in progress).
- MORRISON, N. [1969]. **Introduction to Sequential Smoothing and Prediction**. McGraw-Hill Book Co.
- NAKAMURA, T. [1990]. Vibration Gyroscope Employs Piezoelectric Vibrator, **Journal of Electrical Engineering**, Hi-Tech Report, September, pp 99 to 104.
- OECD [1988]. **Route Guidance and In-Car Communication Systems**. Publication of the Organization for Economic Cooperation and Development, Paris.
- SCHWARZ, K.P., M.E. CANNON and R.V.C. WONG [1989]. A Comparison of GPS Kinematic Models for the Determination of Position and Velocity Along a Traverse. **Manuscripta Geodaetica**, No. 14, pp. 345 to 353.
- THOMPSON - HICKLING [1989]. **Radionavigation/Location Requirements for Surface Users in Canada**. Report Prepared for Transport Development Center, Montreal by Thompson-Hickling Aviation Ltd. Ottawa.
- THOMSON, D.B., E.J. KRAKIWSKY and J.R. ADAMS [1978]. **A Manual for Geodetic Position Computations in the Maritime Provinces**. Department of Surveying Engineering, Technical Report No. 52, University of New Brunswick, Fredericton.
- VAN DIERENDONCK, A.J., S.S. RUSSELL, E.R. KOPITZKE and M. BIRNBAUM [1984]. The GPS Navigation Message. Papers published in **Navigation, Global Positioning System, Volume I**, Institute of Navigation, Washington, D.C..

- WEI, M. and K.P. SCHWARZ [1990]. Testing a Decentralized Filter for INS/GPS Integration, **Proceedings of IEEE PLANS 90**.
- VIEHWEG, C.S., R.D. CROWELL, A. AVERIN, and R.H. FRAZIER [1988]. Differential Loran-C system (DLCS) Project - A Status Report. **Proceedings of the 17th Annual Technical Symposium, Wild Goose Association, Bedford**, pp. 187 to 202.
- WELLS, D.E. [1974]. **Doppler Satellite Control**. Department of Surveying Engineering Technical Report 29, University of New Brunswick, Fredericton.
- WELLS, D., N. BECK, D. DELIKARAOGLOU, A. KLEUSBERG, E.J. KRAKIWSKY, G. LACHAPELLE, R. B. LANGLEY, M. NAKIBOGLOU, K.P. SCHWARZ, J.M. TRANQUILLA, and P. VANIECK [1986]. **Guide to GPS Positioning**. Canadian GPS Associates, Fredericton.
- WONG, R.C. [1987]. **GPS Kinematic Positioning with A Kalman Filter Smoother**. Course Assignment, Space Positioning, Department of Surveying Engineering, University of Calgary.
- YIU, K.P., R. CRAWFORD, and R. ESHENBACH [1982]. A Low Cost GPS Receiver for Land Navigation. Papers published in **Navigation, Global Positioning System, Volume II**, Institute of Navigation, Washington, D.C.

APPENDIX A

COORDINATE TRANSFORMATION FORMULAE

A.1 Transformation of (ϕ, λ, h) to (x, y, z)

The transformation of (ϕ, λ, h) ellipsoidal coordinates to (x, y, z) Cartesian coordinates is given by [Krakiwsky and Wells, 1971; Thomson et al., 1978]:

$$x = x_o + (N + h) \cos \phi \cos \lambda \quad , \quad (A.1)$$

$$y = y_o + (N + h) \cos \phi \sin \lambda \quad , \quad (A.2)$$

$$z = z_o + (N(1 - e^2) + h) \sin \phi \quad , \quad (A.3)$$

where

$$e^2 = \frac{(a^2 - b^2)}{a^2} \quad , \quad (A.4)$$

$$N = \frac{a}{(1 - e^2 \sin^2 \phi)^{1/2}} \quad , \quad (A.5)$$

$$M = \frac{a(1 - e^2)}{(1 - e^2 \sin^2 \phi)^{3/2}} \quad , \quad (A.6)$$

and x_o, y_o and z_o are pre-determined translation components. a and b are based on WGS84 and were previously defined.

A.2 Transformation of (x, y, z) to (ϕ, λ, h)

The transformation of (x, y, z) geocentric Cartesian coordinates to (ϕ, λ, h) ellipsoidal coordinates may be done as follows [Krakiwsky and Wells, 1971].

Let

$$x = x - x_o \quad , \quad (A.7)$$

$$y = y - y_o \quad , \quad (A.8)$$

then

$$\lambda = \tan^{-1} \left(\frac{y}{x} \right) \quad . \quad (A.9)$$

Also, let

$$z = z - z_o \quad , \quad (A.10)$$

and

$$S = (x^2 + y^2)^{1/2} \quad . \quad (A.11)$$

Now, find the first approximations for ϕ and λ ,

$$\phi_1 = \tan^{-1} \left[\frac{(z/S)}{\left(1 - \frac{e^2 a}{a+h}\right)} \right] \quad , \quad (A.12)$$

$$h_1 = (x^2 + y^2 + z^2)^{1/2} - a \quad , \quad (A.13)$$

and then iterate the following equations to get more accurate values for ϕ and h ,

$$N_i = \frac{a}{(1 - e^2 \sin^2 \phi_{i-1})^{1/2}} \quad , \quad (A.14)$$

$$h_i = \frac{S}{\cos \phi_{i-1}} - N_i \quad , \quad (A.15)$$

$$\phi_i = \tan^{-1} \left[\frac{(z/S)}{\left(1 - e^{2*} \frac{N_i}{N_i + h_i}\right)} \right] \quad . \quad (A.16)$$

Equations (A.14), (A.15) and (A.16) are iterated until $|h_i - h_{i-1}|$ and $|\phi_i - \phi_{i-1}|$ are smaller than some pre-determined limit.

A.3 Error Propagation of ϕ , λ , h to X , Y , Z

The error propagation for the three dimensional transformations are taken from [Krakiwsky et al., 1977]. Propagation from ellipsoid coordinates to Cartesian is accomplished by:

$$C_{X,Y,Z} = B C_{\phi,\lambda,h} B^T \quad , \quad (A.17)$$

where B

$$B = \begin{bmatrix} -(M+h) \sin \phi \cos \lambda & -(N+h) \cos \phi \sin \lambda & \cos \phi \cos \lambda \\ -(M+h) \sin \phi \sin \lambda & (N+h) \cos \phi \cos \lambda & \cos \phi \sin \lambda \\ (M+h) \cos \phi & 0 & \sin \phi \end{bmatrix} \quad (A.18)$$

Propagation from Cartesian to ellipsoid coordinates is accomplished by:

$$C_{\phi,\lambda,h} = B^{-1} C_{X,Y,Z} B^{-1T} \quad , \quad (A.19)$$

where

$$B^{-1} = \begin{bmatrix} \frac{-\sin \phi \cos \lambda}{(M+h)} & \frac{-\cos \phi \sin \lambda}{(M+h)} & \frac{\cos \phi}{(M+h)} \\ \frac{-\sin \lambda}{(N+h) \cos \phi} & \frac{\cos \lambda}{(N+h) \cos \phi} & 0 \\ \cos \phi \cos \lambda & \cos \phi \sin \lambda & \sin \phi \end{bmatrix} \quad (A.20)$$

A.4 Transformation of (ϕ, λ) to (x, y) UTM Grid Coordinates

In order to compute the y coordinate from a given (ϕ, λ) the meridian arc-length must be first computed from [eg. Bomford, 1971 ; Krakiwsky, 1973]:

$$S_{\phi} = a(A_0\phi - A_2 \sin 2\phi + A_4 \sin 4\phi - A_6 \sin 6\phi + A_8 \sin 8\phi) \quad , \quad (\text{A.21})$$

where, ϕ is the latitude of the point in radians,

$$A_0 = \left(1 - \frac{1}{4}e^2 - \frac{3}{64}e^4 - \frac{5}{256}e^6 - \frac{175}{16384}e^8 \right) \quad , \quad (\text{A.22})$$

$$A_2 = \frac{3}{8} \left(e^2 + \frac{1}{4}e^4 + \frac{15}{128}e^6 - \frac{455}{4096}e^8 \right) \quad , \quad (\text{A.23})$$

$$A_4 = \frac{15}{256} \left(e^4 + \frac{3}{4}e^6 - \frac{77}{128}e^8 \right) \quad , \quad (\text{A.24})$$

$$A_6 = \frac{35}{3072} \left(e^6 - \frac{41}{32}e^8 \right) \quad , \quad (\text{A.25})$$

and

$$A_8 = -\frac{315}{131072}e^8 \quad . \quad (\text{A.26})$$

Now, the (x, y) grid coordinates can be computed from [Thomas, 1952 ; Krakiwsky, 1973]:

$$\begin{aligned} x = x_o + k_o N [& \Delta\lambda \cos \phi + \frac{\Delta\lambda^3 \cos^3 \phi}{6} (1 - t^2 + \eta^2) + \\ & \frac{\Delta\lambda^5 \cos^5 \phi}{120} (5 - 18t^2 + t^4 + 14\eta^2 - 58t^2\eta^2 + 13\eta^4 + 4\eta^6 - 64\eta^4 t^2 - 24\eta^6 t^2) + \\ & \frac{\Delta\lambda^7 \cos^7 \phi}{5040} (61 - 479t^2 + 179t^4 - t^6)] \quad , \quad (\text{A.27}) \end{aligned}$$

$$\begin{aligned}
y = y_o + k_o * S_\phi + k_o N & \left[\frac{\Delta\lambda^2}{2} \sin \phi \cos \phi + \frac{\Delta\lambda^4}{24} \sin \phi \cos^3 \phi (5 - t^2 + 9\eta^2 + 4\eta^4) + \right. \\
& \frac{\Delta\lambda^6}{720} \sin \phi \cos^5 \phi (61 - 58t^2 + t^4 + 270\eta^2 - 330t^2\eta^2 + 445\eta^4 + \\
& \left. 324\eta^6 - 680\eta^4 t^2 + 88\eta^8 - 600\eta^6 t^2 - 192\eta^8 t^2) + \right. \\
& \left. \frac{\Delta\lambda^8}{40320} \sin \phi \cos^7 \phi (1385 - 3111t^2 + 543t^4 - t^6) \right] , \quad (A.28)
\end{aligned}$$

where

$$\begin{aligned}
\Delta\lambda = \lambda - \lambda_o \quad \lambda_o = -117^\circ \text{ for Calgary} \\
t = \tan \phi \quad , \quad (A.29)
\end{aligned}$$

$$\eta^2 = \left(\frac{a^2 - b^2}{b^2} \right) \cos^2 \phi \quad , \quad (A.30)$$

$$N = \frac{a}{(1 - e^2 \sin^2 \phi)^{1/2}} \quad , \quad (A.31)$$

$$x_o = 500,000.0 \quad m,$$

$$k_o = 0.9996.$$

A.5 Transformation of (x, y) UTM Grid Coordinate to (φ, λ)

In order to compute φ from a given (x, y), the quantity latitude (φ'), which corresponds to a meridian arc length of $S_\phi = y$ must be computed first. The latitude (φ') is usually referred to as the "footpoint latitude" and is computed as follows [Krakiwsky, 1973; Bomford, 1971].

The first approximation of (φ') is computed from

$$\phi'_1 = \frac{y}{a} \quad . \quad (A.32)$$

Then, the Newton-Raphson iteration technique is used to compute the correct value.

The procedure is to compute successive approximations

$$\begin{aligned} \phi'_2 &= \phi'_1 - \frac{f(\phi')}{f'(\phi)} \Big|_{\phi'_1}, \\ \phi'_3 &= \phi'_2 - \frac{f(\phi')}{f'(\phi)} \Big|_{\phi'_2}, \end{aligned} \quad (A.33)$$

etc., until $|\phi'_n - \phi'_{n-1}|$ is smaller than some pre-determined limit, where from equation

(33)

$$f(\phi') = a(A_0\phi' - A_2\sin 2\phi' + A_4\sin 4\phi' - A_6\sin 6\phi' + A_8\sin 8\phi') - y = 0 \quad (A.34)$$

and after differentiation

$$f'(\phi') = a(A_0 - 2A_2\cos 2\phi' + 4A_4\cos 4\phi' - 6A_6\cos 6\phi' + 8A_8\cos 8\phi') \quad , \quad (A.35)$$

where the coefficients $A_i, i = 0, 2, 4, 6, 8$ are computed from equations (A.22) to (A.26).

From the iteration of equations (A.33)

$$\phi' = \phi'_n.$$

Computation of the (ϕ, λ) ellipsoidal coordinates from the given (x, y) grid coordinates is given by [Thomas, 1952; Krakiwsky, 1973]:

$$x = \frac{x - x_0}{k_0} \quad , \quad y = \frac{y - y_0}{k_0}$$

then

$$\begin{aligned}
\phi = \phi' - \frac{tx^2}{2MN} + \frac{tx^4}{24MN^3} (5 + 3t^2 + \eta^2 - 4\eta^4 - 9\eta^2 t^2) - \\
\frac{tx^6}{720MN^5} (61 - 90t^2 + 46\eta^2 + 45t^4 - 252t^2\eta^2 - 3\eta^4 + 100\eta^6 - 66t^2\eta^4 \\
- 90t^4\eta^2 + 88\eta^8 + 225t^4\eta^4 + 84t^2\eta^6 - 192t^2\eta^8) + \\
\frac{tx^8}{40320MN^7} (1385 + 3633t^2 + 4095t^4 + 1575t^6) \quad , \quad (A.36)
\end{aligned}$$

$$\begin{aligned}
\lambda = \lambda_0 + \left[\frac{x}{N} - \frac{x^3}{6N^3} (1 + 2t^2 + \eta^2) + \right. \\
\left. \frac{x^5}{120N^5} (5 + 6\eta^2 + 28t^2 - 3\eta^4 + 8t^2\eta^2 + 24t^4 - 4\eta^6 + 4t^2\eta^4 + 24t^2\eta^6) - \right. \\
\left. \frac{x^7}{5040} N^7 (61 + 662t^2 + 1320t^4 + 720t^6) \right] / \cos \phi' \quad , \quad (A.37)
\end{aligned}$$

where

$$t = \tan \phi' \quad , \quad (A.38)$$

$$\eta^2 = \left(\frac{a^2 - b^2}{b^2} \right) \cos^2 \phi' \quad , \quad (A.39)$$

$$N = \frac{a}{(1 - e^2 \sin^2 \phi')^{1/2}} \quad , \quad (A.40)$$

$$M = \frac{a(1 - e^2)}{(1 - e^2 \sin^2 \phi')^{3/2}} \quad . \quad (A.41)$$

A.6 Error Propagation between Grid and Ellipsoid Coordinates

Transformation of covariance information between the two coordinate systems is as follows [Krakiwsky et al., 1977]. Let

$$C_{X,Y} = \begin{bmatrix} \sigma_X^2 & \sigma_{XY} \\ \sigma_{YX}^2 & \sigma_Y^2 \end{bmatrix} \quad m^2, \quad (\text{A.42})$$

$$C_{\phi,\lambda} = \begin{bmatrix} \sigma_\phi^2 & \sigma_{\phi,\lambda} \\ \sigma_{\lambda,\phi}^2 & \sigma_\lambda^2 \end{bmatrix} \quad rad^2, \quad (\text{A.43})$$

be the covariance matrices of the (X, Y) grid coordinates and (ϕ, λ) ellipsoidal coordinates respectively, and

$$B = \begin{bmatrix} b_{11} & b_{12} \\ b_{21} & b_{22} \end{bmatrix}, \quad (\text{A.44})$$

where

$$b_{11} = 21670\Delta\lambda \cos \phi - 6390000\Delta\lambda \sin \phi, \quad (\text{A.45})$$

$$b_{12} = 6390000 \cos \phi, \quad (\text{A.46})$$

$$b_{21} = 6390000, \quad (\text{A.47})$$

$$b_{22} = 6390000\Delta\lambda \sin \phi \cos \phi, \quad (\text{A.48})$$

then

$$C_{X,Y} = BC_{\phi,\lambda}B^T, \quad (\text{A.49})$$

and

$$C_{\phi,\lambda} = B^{-1}C_{X,Y}B^{-1T}, \quad (\text{A.50})$$

where

$$B^{-1} = \begin{bmatrix} \frac{b_{22}}{b_{11}b_{22} - b_{21}b_{12}} & \frac{b_{12}}{b_{11}b_{22} - b_{21}b_{12}} \\ \frac{b_{21}}{b_{11}b_{22} - b_{21}b_{12}} & \frac{b_{11}}{b_{11}b_{22} - b_{21}b_{12}} \end{bmatrix}. \quad (\text{A.51})$$

It should be noted here that equations (A.45) to (A.48) are accurate enough so that the transformations (A.49) and (A.50) are good to three significant figures, which is sufficient for all practical purposes.

APPENDIX B

NAVIGATION ALGORITHMS

B.1 Navigation Algorithms

The navigation equations can either be formulated in terms of a Cartesian Earth Centred Earth Fixed (ECEF) xyz system or geodetic curvilinear coordinates ϕ, λ, h . The mathematics for both of these methods are described in the following section. GPS formulation is also given in both coordinate frames.

A geodetic coordinate frame was chosen since it is often necessary, when using GPS, to constrain the height to a constant value or to augment it with altimeter information. Given that horizontal speed is also derived from the dead reckoning sensors, this is further justification for using the curvilinear frame. Some investigation was done to consider inputting the height as a weighted range from the origin in the cartesian formulation.

Some systems have opted to work in mapping plane systems, especially when only dealing with dead reckoning sensors, as the computations are somewhat simpler. This not very suitable for GPS computations, however. Rigorous propagation of covariance information between the various coordinate frames is very time consuming for a real time system. Also when dealing with a mapping plane system, zone crossovers must be dealt with. This problem manifests itself in Calgary, where the change in zones runs nearly through the middle of the city.

In both formulations, a Gauss Markov process is incorporated into the velocity equations to account for limitations in the model used. The Gauss Markov process can be used to account for the accelerations which have been neglected in this constant velocity model [Wong, 1987; Harris, 1988; Schwarz et al., 1989].

B.2 Cartesian Formulation

The navigation equations in the Cartesian coordinate frame are as follows:

$$x_k = x_{k-1} + \dot{x}_{k-1} \Delta t_{k-1,k} \quad , \quad (B.1)$$

$$y_k = y_{k-1} + \dot{y}_{k-1} \Delta t_{k-1,k} \quad , \quad (B.2)$$

$$z_k = z_{k-1} + \dot{z}_{k-1} \Delta t_{k-1,k} \quad , \quad (B.3)$$

$$\dot{x}_k = \dot{x}_{k-1} e^{-\left(\frac{a_x \Delta t}{d}\right)} \quad , \quad (B.4)$$

$$\dot{y}_k = \dot{y}_{k-1} e^{-\left(\frac{a_y \Delta t}{d}\right)} \quad , \quad (B.5)$$

$$\dot{z}_k = \dot{z}_{k-1} e^{-\left(\frac{a_z \Delta t}{d}\right)} \quad , \quad (B.6)$$

where

- k refers to the current computation time,
- $k - 1$ refers to the most recent computation time,
- x, y, z are the three dimensional coordinates of the vehicle in motion in an ECEF Cartesian reference frame,
- $\dot{x}, \dot{y}, \dot{z}$ are the corresponding velocities in an ECEF Cartesian reference frame $\left[\frac{dx}{dt}, \frac{dy}{dt}, \frac{dz}{dt} \right]$,
- d is the value computed by taking an average speed value over the time interval Δt for the vehicle, and
- a_x, a_y, a_z are accelerations computed from $\frac{v_k - v_{k-1}}{\Delta t}$, where v represents velocity for x, y, z for each a_x, a_y, a_z .

B.3 Geodetic

The navigation equations in the geodetic coordinate frame are listed below [Harris, 1988]:

$$\phi_k = \phi_{k-1} + \frac{V_N \Delta t}{R} \quad , \quad (B.7)$$

$$\lambda_k = \lambda_{k-1} + \frac{V_E \Delta t}{R \cos \phi_k} \quad , \quad (B.8)$$

$$h_k = h_{k-1} + V_U \Delta t \quad , \quad (B.9)$$

$$V_{N_k} = V_{N_{k-1}} e^{\left(\frac{a_N \Delta t}{d}\right)} \quad , \quad (B.10)$$

$$V_{E_k} = V_{E_{k-1}} e^{\left(\frac{a_E \Delta t}{d}\right)} \quad , \quad (B.11)$$

$$V_{U_k} = V_{U_{k-1}} e^{\left(\frac{a_u \Delta t}{q}\right)} \quad , \quad (B.12)$$

where

- ϕ, λ, h are the latitude, longitude and height of the vehicle in motion,
- V_N, V_E, V_u are the corresponding velocities in the north, east and up directions,
- d is the value computed by taking an average horizontal velocity value over the time interval Δt for the vehicle,
- q is the value computed by taking an average vertical velocity value over the time interval Δt for the vehicle, and
- a_ϕ, a_λ, a_u are accelerations computed from $\frac{v_k - v_{k-1}}{\Delta t}$, where v represents velocity for N, E, u for each a_N, a_E, a_U .

The underlying assumptions for the above velocity equations are as follows (Figure B.1):

$$\Delta S_{\phi} = \Delta \phi R \quad (B.13)$$

rearranging

$$\Delta \phi = \frac{\Delta S_{\phi}}{R} = \frac{V_N \Delta t}{R} \quad (B.14)$$

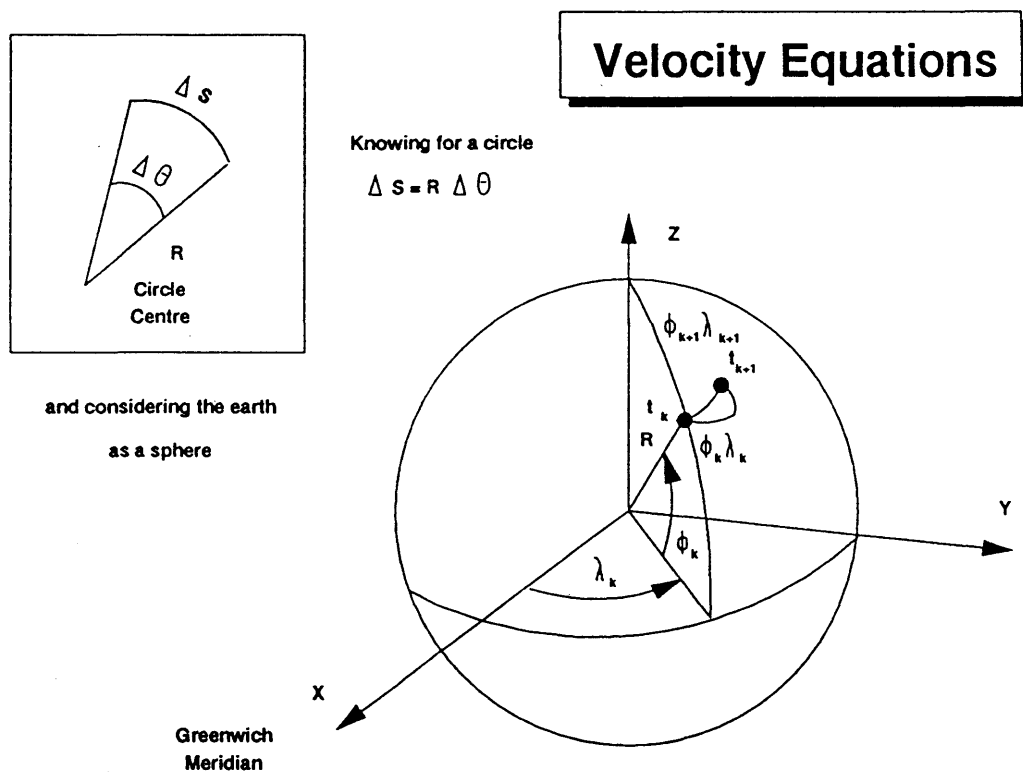


Figure B.1 Velocity Equations

where

$$\Delta S_{\phi} \approx V_N \Delta t \quad (B.15)$$

for small Δt .

$$\Delta S_{\lambda} = \Delta \lambda (R \cos \phi) \quad (B.16)$$

rearranging

$$\Delta\lambda = \frac{\Delta S_\lambda}{R \cos \phi} = \frac{V_E \Delta t}{R \cos \phi} \quad (B.17)$$

where

$$\Delta S_\lambda \approx V_E \Delta t \quad (B.18)$$

for small Δt .

R can be computed from

$$R = \sqrt{MN} . \quad (B.19)$$

Details on the computation of M and N are given in Appendix A.